Monte Carlo technique in modeling ground motion coherence in sedimentary filled valleys

Arrigo Caserta [a,b,*], Massimo Di Bona [a]

[a] Istituto Nazionale di Geofisica e Vulcanologia, Via di Vigna Murata, 605, 00143 Roma, Italy
[b] Charles University, Faculty of Mathematics and Physics, Prague, Czech Republic

ARTICLE INFO

ABSTRACT

Using a Monte Carlo method based on a random walk in ad hoc N-dimensional phase space, we construct N random time series having prescribed coherence spatial decay. We apply the method in seismology by designing a numerical experiment to investigate how the coherence of the bedrock motion relates to the coherence of the surface ground motion in a sedimentary valley. The main features of the coherence behaviour in the valley are found to tie in with data analysis and field observations.

© 2009 Published by Elsevier Ltd.

1. Introduction

The spatial variability of ground motion, even over small distances, has been investigated in seismology because it can be significant for engineering applications. For example in large structures such as bridges or extended power plants, spatially variable excitations at different points along their foundations can cause catastrophic effects. Such variability is mainly expressed in terms of peak amplitudes, phase character, frequency content and coherence. In this paper we will focus on coherence, which is an important ground motion parameter tightly linked to differential motions and aerial damage patterns.

Field observations mainly reveal two features as far as coherence is concerned: the seismic radiation becomes incoherent at a distance of one wavelength in rock-sites (Toksöz et al., 1992) and the coherency level of seismic wave propagation in large sedimentary basins is higher than in rock-sites (Schneider et al., 1992). The former behaviour is ascribed to the scattering that takes place along the propagation path within the Earth's crust (Menke et al., 1990; Toksöz et al., 1992); the latter is attributed to the resonance properties of basins that make seismic wave propagation more coherent (Schneider et al., 1992; Hough and Field, 1996). Both features arise from a wealth of fine structures in the Earth's crust, as well as in the near-surface geological structures that cannot be represented in a detailed enough manner for its behaviour to be described in a deterministic way.

An attempt to numerically model such a *stochastic side* of the coherence behaviour can be found in Caserta et al. (1999). Taking into account effects due to small-scale heterogeneities of the crust, the authors added stochastic noise to the deterministic signals (numerically computed) propagated through the crust. The perturbation (noise) of the deterministic seismic radiation was constructed using the stochastic technique based on Markov-like process generator. Our study has an innovative approach as the stochastic component can be *tuned* to agree with the assumed empirical coherence law. The method is applied in a numerical experiment designed to investigate how the coherence of the bedrock motion relates to the coherence of surface ground motion in a sedimentary valley. This case study deals with the main sedimentary body of the city of Rome, the Tiber valley.

2. The seismological model

The starting point is the deterministic hybrid numerical method called DWFD of Zahradnik and Moczo (1996) and a brief recap of the main steps used in this methods. It is based on the discrete wave-number technique for the seismic source and crustal path and a finite-difference technique to simulate the seismic site response. It is called the hybrid method because the discrete wave-number crustal propagation is numerically

* Corresponding author at: Istituto Nazionale di Geofisica e Vulcanologia, Via di Vigna Murata, 605, 00143 Roma, Italy. Tel.: +39 06 51860494; fax: +39 06 51860605.
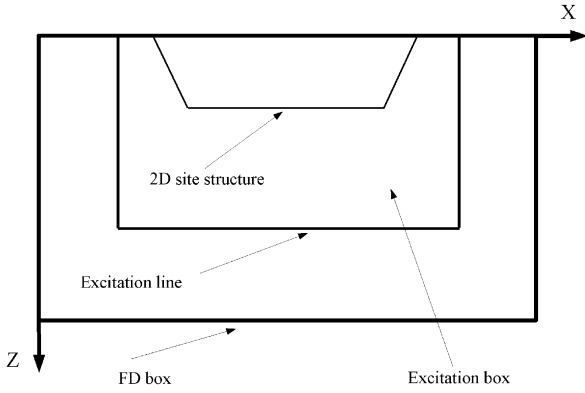
E-mail address: caserta@ingv.it (A. Caserta).

Fig. 1. Schematic representation of DW–FD hybrid method (Zahradnik and Moczo, 1996). Crustal path effects are calculated by DW method and stored at excitation line. DW field is propagated through excitation box via FD numerical method up to free surface. This is to study interaction between seismic radiation and near-surface geological structures. Left, right and bottom sides of FD box are non-reflecting, top side is free.

computed in 3 dimensions, while the elastic site response is computed in 2 dimensions. The coupling between discrete-wave-number and finite-difference (see Fig. 1) is accomplished by computing the discrete wave-number wave-field along the lines belonging to the *excitation box* surrounding the 2D site structure. The discrete wave number seismic radiation represents the data to numerically compute, via the finite difference technique and the 2D elastic response of the alluvial valley under study (for details see Zahradnik and Moczo, 1996).

In this paper we think of seismic wave field below the site under study as made up of the sum of an Earth-model response computed from deterministic techniques (DW in the following) and the stochastic signals (MC in the following) representing the effects of the small scale Earth crustal heterogeneities through scattering phenomena. We construct MC by employing the Monte Carlo method based on random walk to generate suitable stochastic components where the assumed coherence law represents the *target* function. Moreover, for the noise to have a seismological significance, its spectral amplitude needs to be scaled according to the seismological spectral model (Brune (1970) spectrum in the following). These modifications are introduced on the basis of the loss of spatial coherence with distance and frequency arising from field observations (Toksöz et al., 1992; Hough and Field, 1996, among others).

3. The DWMC crustal signal

Adopting the previously mentioned additive model, the new seismic crustal signals, DWMC, can be written as

$$y_l(t) = x_l(t) + \xi_l(t), \quad l = 2, \ldots, N \tag{1}$$

where the index l identifies the N receivers ideally located along the horizontal excitation line of the excitation box (see Fig. 1), $\xi_l(t)$ and $x_l(t)$ represent the deterministic DW and the random MC components at the lth receiver.

The set of random signals $\{\xi_l(t)\}$ are assumed to be stationary with zero mean, therefore the expected value of the seismic signal $E\{y_l(t)\} = x_l(t)$ equals the deterministic component $x_l(t)$. The cross-correlation function for the stationary stochastic process is defined as $R_{l,k}(\tau) = E\{[y_l(t) - x_l(t)][y_k(t+\tau) x_k(t+\tau)]\} = E\{\xi_l(t)\xi_k(t+\tau)\}$ and the cross-spectrum $H_{l,k}(\omega)$ is the Fourier transform of $R_{l,k}(\tau)$ Priestley, 1981). When considering finite duration random

signals, it can be shown (Priestley, 1981) that

$$H_{l,k}(\omega) = \lim_{T \to \infty} E\left\{ \frac{(\hat{\tilde{\xi}}_l(\omega))^* \hat{\tilde{\xi}}_k(\omega)}{T} \right\} \tag{2}$$

where $*$ stands for complex conjugate and the $\hat{\tilde{\xi}}_l(\omega)$ are the Fourier transforms of the random signals $\xi_l(t)$ over a time window of duration T, that is $\hat{\tilde{\xi}}_l(\omega) = \int_0^T \xi_l(t) e^{-i\omega t} dt$. When $l=k$, (2) provides the power spectral densities of the random signals $\{\xi_l(t)\}$. Then, we assume that all of these signals share the same power spectral densities, reflecting a similar frequency content. Moreover, we assume that $H_{l,l} = 1$. This means that the set of random time series $\{\xi_l(t)\}$ will be represented, at the first time-step, by samples of white noise.

In order to quantify the degree of correlation between seismic signals recorded at the lth and the kth receivers, we use the absolute value of the coherence defined as (Priestley, 1981; Toksöz et al., 1991)

$$|W_{l,k}(\omega)| = \frac{|H_{l,k}(\omega)|}{\sqrt{H_{l,l}(\omega) H_{k,k}(\omega)}} \tag{3}$$

The N points on the excitation line have a constant spacing d_0 therefore the distance between the lth and the kth points is $d_{l,k} = |l-k| d_0$. As previously mentioned, the seismic radiation propagating in rock-site environments becomes incoherent over distances greater than one wavelength and the loss of spatial coherence with distance and frequency, can be represented by an exponential function (Menke et al., 1990; Hough and Field, 1996; Riepl et al., 1997). This leads us to choose the following functional form for the coherency decay

$$w_{l,k}(\lambda) = |W_{l,k}(\omega)| = \exp\left(-\frac{d_{l,k}}{\delta(\lambda)}\right), \text{ where } \delta(\lambda) = -\frac{2\pi c}{\omega \ln(0.3)} \tag{4}$$

where c is the wave velocity. The choice (4) represents a 70% coherency decay over one wavelength.

From the above assumptions and equations the absolute value of the cross-spectrum $H_{l,k}(\omega)$ can be represented, for a fixed frequency (or wave-length), by the following symmetric matrix:

$$H = \begin{pmatrix} 1 & \Theta & \cdots & \Theta^{N-2} & \Theta^{N-1} \\ \Theta & 1 & \cdots & \Theta^{N-3} & \Theta^{N-2} \\ \vdots & \vdots & \ddots & \vdots & \vdots \\ \Theta^{N-2} & \Theta^{N-3} & \cdots & 1 & \Theta \\ \Theta^{N-1} & \Theta^{N-2} & \cdots & \Theta & 1 \end{pmatrix} \tag{5}$$

where $\Theta = \exp(-d_0/\delta(\lambda))$. The matrix (5) and the expression (2) suggest estimating the N different elements of such a symmetric matrix as

$$h_{|k-l|} = \frac{1}{T} \left| \frac{\sum_{i=1}^{N-|k-l|} \left(\hat{\tilde{\xi}}_i(\omega)\right)^* \hat{\tilde{\xi}}_{i+|k-l|}(\omega)}{N-|k-l|} \right| \tag{6}$$

with l and k indicating the rows and the columns of the matrix (5), respectively. The estimate (6) is based on the assumption that the spatial variation of the cross-spectrum for the stochastic signals can be represented by a function of the relative distances $d_{l,k}$ between the points on the excitation line.

3.1. Monte Carlo stochastic signal generation

We now describe the method used to generate N random time series $\xi_l(t_j)$ of finite duration T and sampled at M time values $t_j = (1-j)\Delta t, j=1,2, \ldots, M$, with sampling time step Δt. These signals are required to have zero mean and to be correlated amongst themselves according to the expression $|H_{l,k}(\omega)| = \Theta^{|k-l|}$

for the absolute value of the cross-spectrum, previously defined in matrix (5).

The simulation procedure works in the frequency domain, so for a fixed frequency, we initially generate N complex numbers $\hat{\xi}_{0,l} = a_{0,l} + ib_{0,l}$, where $\{a_{0,l}\}$ and $\{b_{0,l}\}$ $l = 1,2, \ldots, N$ are random Gaussian numbers with zero mean and variance equal to $T/2$. The value $T/2$ for the variance comes directly from our assumption $H_{l,l} = 1$ concerning the cross-spectrum (2). In this way, the complex numbers $\{\hat{\xi}_{0,l}\}$ represent the Fourier amplitudes at a fixed

Fig. 2. Number of iterations N_{iter} versus exponent e at different frequency values (1, 10 and 20 Hz as an example).

frequency for N discrete time series of white noise with zero mean and variance equal to $1/\Delta t$. This is because the variance of the random time signals $\{\xi_l(t)\}$ is the integral of their power spectral density ($H_{l,l}(\omega) = 1$) over the frequency window $[-f_N, f_N]$, where $f_N = 1/2\Delta t$ is the Nyquist frequency. Using (6), the estimates $\{h_n\}$ of the absolute value of the cross-spectrum are computed for the complex amplitudes $\{\hat{\xi}_{0,l}\}$ and then compared with the target values $\{\Theta^n\}$ by evaluating the average-weighted misfit

$$D = \sqrt{\frac{\sum\limits_{n=0}^{N-1}(h_n - \Theta^n)^2 \nu_n}{\sum\limits_{n=0}^{N-1} \nu_n}} \tag{7}$$

The weights $\{\nu_n\}$ in (7) describe the loss of accuracy in the estimates $\{h_n\}$ for increasing values of n, and they are evaluated as $\nu_n = N - n/N$.

Each set of complex numbers $\{\hat{\xi}_{0,l}\}$ can be seen as a point in a phase space with N degrees of freedom, and D in (7) can be thought of as the distance between two points in such a *hyperspace*. If $D > D_{th}$, where D_{th} is a threshold, we search the hyperspace for another point perturbing the complex numbers until the misfit D. (7) becomes less than D_{th}, therefore obtaining the new set

$$\hat{\xi}_l = \hat{\xi}_{0,l} + f(D_0)(\phi_l + i\psi_l), \quad l = 1, 2, \ldots, N \tag{8}$$

where φ_l and ψ_l are random numbers uniformly distributed in the range $(-1,1)$, and $f(D_0)$ is a function of the value of the average weighted misfit corresponding to the set $\{\hat{\xi}_{0,l}\}$. We choose $f(D_0) = D_0$ and later in this paper we will explain the reason for this choice. In other words, the rejected set of complex numbers is seen as the center point for a sphere of radius D, we search in such a sphere for a new point generating the random numbers φ_l and ψ_l in (8). In this respect relation (8) can be thought of as our Monte Carlo throw.
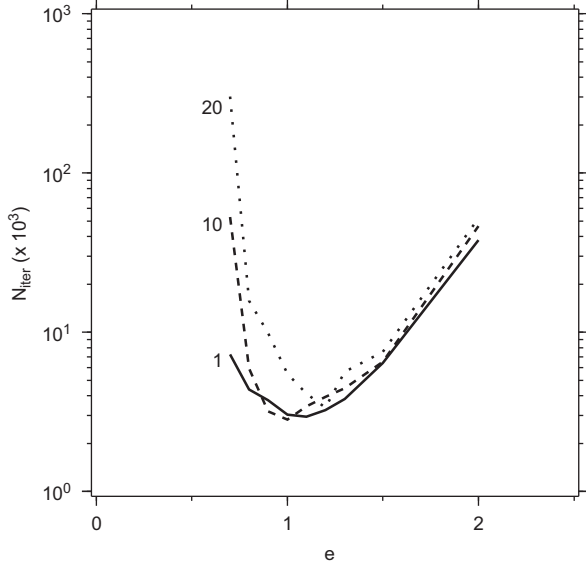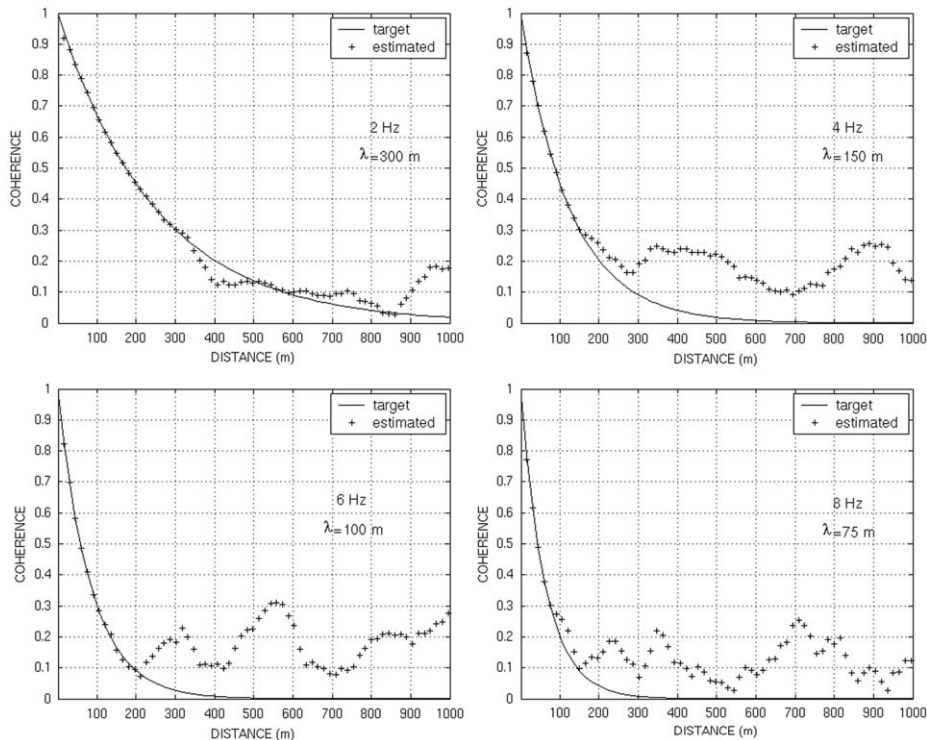

Fig. 3. Comparison between cross-spectrum estimates (6) for complex amplitudes set $\{\xi_l\}$ (crosses) and chosen theoretical coherency decay (4) (solid line). S-wave velocity in Pliocene Bedrock is 600 m/s (see Fig. 6). λ is wavelength. After one wavelength coherency level is degraded to 30%, as prescribed. This happens to all frequencies in range of interest.

The estimates $\{h_n\}$ (6) and the misfit D(7) are updated. If $D > D_0$, the current set $\{\hat{\xi}_l\}$ is replaced by a new one computed through (8). To reiterate, we need another Monte Carlo throw to select another point within the same sphere. This search continues until the misfit D becomes less than D_0. As soon as it happens, the acceptance condition $D < D_{th}$ is checked and if it is fulfilled, the new set of complex numbers are accepted and the procedure restarts for the next discrete value of the frequency. If however the acceptance condition is not fulfilled, we find a point closer to the target point, and we consider the new point as the center of a new sphere which is smaller than the previous one. With the same procedure we scan this new sphere looking for a point for which the acceptance condition is verified.

The function $f(D)$ represents the maximum perturbation for the real and imaginary parts of $\{\hat{\xi}_l\}$ its functional form affects the convergence speed rather than the final result of the Monte Carlo scheme. Choosing $f(D) = D^e$ we investigate the efficiency of the technique for different values of the exponent e.

Fig. 2 shows the number of iterations versus the exponent e for different frequency values (1, 10 and 20 Hz). Higher convergence speeds are obtained for values of the exponent e around 1. This is why we have chosen $f(D) = D_0$ in (8).

Fig. 3 shows the comparison between the target cross-spectrum (4) (exponentially decaying 30% after one wavelength) and the estimated cross-spectrum (6). In the selected range of interest the comparison is shown at all frequencies. The iterative process is run with $e = 1$ and $D_{th} = 0.01$ and the frequency is related to the wavelength through a phase velocity of $60d_0$.

To attach a seismological significance to the stochastic noise $\{\hat{\xi}_l(\omega)\}$ we multiply the latter by the Brune spectrum (Brune, 1970). Details on this operation can be found in Caserta et al. (1999). Here it is worth noting that such an operation has no influence on coherence because only the spectral amplitudes are changed, as seen from Eq. (4), while coherence is insensitive to spectral amplitude variations (Toksöz et al., 1991). Applying the inverse Fourier Transform to the set $\{\hat{\xi}_l(\omega)\}$ we get the stochastic signals $\{\xi_l(\omega)\}$ of (1).

The logical steps that form our technique are summarized in Fig. 4. In the next section we will show how they are applied to our case study: the Tiber valley site.
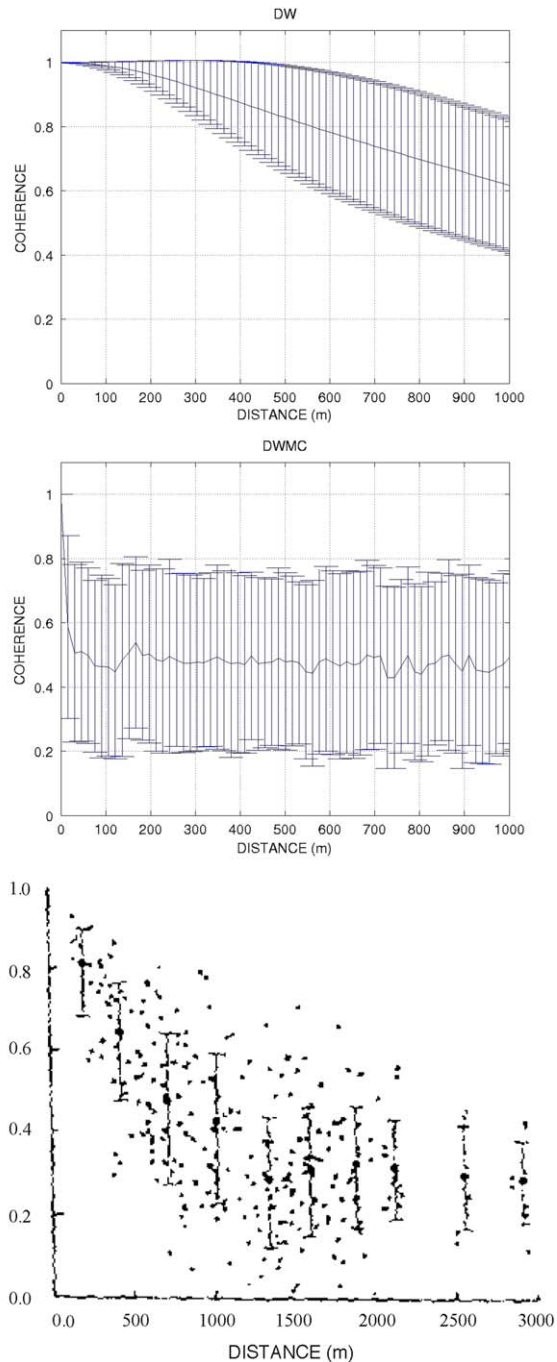

Fig. 5. Comparison between coherence decay with distance between receivers along horizontal excitation line for DW (top), DWMC (middle) and coherence analysis of real data from Toksöz et al., 1992 (bottom). Vertical bars represent ± 1 standard deviation interval. Coherence decay is computed at fixed frequencies. Figure shows comparison at 6 Hz as an example. Wavelength at 6 Hz of Toksöz coherence analysis (bottom) is around 700 m. Toksöz incoherence threshold is fixed at 0.5.
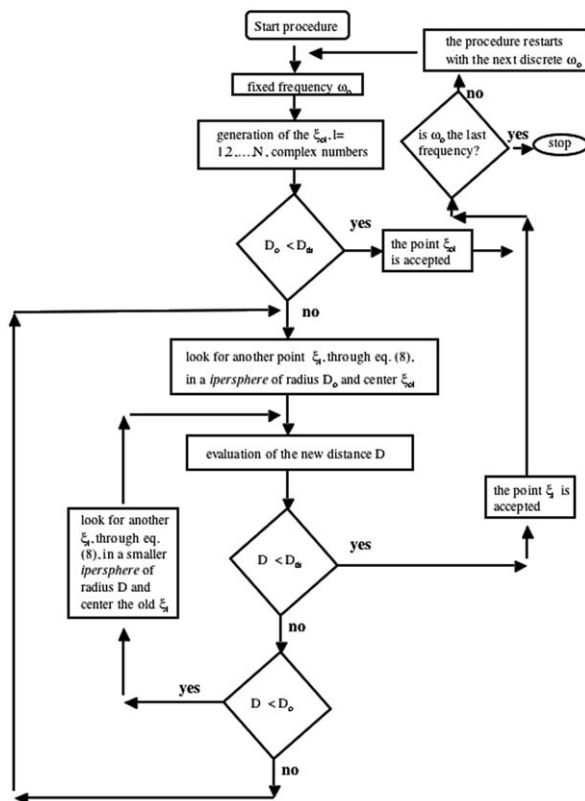

Fig. 4. Flow chart that summarizes main steps of our Monte Carlo method.

4. Numerical test

As a numerical test example, we choose the 2D vertical section of the main sedimentary body of the city of Rome, the Tiber valley. To generate the DW deterministic synthetics we select the 3.6 magnitude earthquake that occurred a few kilometers inside the limit of the urban area in the southernmost part of the city on 12th of June 1995 (see Basili et al. (1996), for details).

For each DW time history along the horizontal excitation lines, the excitation noise is generated by using the procedure explained in Section 3 and it is added to the DW deterministic signals according to Eq. (1) to get the DWMC excitation.

In Fig. 5 the coherency behaviour of the DWMC is shown, in this case taking 6 Hz as an example. The shear wave velocity in the bedrock is 600 m/s, so the wavelength at 6 Hz is 75 m. In Fig. 6 (middle) we see that the DWMC excitation after circa 100 m becomes incoherent. Conversely, the purely deterministic DW wave-field (Fig. 6 top) after one wavelength is fully coherent.

Because our aim is to numerically investigate how a prescribed coherence behaviour under a sedimentary valley is transformed into surface ground motion, we propagate the DWMC input up to the surface using the FD deterministic technique as in Caserta et al. (1999). The geological model is shown in Fig. 6, along with the elastic and anelastic parameters used in the computations. The results are summarized in Fig. 7, which shows the coherence versus distance across the basin related to the simulated DWMC–FD shaking on the basin's surface. The surface motion is more coherent around the basin resonance frequency (1–2 Hz) than elsewhere in the frequency band under study. The bottom panel shows the coherence behaviour for the pure deterministic DW–FD simulation; it reflects a negligibly slow coherence decay due to the deterministic DW crustal propagation.

The results shown in Fig. 7 are in agreement with field observations (Schneider et al., 1992; Hough and Field, 1996) that seismic propagation in large sedimentary basins represent a
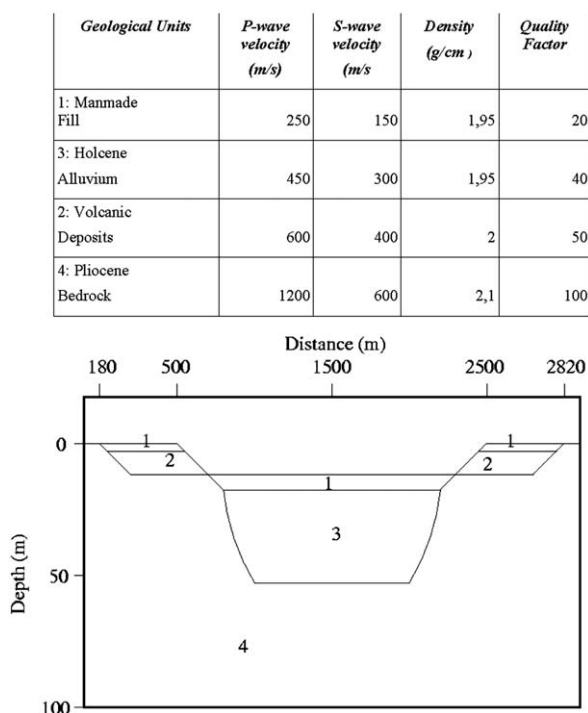

Geological Units	P-wave velocity (m/s)	S-wave velocity (m/s)	Density (g/cm)	Quality Factor
1: Manmade Fill	250	150	1,95	20
3: Holcene Alluvium	450	300	1,95	40
2: Volcanic Deposits	600	400	2	50
4: Pliocene Bedrock	1200	600	2,1	100

Fig. 6. Cross-section of Tiber valley as modeled in this paper. Table provides key to the individual geologic blocks, along with material properties used in numerical simulations.
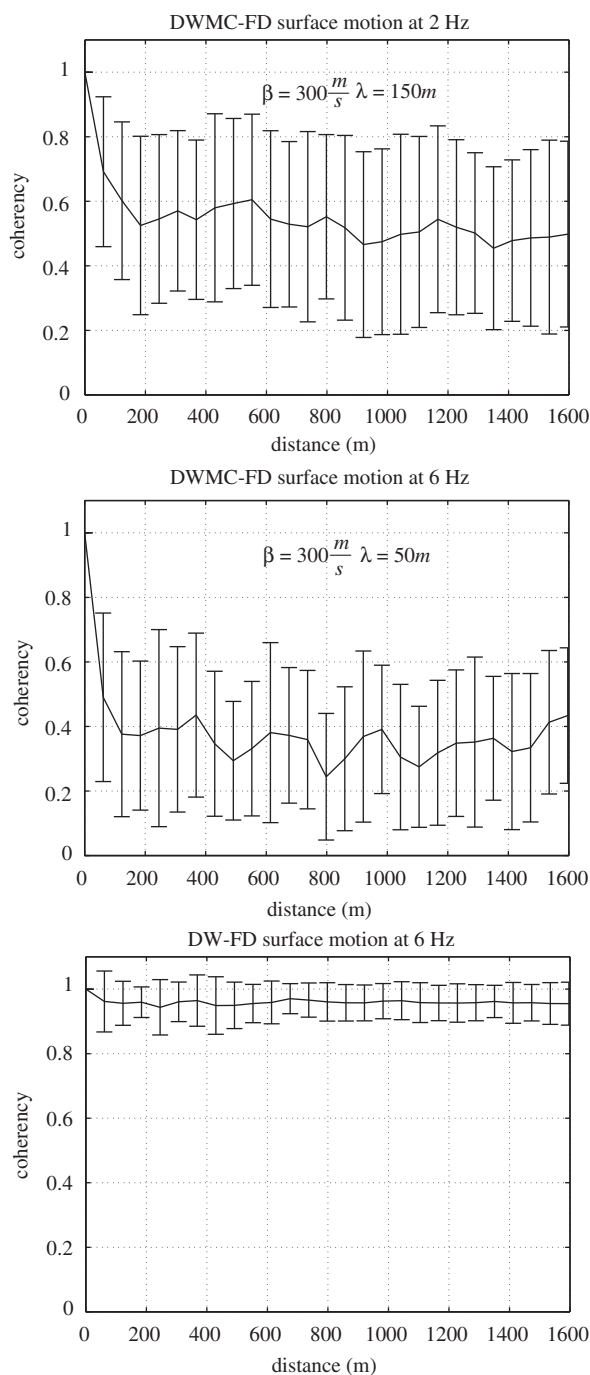

Fig. 7. Coherence versus distance of surface motion along valley close to resonance frequency (1–2 Hz), and far from valley resonance (6 Hz). Vertical bars represent ± 1 standard deviation interval. Bottom panel shows coherence versus distance on free surface along valley of DW–FD pure deterministic simulation.

resonance effect; therefore, ground motions may be uniform over kilometers before being degraded by scattering.

5. Conclusions

Using a Monte Carlo method based on a random walk in an *ad hoc N*-dimensional phase space, we constructed *N* random time series (MC). Such MCs have been used in seismology, with the aim to improve the tuning of the stochastic component of the wave-field to agree with the assumed empirical coherence law.

Moreover, our Monte Carlo technique does not depend neither on the coherency decay law nor on the incoherence threshold over one wavelength, both given in expression (4); the method also works with other decay laws.

A numerical experiment was designed to investigate how the presence of a sedimentary basin transforms a prescribed bedrock coherence behaviour. We find that the main features of the coherence behaviour in the valley are in agreement with field observations. Nonetheless, our Monte Carlo technique is not solely applicable to the selected Roman earthquakes or to the Tiber valley, which have only been used here as a case study, but is applicable to any other earthquakes (i.e., different focal mechanisms and/or source parameters) and sedimentary basins. Our method is of interest mainly for applications in both strong motion seismology and engineering seismology and currently focuses on these fields. Nevertheless, if interest outside the above mentioned is presently modest, it is worth considering that the method can be applied in every other scientific field where a set of stochastic time series with a prescribed spatial decay of coherence needs to be generated.

Acknowledgements

References

Basili, A., Cantore, L., Cocco, M., Frepoli, A., Margheriti, L., Nostro, C., Selvaggi, G., 1996. The June 12, 1996 microearthquake sequence in the city of Rome. Annali di Geofisica XXXIX, 1167–1175.

Brune, J.N., 1970. Tectonic stress and the spectra of seismic shear from earthquakes. Journal of Geophysical Research 76, 5002.

Caserta, A., Zahradnik, J., Plicka, V., 1999. Ground motion modelling with a stochastically perturbed excitation. Journal of Seismology 3, 45–59.

Hough, S.E., Field, E.H., 1996. On the coherence of ground motion in the San Fernando valley. Bulletin of Seismological Society of America 86, 1724–1732.

Menke, W., Lerner-Lam, A.L., Dubendroff, B., Pacheco, J., 1990. Polarization and coherence of 5–30 Hz seismic wave fields at hard-rock site and their relevance to velocity heterogeneities in the crust. Bulletin of Seismological Society of America 80, 430–449.

Priestley, M.B., 1981. In: Spectral Analysis and Time Series first ed. Academic Press, New York, NY.

Riepl, J., Oliveira, C.S., Bard, P.-Y., 1997. Spatial coherence of seismic wave fields across an alluvial valley (weak motion). Journal of Seismology 1, 253–268.

Schneider, J.F., Stepp, J.C., Abrahamson, N.A., 1992. The spatial variation of earthquake ground motion and effects of local site conditions. In: Proceedings of the Tenth World Conference Earthquake Engineering, Madrid, Spain. pp. 967–972.

Toksöz, M.N., Dainty, A.M., Charrette, E.E., 1991. Coherency of ground motion at regional distances and scattering. Physics of the Earth and Planetary Interior 10, 53–77.

Toksöz, M.N., Dainty, A.M., Coates, R., 1992. Effects of lateral heterogeneities on seismic motion. In: Proceedings of the International Symposium on the Effects of Surface Geology on Seismic Motion, Odawara, Japan. pp. 33–64.

Zahradnik, J., Moczo, P., 1996. Hybrid seismic modelling based on discrete-wave number and finite-difference methods. Pure Applied Geophysics 158, 21–38.

STATISTICAL FEATURES OF THE SEISMIC NOISE-FIELD

A. Caserta[1], G. Consolini[2] and P. De Michelis[1]

1   Istituto Nazionale di Geofisica e Vulcanologia, Via di Vigna Murata 605, 00143 Rome, Italy (caserta@ingv.it, demichelis@ingv.it)

2   Istituto di Fisica dello Spazio Interplanetario -I.N.A.F., Via del Fosso del Cavaliere 100, 00133Rome, Italy (giuseppe.consolini@ifsi-roma.inaf.it)

ABSTRACT

We present a preliminary study of the dependence of the statistical features of the soil motion due to seismic noise on the near-surface geology in the frequency range from 1 Hz to ~ 40 Hz. In detail, we have investigated the 3D average squared soil displacement $\langle r^2 \rangle$ and the distribution function of the displacement flctuations at different geological sites. The anomalous scaling of the average squared soil displacement $\left\langle r^2 \left(\tau \right) \right\rangle \sim \tau^\alpha$, and the Gaussian shape of the probability distribution function of its fluctuations suggest that the soil motion under the influence of the seismic noise is consistent with a persistent fractional Brownian motion (fBm) characterized by a scaling exponent $1.5 < \alpha < 2$. Therefore, the seismic noise-field, thought as a stochastic process, shows a markovian character with a memory longer than a pure Brownian motion ($\alpha = 1/2$). Moreover, a dependence of such persistent behavior of the noise-field dynamics on the near-surface local geology has been found and it is discussed.

K e y   w o r d s : seismic noise, fractals, scale invariant process, superdiffusion

1. INTRODUCTION

In seismology the ambient vibration is studied to achieve information on the near-surface geology and the inner Earth structure. While the former mainly concerns site effect studies for seismic risk assessment and engineering seismology purposes (see the review of *Bard (1999)* and references therein), the latter is more oriented to get information on the structure of the Earth's crust and upper mantle (*Shapiro and Campillo, 2004*).

The two afore-mentioned topics usually investigate the seismic noise-field features in two different frequency ranges: 1 to 15 Hz for site effects and 5×10^{-3} to 1 Hz for crust and upper mantle images. It is worth noticing that 1 Hz has been conventionally chosen as the border between the two topics although some times both engineering seismology is interested in frequencies lower than 1 Hz and some times crustal studies involve the shallow geological layers as part of the Earth crust. However, both topics are mainly

based on the analysis of the dispersion curves of surface waves, which are hidden in the seismic noise-field, and are one of the main sources of information (*Lachet and Bard, 1994*; *Campillo and Paul, 2003*; *Shapiro and Campillo, 2004*; *Wathelet et al., 2005*).

To use the dispersion curves of the surface waves from the noise-field, it is necessary to get information from the so called ballistic component of the diffused wave-field. This can be done by different approaches. For example, *Wathelet et al. (2004,2005)* realize the surface-wave inversion numerically by means of a Monte Carlo technique. This numerical technique, is not a method to estimate the dispersion curves of the surface waves. On the contrary, it is applied to the ambient vibration time series in order to assess the subsurface structure and, in particular, the shear-wave velocity profile.

On the other hand, *Shapiro and Campillo (2004)* showed how coherent information about the structure of the Earth's crust and the upper mantle can be recovered analyzing the ballistic content of the seismic noise-field. Their study concerns how to extract the Green function of the elastic medium under study by the diffused or random wave-field and the seismic noise-field. The theoretical roots of their work are in the paper of *van Tiggelen (2003)* who showed that correlation of diffuse waves can be used to retrieve ballistic waves between two points in the space-time. The van Tiggelen method is based on a passive method of imaging. This is very useful when active sources are whether expansive or impracticable as it often happens in seismology.

Although it is well known that the energy transport process through heterogeneous media can be described both in terms of a diffusion process and wave propagation (*Sheng, 1990,2006*), all of the afore-mentioned approaches are focused on the deterministic component of the seismic noise-field. Indeed, all efforts are spent to recover the ballistic component, represented by surface waves, and to invert for the velocity profile.

Conversely to what is stated above, this paper approaches the problem of the characterization of the noise-field features and of its relationship with the soil geo-morphology from a stochastic point of view. We will focus on investigating the statistical and dynamical features of the noise-field without considering its deterministic and diffusive component. In other words, we assume the seismic noise-field to be a result of the stochastic nature of the energy transport process through a heterogeneous medium.

We will show that the seismic noise-field statistical features are in good agreement with those of a particular diffusive process called fractional Brownian motion (fBm). Its statistical (scale-invariant) and physical (how the diffusion drives the energy transport process) features are analyzed and discussed. Moreover, the super-diffusive character of the fBm has been found to be dependent on the near-surface local geological conditions.

2. DATA DESCRIPTION AND ANALYSIS

Data used in this work were collected during a measurement campaign at three different sites in Umbria (Central Italy): the Verchiano valley, the Nocera Umbra site and the Colfiorito plain (Fig. 1). These sites are Quaternary intra-mountain basins located in the Northern Apennines arc, which were created by extensional tectonics related to the opening of the Tyrrhenian Sea (*Calamita et al., 1994*). In detail, they consist of a valley filled with soft sedimentary deposits of alluvial origin dominated by hills consisting of consolidated soil. All these sites are well known and have been widely studied during the
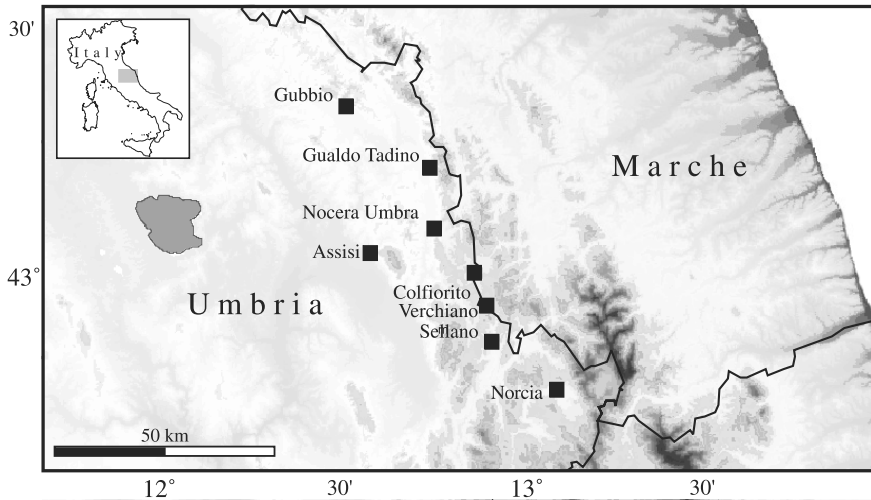
Fig. 1. Map of the area where the sites of the present study are located. Redrawn from *Marra et al. (2000).*

1997 Umbria-Marche seismic sequence (see *Gaffet et al., 2000*; *Caserta et al., 2000*; *Rovelli et al., 2001*, among others). Each site consists of three different prototypical zones of different geological structures: (A) an unconsolidated soil-alluvial deposit; (C) a firm soil-marl sandstone; and (B) a transition -colluvial and debris deposit (Fig. 2).

Seismic noise measurements were performed using a portable seismic station, a Marslite digital recorder equipped with a 3D, 5-second seismometer (Lennartz LE-3D/5s). Data were collected at a sampling frequency of 256 Hz. The instrument response of the seismometer is flat in the range 0.2−40 Hz. Moreover, the Marslite digital recorder spectrum is flat in the range 10 mHz−10 kHz (see the technical section at the website *http://www.lennartz-electronic.de/MamboV4.5.2/index.php*). Based on these technical characteristics we limited our study to periods from 1 s to 0.028 s.

In each site we collected more than one time record at each prototypical zone (see Table 1). A 5-minute time series characterized by the least variance, was selected for each record to deal with stationary time windows only. As a matter of fact a local noise source (like cars, trains, etc.) produces bumps and/or spikes in the signal that might hide the scale-invariance properties of the noise free-field.

Furthermore, because both seismic sensors and digitizers can affect the recorded signal with their own noise, we checked that the observed signal amplitude exceeds the instrumental electronic noise. The comparison between measured and electronic noise showed that the latter is much smaller, by almost 20 dB, than the former in the range of frequencies under study, i.e., 1−40 Hz. This ensure that the records have physical content. Moreover, we note that the electronic noise spectrum is flat (white noise) over the entire range of investigated frequencies.

Last, but not least, because a seismic sensor couples differently with different types of media and to be sure that the sensor was precisely moving with the soil, we adopted all the
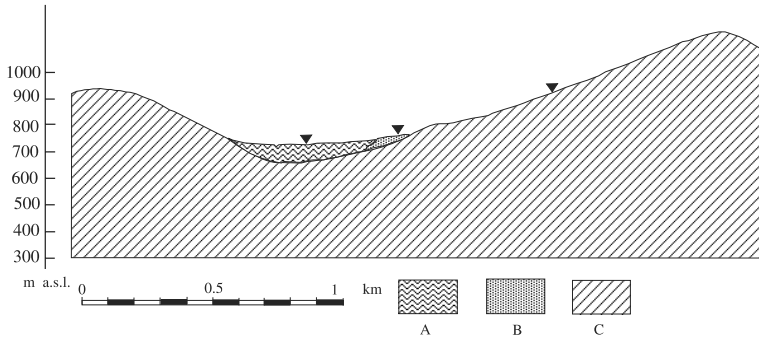
Fig. 2. Geological setting common to all three sites investigated. The three prototypical zones are also shown. The black triangles are seismic stations. Redrawn from *Gaffet et al. (2000)*.

recommendations listed in the SESAME Deliverable WP12 D23.12 (2004; available at the web site *http://sesame-fp5.obs.ujf-grenoble.fr/SES-TechnicalDoc.htm*). Where it is needed, we dig a hole to realize better soil-sensor coupling.

Since the observables are particle velocities, we computed the three dimensional (3D) soil displacement vector by simply integrating the measurements:

$$x_i(t) = \int_0^t v_i(t')\,\mathrm{d}t', \tag{1}$$

where x_i and v_i are the *i*-th component of the ground displacement and velocity, respectively. Fig. 3 shows the behavior of the 3D soil motion in the case of two different records in Verchiano, V1 and V5 (see Table 1), relative to different geological prototypes (A and C, respectively). Note the different behavior of the short time-scale motion. The higher roughness of the trajectory in the case of unconsolidated soil (V1 in Fig. 3) suggests a different diffusive nature of soil displacement in alluvial deposits with respect to firm soil.

To quantify such differences in roughness, we investigate the fractal nature of the 3D soil motion. Although the standard procedure for investigating fractal properties of time series is to look at the power spectrum features, this method is often biased by artefacts when we are interested in determining the spectral exponent (*Hergarten, 2002*). To overcome such difficulties we use the well-known variogram analysis (*Matheron, 1963*) that is less affected by artefacts (*Hergarten, 2002*).The variogram, $\Gamma(\tau)$, of a stochastic process *f(t)* is defined as the following expected value (*Hergarten, 2002*)

$$\Gamma(\tau) = E\big(f(t+\tau) - f(t)\big)^2,$$

where *E* indicates the expectation value. Thus, $\Gamma(\tau)$ can be seen as the generalization of variance $\sigma^2(t) = E\big(f(t)\big)^2$ for stochastic functions that do not satisfy the condition $f(0) = 0$. The variogram quantifies the dependence of the variance $\sigma^2(t)$ on time *t*, and can be thought as a generalization of the standard study of Brownian motion, which is the

258

Table 1.   Summary of the main features of data samples. A, B and C identify the geological prototype (see Fig. 2). $\alpha \pm$ its standard deviation, and ΔT are the scaling exponent and the fitting time interval, respectively.

Sample	Site	Geological Prototype	α	ΔT [s]
V1	Verchiano	A	1.71 ± 0.01	$0.028 \div 1.000$
V2	Verchiano	B	1.82 ± 0.01	$0.028 \div 1.000$
V3	Verchiano	C	1.89 ± 0.01	$0.028 \div 1.000$
V4	Verchiano	C	1.93 ± 0.01	$0.028 \div 1.000$
V5	Verchiano	C	1.93 ± 0.01	$0.028 \div 1.000$
V6	Verchiano	C	1.91 ± 0.01	$0.028 \div 1.000$
N1	Nocera	A	1.73 ± 0.02	$0.096 \div 1.000$
N2	Nocera	B	1.88 ± 0.01	$0.028 \div 1.000$
N3	Nocera	C	1.95 ± 0.01	$0.028 \div 1.000$
N4	Nocera	C	1.89 ± 0.01	$0.128 \div 1.000$
N5	Nocera	C	1.88 ± 0.01	$0.028 \div 1.000$
C1	Colfiorito	A	1.78 ± 0.01	$0.028 \div 1.000$
C2	Colfiorito	A	1.59 ± 0.01	$0.028 \div 1.000$
C3	Colfiorito	C	1.93 ± 0.01	$0.028 \div 1.000$

simplest example of a random scale-invariant motion (random fractal). In other words, the variogram quantifies the temporal correlation that describes how the probability density spreads through time.

In geostatistics, the semivariogram $\gamma(\tau) = \frac{1}{2}\Gamma(\tau)$ is more popular than the variogram (*Turcotte, 1997*), but the difference is nothing more than a factor two. We adopt the variogram because we do not see any reason, neither statistical nor physical, to prefer the semivariogram in the present work.

Geophysical studies generally deals with velocity, which is the correct quantity to investigate or estimate the diffusion coefficient of the stochastic process under study (*Risken, 1989*). Anyway, because the main target of this work is to check the existence of time-correlations and scaling invariance in the noise field, and to discuss these features in connection with wave diffusion and transport, we analyze the ground displacement instead of velocity. Moreover, we consider the 3D soil displacement instead of its three components because we are interested in studying the global soil motion under the effect of seismic noise; considering and comparing the motion in each component separately (H/V spectral ratio, etc.), could be done in a next paper.

Within such a framework it is natural to generalize the variogram analysis to the 3D case by evaluating the expectation value of the squared soil displacement $E\left(r^2(\tau)\right) \equiv \left\langle r^2(\tau) \right\rangle$, which has been defined according to the following expression:

$$\left\langle r^2(\tau) \right\rangle = \left\langle \sum_{i=x,y,z} \left[x_i(t+\tau) - x_i(t) \right]^2 \right\rangle \tag{2}$$

as a function of the τ in the period temporal range from 0.028 s to 1 s. Here, $\langle \cdot \rangle$ indicates time averaging. Note that the use of definition (2) for the average soil displacement, instead of the average time differences of the magnitude of the vector displacement, retains the additional information on angular variations.

In the case of a scale-invariant motion the average squared displacement is expected to scale with the time delay τ as follows (*Hergarten, 2002*):

$$\left\langle r^2 (\tau) \right\rangle \propto \tau^\alpha, \tag{3}$$

where for a simple Brownian motion $\alpha = 1$. If $\alpha \neq 1$, the process may be sub-diffusive ($\alpha < 1$) or super-diffusive ($\alpha > 1$), i.e., representing anti-persistent or persistent motion (*Hergarten, 2002*). We recall that $\alpha = 2$ represents ballistic motion (e.g., $x(t) = vt$) (*Sornette, 2000*). Furthermore, the scaling exponent α is directly related to the well-known Hurst exponent H by the relation

$$\alpha = 2H . \tag{4}$$

Fig. 4 shows the behavior of $\left\langle r^2 (\tau) \right\rangle$ as a function of τ for three samples representing the different geological prototypes (see Table 1) investigated in our work. The average square soil displacement follows a power-law $\left\langle r^2 (\tau) \right\rangle \sim \tau^\alpha$, characterized by an exponent $\alpha > 1$. This is a common feature in all the sites investigated here and it is evidence of self-similarity of the soil motion in the studied time interval (*Mandelbrot,*
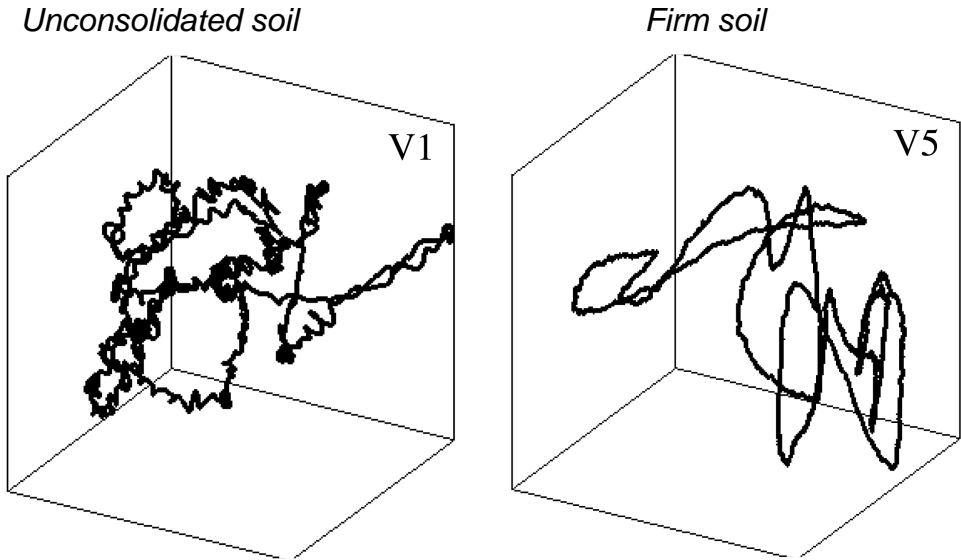
Unconsolidated soil   *Firm soil*

Fig. 3. The 3D soil motion as reconstructed by means of Eq.(1) in the case of two different records (V1 and V5 in Table 1).

1983; Sornette, 2000). The occurrence of self-similarity in the soil motion might be read as the signature of a scale-invariance in the noise-field, at least in the range of scales investigated. As a matter of fact, as the soil motion is a proxy of the noise field, we can link the soil motion features to those of the noise field. The observed self-similarity seems to be a common feature of the stationary part of the noise, although different sites are characterized by different scaling exponents. Furthermore, as our measurements have not been recorded simultaneously, this self-similarity property can be considered to be time-independent.

The observed scaling exponents α $(\alpha > 1)$ allow us to conclude that the soil motion (soil shaking) in the investigated range of scale appears to be more persistent than a simple Brownian motion. The main feature of the ground motion under the action of the seismic noise-field is that of a correlated random motion; in other words, we deal with a process with a memory longer than the Brownian one, i.e., a sort of super-diffusive process (*Hergarten, 2002*). However, in order to avoid misunderstanding the use of the term "diffusive", it is necessary to remark that our results do not deal with a real diffusion of the soil, but conversely with a soil-shaking motion which is the result of a wave-field diffusion.

Another relevant result that emerges from our analysis is that the scaling exponents α (as reported in Table 1) suggests a dependence of the diffusive properties on the near-surface geology. To better highlight whether the dependence exists or not, we have
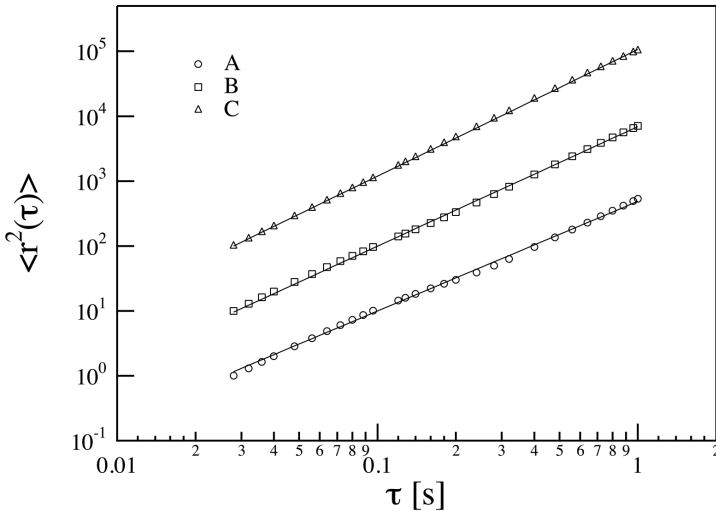

Fig. 4.   The behavior of the average squared soil displacement $\left\langle r^2(\tau) \right\rangle$ as a function of the timescale τ for three different samples representing each of the three different geological prototypes as reported in the legend. Light dots, squares and triangles refer to samples V1, N2 and N3, respectively (see Table 1). Solid lines are power-law best fits. Plots are scaled by factors 1, 10 and 100 for convenience.

Table 2. The average scaling exponent $\langle\alpha\rangle$ for the 3 geological prototypes. The error is the standard deviation.

Geological Prototype	$\langle\alpha\rangle$
A	1.70 ± 0.08
B	1.85 ± 0.01
C	1.91 ± 0.03

evaluated the average scaling exponent $\langle\alpha\rangle$ for the three different geological prototypes (Table 2). Different geological prototypes seem to be characterized by similar but clearly distinct values of $\langle\alpha\rangle$; i.e., the fractal features of the soil motion due to seismic noise seems to depend on the nature of the near-surface geology. Moreover, while the soil motion in the firm soil zones (C) tends to be ballistic ($\langle\alpha\rangle \sim 2$), in the soft unconsolidated soil zones (A) it has a more diffusive character ($\langle\alpha\rangle < 2$). Here, the term ballistic refers to a motion where the walker moves with a given velocity instead of randomly hopping at each time (*Sornette, 2000*).

In looking at Table 2 it is clear that different soils correspond to different and clearly distinct numerical values (numerical inconsistency) of the scaling exponent. This means that, if we add to each numerical value its own error, no overlapping of the numerical values of α is observed. As a consequence, we can conclude that the more the soil is consolidated, the more the behavior of the soil motion is super-diffusive. This property is also evident from the roughness of the 3D motion shown in Fig. 3.

We believe that differences observed in the self-similarity property could arise from the effects of different dynamical properties and/or structural heterogeneity (e.g., local small-scale inhomogeneities and/or a randomness of soil properties in the first hundreds of meters) of the soil layers near the Earth's surface. As a matter of fact, it has been well established that irregular changes of the soil structure in the form of inhomogeneities affect the ground motion (*Safak, 2001*; *Manolis, 2002*).

Information concerning $\langle r^2(\tau)\rangle$ is not enough to characterize the ground motion behavior. Information about its fluctuations is also needed. Thus, in order to better characterize the nature of the ground motion, we analyzed the probability distribution function (PDF) of the displacement fluctuations.

Fig. 5 shows the normalized PDFs of the displacement fluctuations at the smallest scale investigated ($\tau = 0.028$ s) for the three examples of geological prototypes reported in Fig. 4. For each example the PDF has been averaged over the three components. The shape of the PDFs agrees with a Gaussian distribution, thus suggesting that the observed statistical self-similarity is analogous to that of fractional Brownian motion (fBm). It is important at this point to stress that because the observed PDFs are nearly Gaussian at the smallest scale here investigated, in virtue of the Central Limit Theorem, these PDFs are expected to be Gaussian at all time scales.
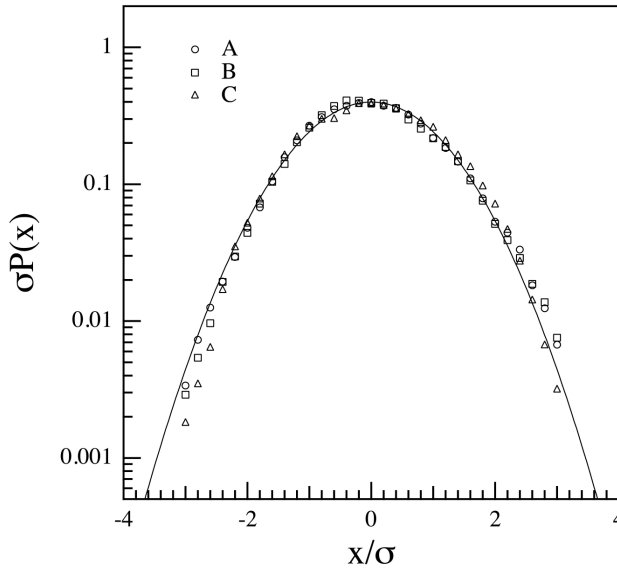
Fig. 5. The normalized PDFs of displacement fluctuations at the smallest time scale here investigated ($\tau = 0.028$) for the same samples reported in Fig. 4. Solid line is a Gaussian distribution with unit variance for comparison.

To elucidate the meaning of fractional Brownian motion, we simulated long range correlated random 3D signals characterized by different values of the scaling exponent α, using the successive random additions method as described by *Mandelbrot (1983)*. In order to take into account three different dynamics (sub-diffusive, diffusive (Brownian) and super-diffusive), different values of the scaling exponent α (0.4, 1, and 1.6) have been considered.

Fig. 6 shows the obtained results. Although self-similar signals (Fig. 6) clearly display scaling features for the average squared displacement $\left\langle r^2(\tau) \right\rangle$ but with different degree of Markovian character (memory), the PDF of the fluctuations for all three simulated time series (Fig. 6. Inset) are in agreement with a Gaussian distribution as it is expected for a fBm (*Hergarten, 2002*). The result of the 3D numerical simulation points towards a fBm nature of the soil motion (shaking).

3. DISCUSSION AND CONCLUSIONS

In this paper we have presented a summary of experimental observations, data analysis and numerical simulations dealing with the self-similarity features of seismic noise. In summary, the 3D average squared soil displacement $\left\langle r^2(\tau) \right\rangle$, and the PDF of the displacement fluctuations suggest the nature of the noise-field soil motion to be analogous to that of a persistent fractional Brownian motion ($\alpha > 1$). Moreover, a dependence of the
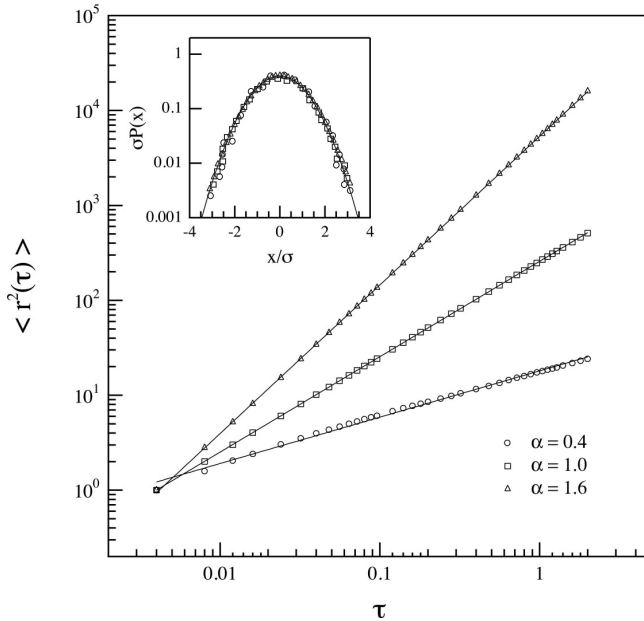
Fig. 6. The average squared displacement $\left\langle r^2(\tau) \right\rangle$ versus τ for three simulated 3D fBm characterized by different scaling exponents (α = 0.4, 1.0 and 1.6), and the normalized PDF of the small scale fluctuations relative to the 3D fBm with α = 1.6 in comparison with a Gaussian distribution - inset. Solid lines are power-law best fits.

scaling exponent α (i.e. Hurst exponent H) on the geological nature of the site has been found. In detail, while for a consolidated soil zone the seismic noise has a nearly ballistic character ($\alpha \sim 2$), for unconsolidated soil zones the motion tends to be more diffusive ($1 < \alpha < 2$). To summarize, we have found that:

- seismic noise is neither a White nor Brownian stochastic processes;
- it is a self-similar (or fractal) stochastic signal that can be described in terms of persistent fBm ($\alpha > 1$). Persistency means a process with a memory longer than the Brownian motion, as it is in the case of super-diffusive stochastic processes;
- a dependence of statistical features of the soil motion on the geological nature of the site seems to exist;
- we obtain these results without any a priori hypothesis neither on the noise field nor on its spectrum. It is worth noting that White and Brownian processes are just particular cases of a more general stochastic process, named the fractional Brownian motion (*Hergarten, 2002*).

Regarding the observed dependence of the soil motion self-similarity on the near-surface geology, although we cannot exclude that some of the observed differences might arise from factors like wave focusing, basin geometry and topography, our feeling is that our results could be better understood in terms of transport of seismic radiation in random

media (*Zhang et al., 1999*; *Jia, 2004*), i.e., in terms of strong nonlinearity and randomness of soil media. As a matter of fact, assuming that the nature of the seismic noise source of the different sites is statistically the same, the observed differences should be due to a different degree of dynamical behavior and/or structural heterogeneity of the geological prototypes. In other words, differences in the structural heterogeneity would produce differences in the multiple scattering of the seismic noise-field, changing the character of the motion from nearly ballistic to diffusive. Recent studies have clearly shown that the effects of randomness on seismic wave transport may be treated in terms of nonlinearity involving scaling and dispersion in the soil motions, and that the soil stochasticity must be considered to describe the motion at high frequencies, i.e., $f > 1$ Hz (*O'Connell, 1999*; *Manolis, 2002*; *Larose et al., 2004*; *Grêt et al., 2006*).

To better assess the seismic radiation transport process in the noise-field, a link between the determistic (wave) and stochastic (diffusive) description must be found. In our opinion such a link should be in the transition, of the energy propagation process, from the diffusive to the wave regime (and vice versa). Such studies can not be done using records from a single station, as in the present paper, but from arrays of seismic stations. We emphasize that our dataset comes from records at three different geographical sites only: Verchiano valley, Colfiorito plain and Nocera Umbra site. They are located in Italy in the same tectonic zone: Northern Appennine arc. Another important point is that we have analyzed records of 5 minute-length only without making any distinction between day and night. Indeed, seismic noise could be affected by night and day variations mainly due to human activity (see, among others, *Mc Namara and Bouland, 2004*). For these reasons our results must be considered as preliminary.

The analysis of the afore-mentioned transition in the dynamical behavior of the energy propagation process and a data analysis on a wider dataset including differences between night and day will be the topic of forthcoming papers.

References

Bard P.-Y., 1999. Microtremor measurements: A tool for site effects estimation? In: K. Irikura, K. Kudo, H. Okada and T. Sasatani (Eds.), *Effects of Surface Geology on Seismic Motion*, Balkema, Rotterdam, The Netherlands, 1251−1279.

Calamita F., Cello G., Delana G. and Paltrineri W., 1994. Structural styles, chronology rates of the fluctuations, and time-space relationships in Umbri-Marche trust system (Central Appennines -Italy). *Tectonics*, **13**, 873−881.

Campillo M. and Paul A., 2003. Long-range correlations in the diffuse seismic coda. *Science*, **299**, 547−549.

Caserta A., Bellucci F., Cultrera G., Donati S., Marra F., Mele G., Palombo B. and Rovelli A., 2000. Study of site effects in the area of Nocera Umbra (Central Italy) during the 1997 Umbria-Marche seismic sequence. *J. Seismol.*, **4**, 555−565.

Gaffet S., Cultrera G., Dietrich M., Corboulex F., Marra F., Bouchon M., Caserta A., Cornou C., Deschamps A., Glot J.P. and Guiguet R., 2000. A site effect study in Verchiano Valley during the 1997 Umbria-Marche (Central Italy) earthquakes. *J. Seismol.*, **4**, 525−541.

Grêt A., Sneider R. and Scales J., 2006. Time-lapse monitoring of rock properties with coda wave interferomtery. *J. Gephys. Res.*, **111**, B03305.

Hergarten S., 2002. *Self-Organized Criticality in Earth Systems*. Springer Verlag, Berlin, Heidelberg.

Jia X., 2004. Codalike multiple scattering of elastic waves in dense granular media. *Phys. Rev. Lett.*, **93**, 154303.

Lachet C. and Bard P.-Y., 1994. Numerical and theoretical investigations on the possibilities and limitations of Nakamura's technique. *J. Phys. Earth.*, **42**, 377−397.

Larose E., Margerin L., van Tiggelen B.A. and Campillo M., 2004. Weak localization of seismic waves. *Phys. Rev. Lett.*, **93**, 048501.

Mac Namara D.E. and Buland R.P., 2004. Ambient noise levels in the continental United States. *Bull. Seismol. Soc. Amer.*, **94**, 1517−15277.

Mandelbrot B.B., 1983. *The Fractal Geometry of Nature*. W.H. Freeman, New York.

Manolis G.D., 2002. Stochastic soil dynamics. *Soil Dyn. Earthq. Eng.*, **22**, 3−15.

Matheron G., 1963. Principles of geostatistics. *Econ. Geol.*, **58**, 1246−1258.

O'Connell D.R.H., 1999. Replication of apparent nonlinear seismic response with linear wave propagation models. *Science*, **283**, 2045−2050.

Risken H., 1989. *The Fokker-Plank Equation. Methods of Solution and Applications*. Springer-Verlag, Berlin; New York.

Rovelli A., Scognamiglio L., Marra F. and Caserta A., 2001. Edge-diffracted 1-sec surface waves observed in a small-size intramountain basin (Colfiorito central Italy). *Bull. Seismol. Soc. Amer.*, **91**, 1851−1866.

Safak E., 2001. Local site effects and dynamic soil behavior. *Soil Dyn. Earthq. Eng*., **21**, 453−461.

Shapiro N.M. and Campillo M., 2004. Emergence of broadband Rayleigh waves from correlations of the ambient seismic noise. *Geophys. Res. Lett.*, **31**, L07614.

Sheng P., 1990. *Scattering and Localization of Classical Waves in Random Media*. World Scientific Publ. Co., Singapore.

Sheng P., 2006. *Introduction to Wave Scattering Localization and Mesoscopic Phenomena*. Springer Verlag, Berlin, Heidelberg.

Sornette D., 2000. *Critical Phenomena in Natural Sciences*. Springer Verlag, Berlin, Heidelberg.

van Tiggelen B.A., 2003. Green function retrieval and time reversal in a disordered world. *Phys. Rev. Lett.*, **91**, 243904.

Turcotte D.L., 1997. *Fractals and Chaos in Geology and Geophysics*. Cambridge University Press, New York.

Wathelet M., Jongmans D. and Ohrnberger M., 2004. Surface wave inversion using a direct search algorithm and its application to ambient vibration measurements. *Near Surface Geophysics*, **2**, 211-221.

Wathelet M., Jongmans D. and Ohrnberger M., 2005. Direct inversion of spatial autocorrelation curves with the Neighborhood algorithm. *Bull. Seismol. Soc. Amer.*, **95**, 1787−1800.

Zhang Z.Q., Jones L.P., Schriemer H.P., Page J.H., Weitz D.A. and Sheng P., 1999. Wave transport in random media: The ballistic to diffusive transition. *Phys. Rev. E*, **60**, 4843−4840.

Static and dynamic characterization of alluvial deposits in the Tiber River Valley: New data for assessing potential ground motion in the City of Rome

F. Bozzano,[1] A. Caserta,[2,3] A. Govoni,[4] F. Marra,[2] and S. Martino[1]

[1]   The paper presents the results of a case study conducted on the Holocene alluvial deposits of the Tiber River valley, in the city of Rome. The main test site selected for the study, Valco S. Paolo, is located about 2 km South of Rome's historical centre. The alluvial deposits were dynamically characterized in a comprehensive way via site investigations and geotechnical laboratory tests. Normalized shear modulus decay and damping curves (G/G_0 and D/D_0 vs γ) were obtained for the dominantly fine-grained levels. The curves demonstrate that these levels have a more marked shear stiffness decay if compared with the underlying Pliocene bedrock. Decay curves from laboratory tests for the Tiber alluvia correlated well with the trend of the function proposed by Hardin and Drnevich, making it possible to derive their specific interpolation function coefficients. Use was made of the extrapolation of the findings from the Valco S. Paolo test site to a large part of Rome's historical centre by means of two other test sites, supported by an engineering-geology model of the complex spatial distribution of the Tiber alluvia. The experimental Valco S. Paolo Vs profile was extrapolated to the other test sites on the basis of a stratigraphic criterion; the analysis of seismic noise measurements, obtained for the three test sites, validated the engineering-geology based extrapolation and showed that the main rigidity contrast occurs inside the alluvial body (at the contact with the underlying basal gravel-level G) and not between the alluvia and the Plio-Pleistocene bedrock, composed of highly consistent clay (Marne Vaticane). The 1D modeling of local seismic response to the maximum expected earthquakes in the city of Rome confirms that the deposits have one principal mode of vibration at about 1 Hz. However, the simulation also evidenced that the silty-clay deposits (level C), making up the most part of the Tiber alluvial body, play a key role in characterizing the soil column deformation profile since it can be affected by non linear effects induced by the maximum expected earthquake when some stratigraphic conditions are satisfied.

1.   Introduction

[2]   Assessment of potential strong ground motion within the city of Rome is crucial to preserving its millenary monumental heritage and protecting its large urban settlements. Rome is located at a distance of some tens of kilometers from the central Apennines seismogenic zone, where earthquakes of tectonic origin and of a magnitude of up to 7.0 can be expected. The most recent of these major earthquakes took place in 1915 near Avezzano, 100 km NE of Rome and caused severe damage to the city of Rome [*Ambrosini et al.*, 1986]. Even smaller and local earthquakes (in 1812 and 1895) induced damage to the architectural heritage, including collapse of a small portion of the southern arcade of the Colosseum [*Molin and Guidoboni*, 1989]. A study by *Ambrosini et al.* [1986] reported that the 1915 earthquake caused the most severe damage to buildings located on the Holocene alluvial fill of the Tiber valley (Figure 1), thereby stressing the role of local geology in amplifying ground shaking. Similarly, *Boschi et al.* [1995] and *Funiciello et al.* [1995] showed the close relationship that exists between selective damage to monuments, such as the Antonina Column and the Colosseum, and occurrence of soft alluvial sediments underneath. Since then, several studies have been conducted to quantify the expected site

[1]Università di Roma "La Sapienza" - Dipartimento di Scienze della Terra, Rome, Italy.
[2]Instituto Nazionale di Geofisica e Vulcanologia, Rome, Italy.
[3]Charles University, Faculty of Mathematics and Physics, Prague, Czech Republic.
[4]Instituto Nazionale di Oceanografia e di Geofisica Sperimentale-OGS, Udine, Italy.

Figure 1. Tiber valley near the city of Rome: the dashed line marks the boundary of the recent alluvia of the Tiber River and of its tributaries; the two boxes identify the areas of Rome's historical center (A) (Figures 2 and 3) and of Valco S. Paolo (B) (Figure 4).

effects within the city of Rome, including simulations via the finite-difference technique applied to 2D models [*Rovelli et al.*, 1994, 1995], as well as a hybrid technique based on mode summation and finite differences [*Fäh et al.*, 1993]. However, all these studies relied on theoretical values from the scientific literature for the elastic and inelastic properties of geological materials and were not supported by *in situ* measurements and specific engineering-geology studies for the city of Rome.

[3] In order to fill this gap and better understand and quantify the expected ground shaking within the city of Rome, a multidisciplinary research project was carried on and a detailed analysis was made of the physical and mechanical properties of the different lithotypes constituting the recent sedimentary fill of the Holocene Tiber River valley, as well as the corresponding bedrock [*Salvi et al.*, 1991], under both static and dynamic conditions. The project involved the installation of a permanent seismic

Table 1. Historical Earthquakes Yielding I ≥ 6 in Rome

Age	I_o	I_{felt}	Epicentral Area
801	?	VII–VIII	Central Apennine
1349	X	VII–VIII	Central Apennine
1703	X	VI–VII	Central Apennine (Val Nerina)
1703	X	VII	Central Apennine (L'Aquila)
1812	VII	VII	Rome
1895	VII	VII	Rome
1899	VII–VIII	VI	Colli Albani
1909	VI	VI	Rome
1915	XI	VI–VII	Fucino Plain (Avezzano)

array and a detailed classification of the physical and mechanical properties of the rocks constituting the geological subsoil of Rome, under both static and dynamic conditions.

[4] As the dynamic behavior of recent clay deposits might disagree with the most widespread empirical relations used in numerical modeling, the dynamic properties of the Holocene alluvial deposits of the Tiber River, identified in this study, were compared with the results obtained by other authors [*Carrubba and Maugeri*, 1988; *Crespellani et al.*, 2001; *Lo Presti et al.*, 2002] for different Holocene Italian deposits.

[5] This paper deals with the results of on-site geophysical investigations and laboratory tests and the related effects on the assessment of potential ground motion in the city area; 1D numerical models of local seismic response to possible strong motion (PGA of up to 0.06 g) in the city of Rome were built. These models highlight the important role that an up to 50-m-thick silty-clay level inside the Tiber alluvia can play in terms of ground motion effects.

2. Seismicity of the Area of Rome

[6] The millenary history of Rome has extensive records of felt earthquakes. A detailed study of historical sources allowed *Molin and Guidoboni* [1989] to produce a catalogue, which was supplemented with a renewed assessment of several minor events [*Riguzzi and Tertulliani*, 1993]. On the basis of this historical record, nine events have occurred in Rome since 801 AD, yielding an $I_{felt} ≥ VI$ according to the MCS scale (Table 1). Five of these events were localized in the regional seismogenic zone of the central Apennines and caused an I_{felt} as high as VII–VIII within the city. The seismogenic sources of this regional seismicity are located as close as 60 km from Rome; they have a focal depth of about 10–15 km and can produce earthquakes of a maximum magnitude of up to 7. Smaller earthquakes, with a focal depth of ≤6 km and a maximum magnitude of 4–5, are generated in the Colli Albani hills volcanic area [*Amato et al.*, 1994], whereas local seismicity in the urban area can produce earthquakes of a maximum magnitude not exceeding 4 [*Tertulliani et al.*, 1996]. These smaller events are expected to produce a maximum $I_{felt} = VI–VII$ in Rome.

3. Geological Setting

[7] The area of Rome was characterized by marine sedimentary conditions from Pliocene through early Pleistocene times (4.5-1.0 Myr). In this period, a thick (>1,000 m) succession of sediments (Monte Vaticano Unit [*Marra and Rosa*, 1995]) was deposited. This Plio-Pleistocene succes-

sion consists of alternating, decimeter-thick levels of clay and sand, with an overconsolidation ratio (OCR) of >5 and low compressibility [*Bozzano et al.*, 1997].

[8] Subsequently, at about 0.9 Myr, a delta of the palaeo-Tiber delta developed in the area of Rome [*Karner et al.*, 2001]. During middle-late Pleistocene and Holocene times, sedimentary processes were confined to fluvial channels and coastal plains and strongly controlled by glacio-eustatic sea-level changes [*Karner and Renne*, 1998; *Karner and Marra*, 1998; *Marra et al.*, 1998]. In the same time interval, the region also experienced strong volcanic activity, causing the emplacement of a thick pyroclastic cover that became intercalated into the continental sedimentary deposits.

[9] The present-day hydrographic network of the Tiber valley and its tributaries originated during the Würm glacial (18 ka) through re-incision and deepening of the valleys which had developed during previous glacial-interglacial phases. During the latest glacial, the combination of sea-level fall (more than 120 m, *Bard et al.*, 1996) with regional uplift (about 20 m [*Hearty and Dai-Pra*, 1986; *Bordoni and Valensise*, 1998]) caused deep erosion of Rome's fluvial valleys, also cutting their Pliocene bedrock down to 60 m below the present sea level [*Marra and Rosa*, 1995]. The return of temperate climate conditions melted the glaciers in the northern hemisphere and the sea level rose in a relatively fast way, filling the fluvial incisions up to the present level of deposition. The sediments filling the Holocene incisions are generally characterized by a fining-upward succession, with a relatively thin level of gravel at the base grading into a thick pack of sand and clay [*Bozzano et al.*, 2000]. This fine-grained portion of the deposit is represented by normally to weakly overconsolidated clay-sandy silt, saturated in water, with low deformability moduli [*Bozzano et al.*, 2000].

4. Engineering-Geology Characterization of the Main Alluvial Body of the Tiber River in the Area of Rome

[10] The paper reports new engineering-geology data collected at the Valco S. Paolo test site. The site was selected on the basis of technical and locational considerations. The data were extrapolated, under geological criteria, to the entire alluvial body making up the subsoil of the most part of the city of Rome. These criteria refer to new geological and stratigraphic data on the Roman subsoil which derive from an original collection and interpretation of data from geognostic investigations; these investigations were conducted as part of the project for construction of a new line of Rome's underground transportation.

[11] Beside a 5.5 km-long section previously reconstructed by means of 57 boreholes [*Bozzano et al.*, 2000], the paper presents two new stratigraphic sections. These sections were reconstructed using 58 new boreholes drilled at depth of 10–65 m below ground level. Eight ^{14}C age determinations were also made on organic matter recovered at different depths in the alluvial sediments, in order to evaluate the history of the Tiber River depositional system.

[12] Reconstruction of the alluvial deposits shows that the Tiber palaeo-valley in Rome's historical centre has a depth from about 60 m to the North to about 70 m to the South.
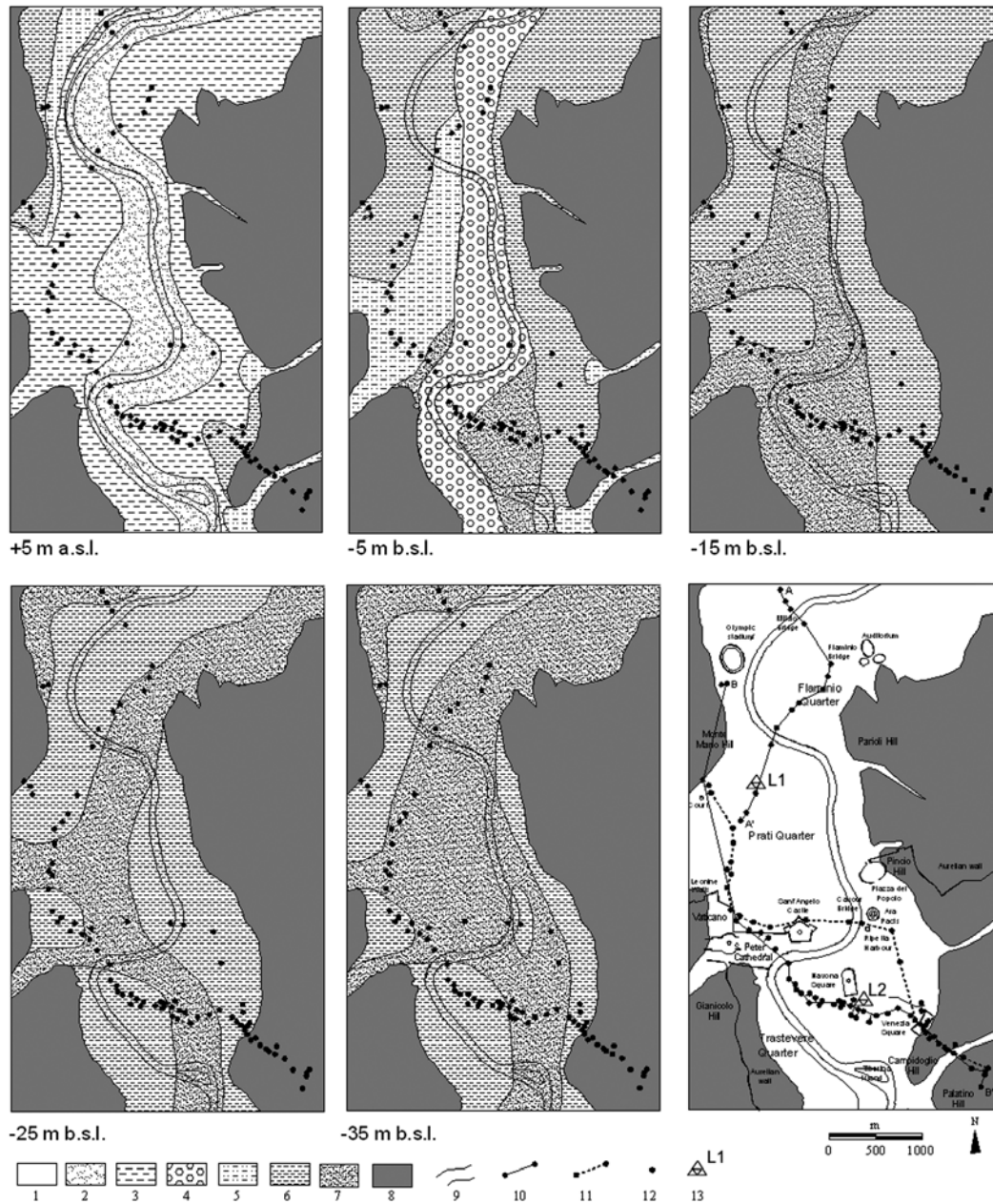
Figure 2. Distribution of alluvia in Rome's historical center at different elevations above sea level (asl): 1) Tiber alluvia; 2) level A1; 3) level A2; 4) level B1; 5) level B2; 6) level C; 7) level D; 8) Plio-Pleistocene bedrock; 9) current Tiber channel; 10) trace of section AA' along the routes of the future lines T1 and T2 of Rome's underground; 11) trace of section BB', which was built on the basis of the geognostic survey of 1996–1997; 12) boreholes; 13) seismic noise array.

The valley, which is enclosed by steep slopes, has a flat floor slightly dipping southwards (Figures 2 and 3).

[13] The Pliocene bedrock is continuously overlain by a level of gravel (level G), whose thickness ranges from roughly 8–10 m on average to a maximum of about 12m.

[14] Above is a level of sand (level D), which extends throughout the valley and is approximately 2m-thick. Above these sand, the valley is filled with about 30m-thick heteropic sandy (level D) and silty-clay (level C) deposits. The silty-clay deposits of level C are dominant at the margins of the valleys. In particular, on the right bank of

the river, both of the reconstructed sections exhibit a body C; this body, which has a maximum thickness of 30m, is frequently in heteropic contact with level D. On the left bank, the silty clay of level C display more depositional continuity and reach a maximum thickness of about 50 m (near Piazza Venezia square).

[15] Above lithotypes D and C, the alluvial deposits sharply reverse their grain size: level B1 (medium-coarse sand) near the main valley and level B2 (silty sand and clay) near the Tiber tributaries have lenticular or tabular geometries, respectively.
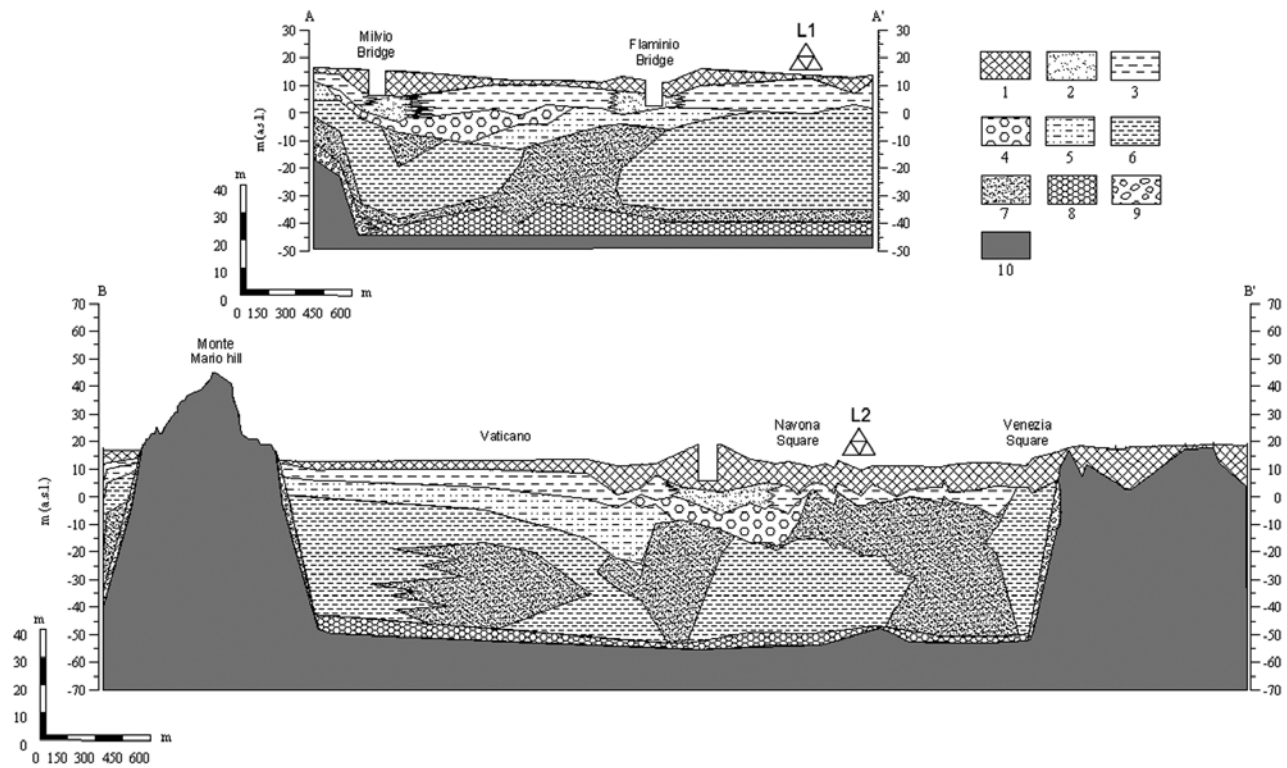
Figure 3. Geological sections in the area of Rome's historical centre; traces are shown in Figure 2. 1) man-made fills; 2) level A1; 3) level A2; 4) level B1; 5) level B2; 6) level C; 7) level D; 8) level G; 9) slope debris and/or palaeo-slope; 10) Plio-Pleistocene bedrock.

[16] The historical alluvia of the Tiber (level A) close the sedimentary succession. The grain size of these deposits is finer than the one of level B. Two facies can be distinguished: level A1 (silty sand), which follows the trend of the present Tiber channel, and level A2 (clay silt), which is depositionally more continuous on the right bank of the river, albeit present also on its left bank. The total thickness of level A and of the overlying man-made fill (level R) is comparable on both banks.

[17] By using the three geological sections (built through the deposits of the main alluvial valley of the Tiber), horizontal correlations were established at +5 m, −5 m, −15 m, −25 m and −35 m above sea level (asl), obtaining five lithotechnical maps (Figure 2). The maps show the planar distribution of the Tiber valley alluvia in Rome's historical centre (Figure 1).

[18] At +5 m asl, the deposits are likely to have an age of about 2,500 a BP, as suggested by the estimated age (2,550 ± 190 a) of a sample taken from level A, which is in agreement with the estimated age of another sample referred to the same level (2,741−2,360 a [*Bozzano et al.*, 2000]).

[19] At −5 m asl, the planar distribution of the deposits evidences a body B1 at the centre of the valley. This body extends rectilinearly towards N−S and is flanked by the deposits of level B2 on the right bank and of level C on the left bank. Two samples of organic matter collected from a borehole in level B (at −3.7 m and −7.5 m asl, respectively) yielded an age of 4,990 ± 70 and 6,060 ± 40 a BP, respectively. The deposits lying at −5 m asl were thus determined to be 6,000−5,000 a old.

[20] At −15 m asl, the deposits that may be directly ascribed to the Tiber channel are those of level D, which lies in the middle of the valley. On the right bank, two secondary bodies of level D (sided by level C everywhere) may be attributed to the streams of the Valle dell'Inferno and Gianicolo valley, respectively. A sample of organic matter collected at −12.2 m asl from a hole drilled into level C was determined to have a radiocarbon age of 7,380 ± 40 a BP. Furthermore, based on the calculated age of a peat sample collected from a hole, an age of 9,498 and 9,450 a BP was attributed to the deposits lying at −15 m asl [*Bozzano et al.*, 2000]. Overall, these deposits are assumed to have an age range of 9,500−7,500 a BP.

[21] At −25 m asl, the planar distribution of the alluvial deposits shows a markedly meandering pattern of level D inside the Tiber valley, but a reversal of the sinuosity of the palaeo-channel vs. the present one. An organic sample taken from a hole drilled at −20.5 m asl into level C gave a radiometric age of 9,140 ± 120 a; therefore, the deposits lying at −25 m are estimated to have an age of about 10,000 a BP.

[22] At −35 m asl, the depositional body supposedly belonging to level D is always dominant; however, its pattern is less markedly meandering. Basal gravel (level G), which were emplaced by the Tiber in a braided depositional system, are found beneath this level and throughout the valley. Radiometric dating inside the gravelly level a few kilometers South of Rome's historical centre yielded an age of about 14,500 a BP (G. Calzoletti, personal communication). Considering this age and the fact that the gravelly
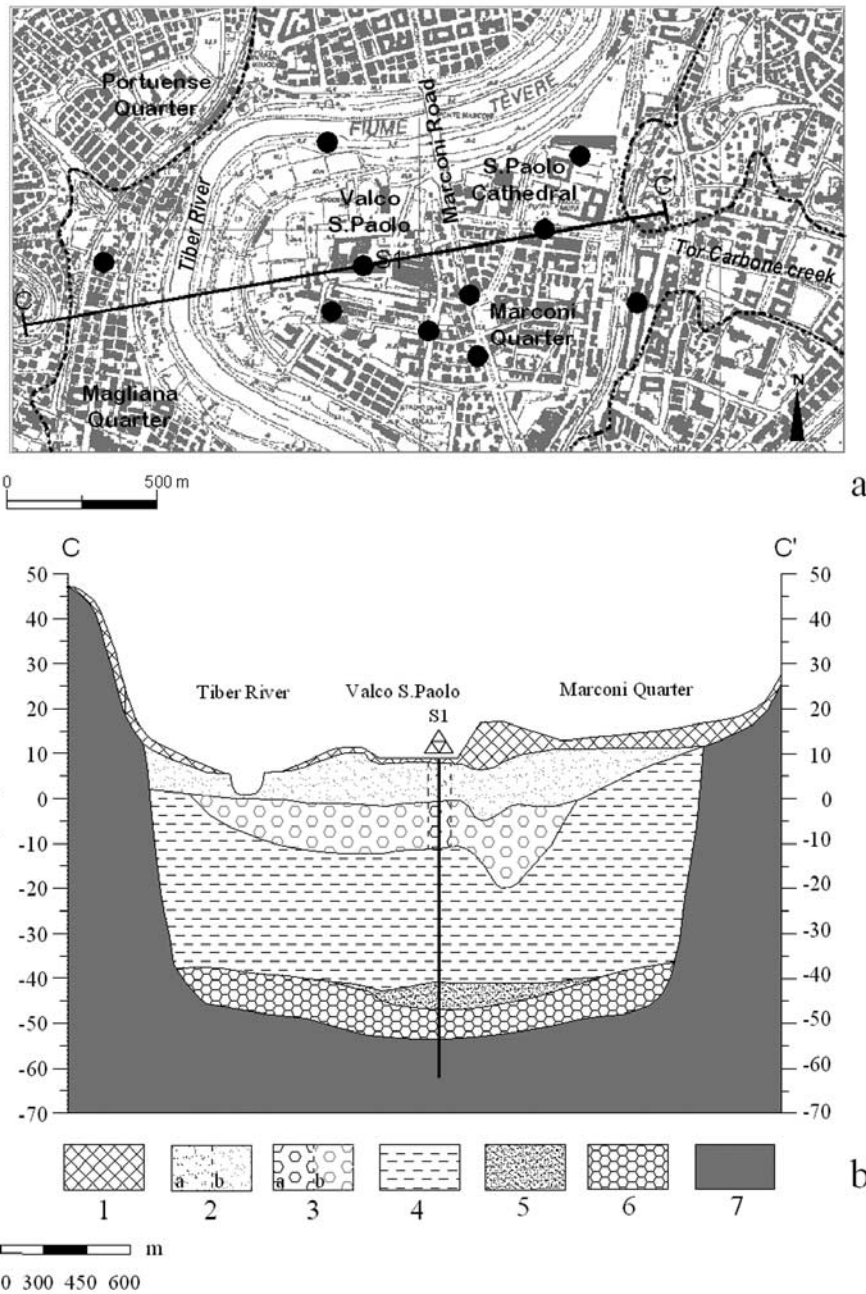
Figure 4. Geological section of the Tiber valley at Valco S.Paolo and location of hole S1. 1) man-made fills; 2) level A1 (a) and undifferentiated level A (b); 3) level B1 (a) and undifferentiated level B (b); 4) level C; 5) level D; 6) level G; 7) Plio-Pleistocene bedrock.

basal level must have been deposited in the time interval of 18,000–14,000 a BP, the deposits lying at a depth of −35 m a.s.l. may be estimated to have an age of about 13,000 a BP.

5. Static and Dynamic Engineering-Geology Characterization at the Valco S. Paolo Site

[23] Based on available literature about the Tiber alluvial body in the city of Rome, the Valco S. Paolo site may be reliably regarded as representative of the main Tiber valley in the urban area of Rome, from which it lies about 2 km away (Figures 1 and 4). The location of the site has a number of advantages, including its low urbanization.

[24] Geognostic investigations were conducted in the Autumn of 2003:

[25] a borehole was drilled at a depth of 72 m, from which both high- and low-quality soil samples were collected;

[26] on-site tests were made on core samples;

[27] down-hole tests were conducted down to 71 m;

[28] core penetration testing (CPT) with electrical cone penetrometer was made down to 45 m from ground level.
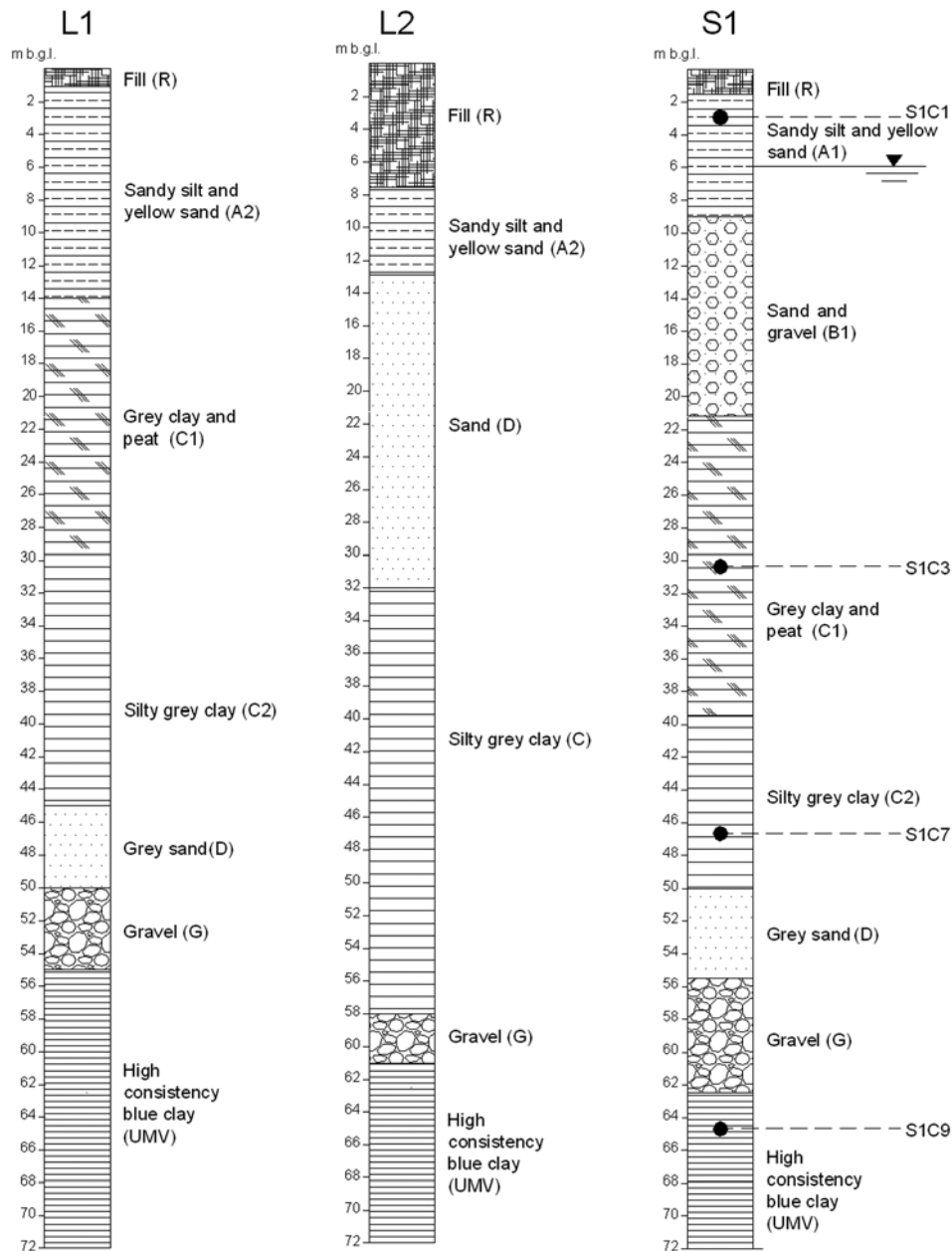
Figure 5. Stratigraphy of borehole S1 (see Figure 4), showing the points where undisturbed samples were collected, and synthetic stratigraphies of sites L1 and L2 (see Figures 2 and 3).

[29] Site tests were supported by lab tests for classifying the sampled soils and characterizing them physically and mechanically under both static and dynamic conditions.

[30] The stratigraphic succession reconstructed via the borehole (Figure 5) is similar to the one considered for the Tiber alluvia in Rome's historical centre. With reference to the lithotechnical groups distinguished by *Bozzano et al.* [1997, 2000], *Corazza et al.* [1999] and *Amorosi et al.* [2002] (the latter with another nomenclature and for the nearby historical site of ''Vasca Navale'' (naval basin-ship testing laboratory)), the reconstructed stratigraphy (S1 in Figure 5) consists of: about 1.5 m of man-made fill (level R); about 7.5 m of ''historical'' alluvia, i.e., clay silt evolving into sandy silt and into weakly silty sand with

diffuse organic matter (level A1); roughly 10 m of yellow-ish to black sand with a gravelly basal layer having millimeter-scale elements in a sandy matrix (level B1); approximately 30 m of silty clay with diffuse organic matter and scarce sandy intercalations (level C); gray sand gradu-ally passing to gravel downwards (level D); about 12.5 m of prevalently calcareous-marly gravel with heterometric cen-timeter-scale elements (level G). Starting from about 63m from ground level, this alluvial succession of Holocene age (14,000 a to present) rests, with erosional contact, on consistent clay of Pliocene age (Marne Vaticane - UMV); these marls represent the geological bedrock of the Roman area. An aquifer was encountered at 6 m from ground level.

Table 2. Undisturbed Samples Collected From Hole S1, Related Physical Characterization and Classification

Sample	z, m	γ_n, kN/m³	w, %	γ_S, kN/m³	Sand, %	Silt, %	Clay, %	w_{LL}, %	w_{PL}, %	PI, %	OCR	Cc	Group	USCS
S1C1	3,00–3,50	20.30	19.45	15.75	32	46	22	36.26	19.82	16.44	11	0.19	A1	CL
S1C3	30.00–30.50	17.20	48.66	10.72	8	52	40	61.54	27.18	34.36	1	0.55	C1	CH
S1C7	46.50–47.00	18.31	31.28	12.92	7	45	48	61.03	25.53	35.50	1	0.32	C2	CH
S1C9	64.50–64.80	20.94	20.33	16.13	8	59	33	56.27	21.75	34.52	2	0.11	UMV	CH

[31] The values of the physical properties and of the index parameters for the rock core samples collected at Valco S. Paolo (Table 2) perfectly match those reported by *Bozzano et al.* [2000], except for the grain size of level A1. Indeed, at Valco S. Paolo, the latter level is sandier than average. The average natural water content is about 45% (clay silt of level C at −25−35 m from ground level). This content stabilizes around 18% in the first 10 m of the Marne Vaticane (Figure 6).

[32] In the plasticity map, level C samples are classified as inorganic silty clay of average-high compressibility, whereas the Marne Vaticane and lithotypes A1 and D are defined as silty clay with average-low compressibility.

[33] Based on oedometer test results and similarly to what has already been observed in other sectors of the Tiber alluvial body in the city of Rome, the silty clay referable to level C are normal-consolidated, whereas level A1 clay silt are overconsolidated (OCR ≈ 10), presumably by desiccation and groundwater level fluctuations. Conversely, the Marne Vaticane (Pliocene bedrock) are overconsolidated (OCR ≈ 2), in line with their geological history.

[34] The electrical cone penetrometer resistance (qc) measured with CPT down to about 45cm from ground level (Figure 7) has values that do not exceed 6 MPa in level A1 silty sand, of about 16 MPa in level B sand and about 2 MPa in level C clay silt. The values of Fr% are close to zero inside level B1, about 2.5% in level C and above 5% in level A1. On the basis of these values and under the Douglas and Olsen classification (1981), level A1 can be classified as "fine-grained soil", level B1 as "non-cohesive coarse-grained soil" and level C as "sensitive mixed soil" (Figure 8).

[35] Four undisturbed samples collected at Valco S. Paolo were tested via resonant column (RC) and cyclical torsional shear at 1 Hz (TTC_1Hz) at the Laboratorio di Geotecnica (Politecnico di Torino) laboratory. For selecting the TTC test frequency, account was taken not only of standard procedures, but also of the results obtained by *Rovelli et al.* [1995] in previous numerical modeling of the seismic response of the main Tiber valley.

[36] The tested four samples (Figure 5) had been collected as follows: one from the historical alluvia of level A1 (3.00–3.50 m from ground level, S1C1), two from the clay silt of level C (30.00–30.50 m and 46.50–47.00 m from ground level, S1C3 and S1C7) and one from the upper portion of the Marne Vaticane (64.50–64.80 m from ground level, S1C9). The tests were carried out by confining the samples at pressures approximately equal to the vertical effective stresses of the site. These stresses were estimated at the depth of collection of the samples, based on a model
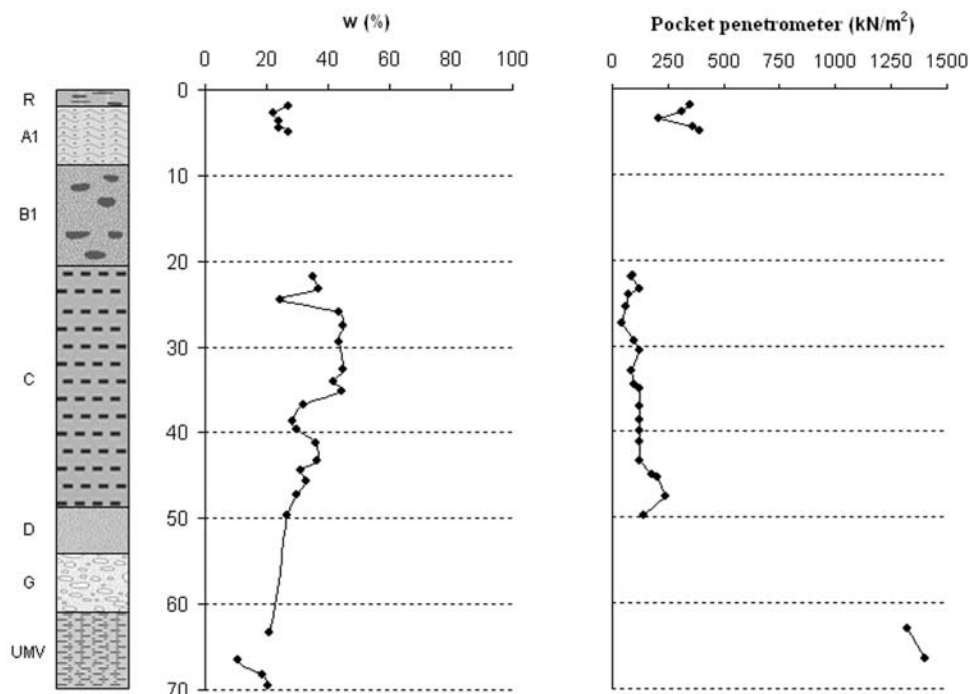
Figure 6. Variations of natural water content (w%) and of pocket penetrometer resistance vs. depth.
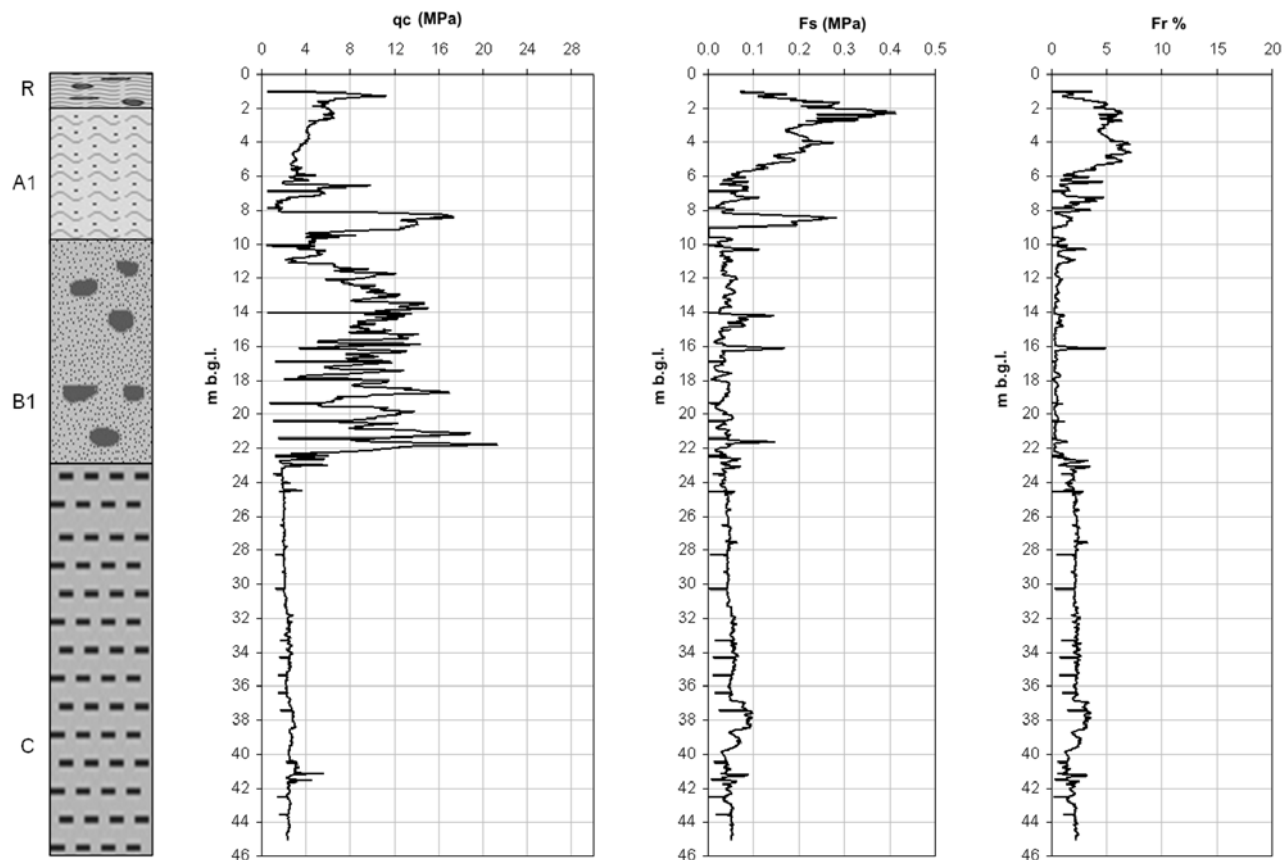
Figure 7. Values of electrical cone penetrometer resistance (qc), lateral resistance (Fs) and friction ratio (Fr%) obtained from CPT at Valco S. Paolo.

of vertical propagation of shear waves, as well as on thickness and density of individual levels and depth of the aquifer.

[37] The dynamic deformability properties of the tested samples (Figures 9 and 10) reveal a sharp distinction between the alluvial covers and the Pliocene clay bedrock, with a shear modulus difference of about 100 MPa. Conversely, the differences measured inside the alluvia are less significant and anyway in the 50–100 MPa range (Figure 9a). In the alluvia, the dynamic shear modulus differences resulting from the comparison between RC and TTC_1Hz tests are of less than 20 MPa, whereas in the Marne Vaticane they are approximately equal to 50 MPa.

[38] The measurable linearity threshold evidences deformations in the range of 0.005% for the Marne Vaticane and of 0.01%–0.02% for the alluvia (Figure 9a). The measurable plasticity threshold (Figure 10) for the alluvia ranges from 0.02% to 0.04% (samples S1C3 and S1C7). For the samples ascribable to the Marne Vaticane and to level A, such threshold cannot be measured owing to testing anomalies (see relevant portions of the decay curves $G/G_0(\gamma)$ and $\Delta u/\sigma'(\gamma)$ in Figure 10b).

[39] Generally, the normalized shear modulus decay curves (G/G_0 vs γ) proposed in the literature (V&D - [*Vucetic and Dobry*, 1991], [*Sun et al.*, 1988], I&Z – [*Ishibashi and Zhang*, 1993], [*Zhang et al.*, 2005]) are not in agreement with the laboratory results reported here
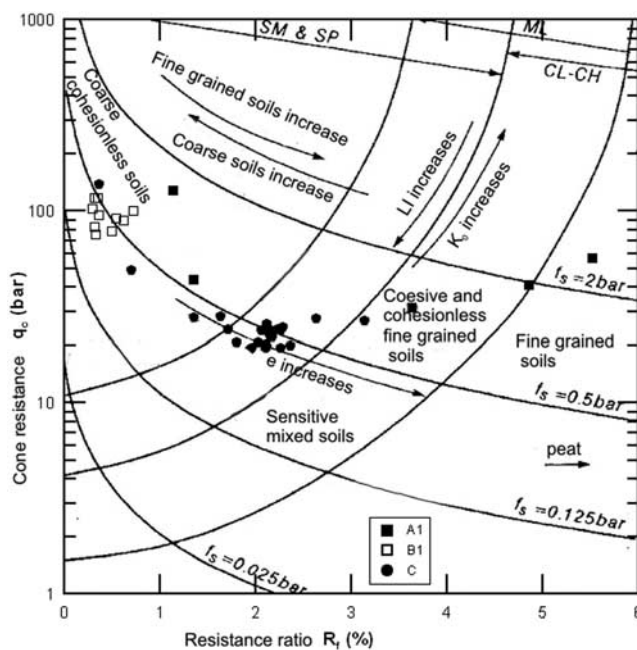

Figure 8. Douglas and Olsen (1981) classification applied to the soils crossed by the electrical cone penetrometer at the Valco S. Paolo site.
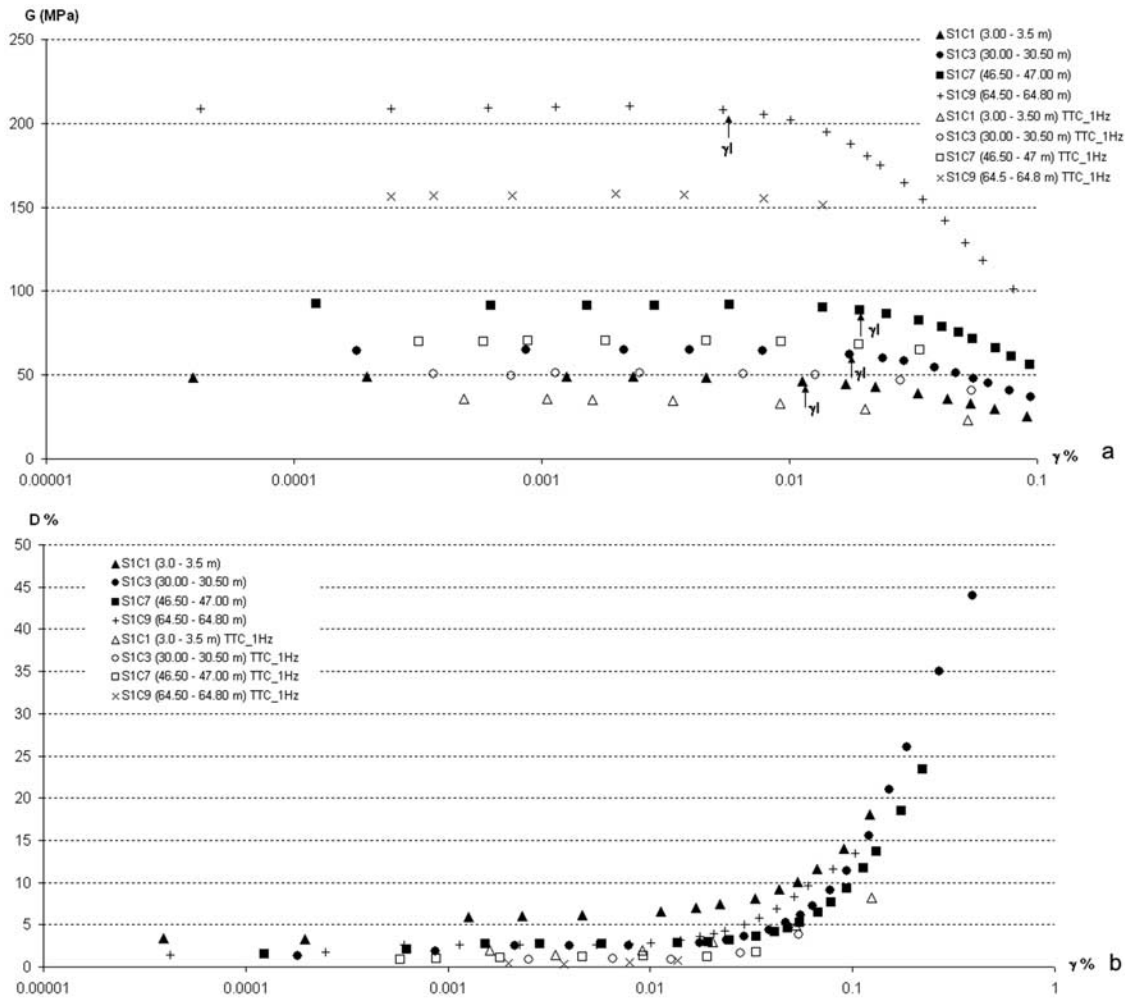
Figure 9. Decay curves $G/G_0(\gamma)$ (a) and damping curves $D/D_0(\gamma)$ (b) obtained for undisturbed samples collected from the Valco S.Paolo borehole and undergoing resonant column (RC) tests and cyclical torsional shear (TTC) tests at 1 Hz; the position of the linearity thresholds γ_l is shown.

(Figure 11). The observed differences concern not only the shape of the curves, but also the values of the linearity threshold. In particular, a marked inconsistency (curve shape and threshold values, Figure 11a) is noted with respect to the curves proposed by *Vucetic and Dobry* [1991]. However, samples S1C3 and S1C7 responded to dynamic tests with decay curves $G/G_0(\gamma)$ that are very similar to those reported by *Ishibashi and Zhang* [1993] and, more recently, by *Zhang et al.* [2005]; the latter curves take into account not only the confinement and plasticity index of the sample, but also its age (Holocene, Tertiary and even older) (Figure 11b). The experimental curves proposed here significantly deviate from those reported in the literature for threshold values. Even more pronounced are, in general, the differences in comparison with the curves proposed by *Sun et al.* [1988] and largely used in software codes for modeling local seismic response and decay of NC clay (Figure 11c).

[40] The normalized decay curves obtained for the samples of level C of the Tiber alluvia in Rome's urban area fall within the variability range of the experimental decay curves obtained for the Holocene alluvial clay of Nocera

Umbra by *Crespellani et al.* [2001], for the Catania alluvial clay by *Carrubba and Maugeri* [1988] and for the Pisa clay (level B) by *Lo Presti et al.* [2002] (Figure 12). The normalized decay curves compare better with the curves built according to the relation proposed by *Hardin and Drnevich* [1972a, 1972b]. In particular, for the Tiber alluvial clay, the interpolation function according to the *Hardin and Drnevich* [1972] relation is (Figure 12a):

$$G/G_0 = 1/\left(1 + \left(15.72\lambda\%^{1.445}\right)\right)$$

[41] For all the tested samples, damping values (D%) remain in the 5% range, below the plasticity threshold, except for the deposits represented by the sample of level A, for which D% values are slightly higher (Figure 9b).

[42] Always on the basis of the *Hardin and Drnevich* [1972a, 1972b] relation, the damping of level C samples may be expressed by the relation (Figure 12b):
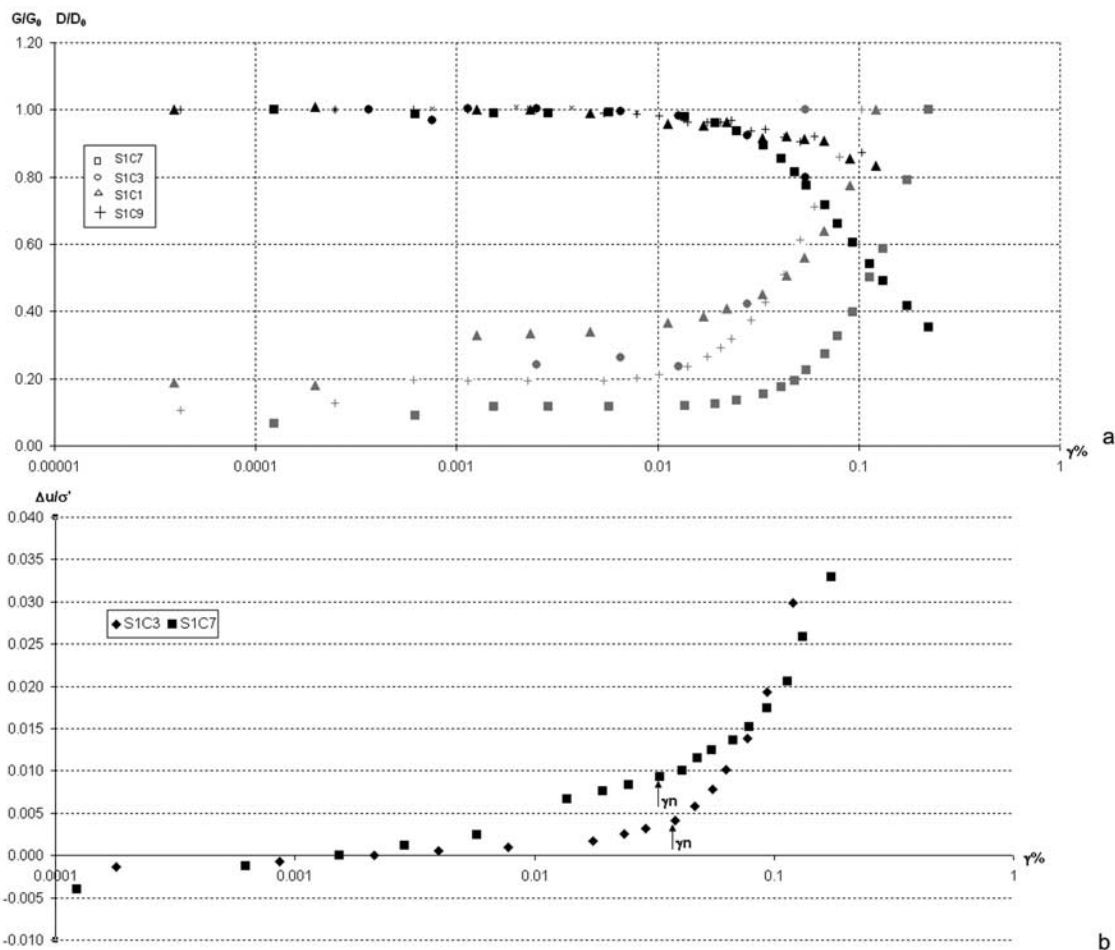
$$D\% = 68.25\exp(-3.1G/G_0)$$

Figure 10. (a) Normalized decay curves $G/G_0(\gamma)$ (black) and damping curves $D/D_0(\gamma)$ (gray) obtained for undisturbed samples collected from the Valco S. Paolo borehole and undergoing resonant column (RC) tests and cyclical torsional shear (TTC) tests at 1Hz; (b) variations of water overpressures normalized during resonant column tests on samples S1C3 ed S1C7; volumetric thresholds (γ_l) are shown.

[43] Table 3 summarizes the Vs values obtained from the down-hole test at the Valco S. Paolo site. So far, these data represent the most comprehensive dynamic characterization of the entire alluvial succession of the main Tiber valley near Rome's historical centre. The comparison of these results with previous technical reports on down- and cross-hole tests demonstrates that: i) the only down-hole data from the literature that can be extrapolated to the Holocene alluvial covers do not permit to distinguish among the lithotechnical levels into which the alluvial deposit may be divided and, ii) the only comparable cross-hole data from the literature are the values of Vs in the Marne Vaticane, which match those obtained at Valco S. Paolo.

[44] The comparison between shear wave velocities (Vs) obtained via down-hole tests and those calculated from lab tests for small deformations (Figure 13) indicates a good match between the values of level C clay silt, but a significant deviation of the values of the samples from level A1 and the Marne Vaticane, equal to roughly 100 and 150 m/s, respectively.

[45] These discrepancies give insight into the effects due to primary and/or secondary structures at the deposit scale. In this connection, the differences recorded between the site- and lab-characterized dynamic behavior of level A1 may be attributed to the depositional heterogeneity and status of the deposit. For the Marne Vaticane, the overestimation of site Vs values vs. lab Vs values might depend on the occurrence of either gravel in level G (approximately at the depth of measurement) or sandy levels interbedded in the clay formation, as directly observed, for instance, upon boring of the "Passante a NW" road tunnel [*Bozzano et al.*, 2006b].

[46] Furthermore, both site and lab tests substantiate the occurrence of two levels, clearly distinguishable by their static properties, inside level C clay silt. The first of these levels lies at about 20–37m from ground level, while the second at 37–51 m from ground level. In particular, the second level of level C has electrical cone penetrometer resistance values higher than the first one. Nonetheless, these differences do not emerge from their dynamic behavior, taking into account the different average confinement of
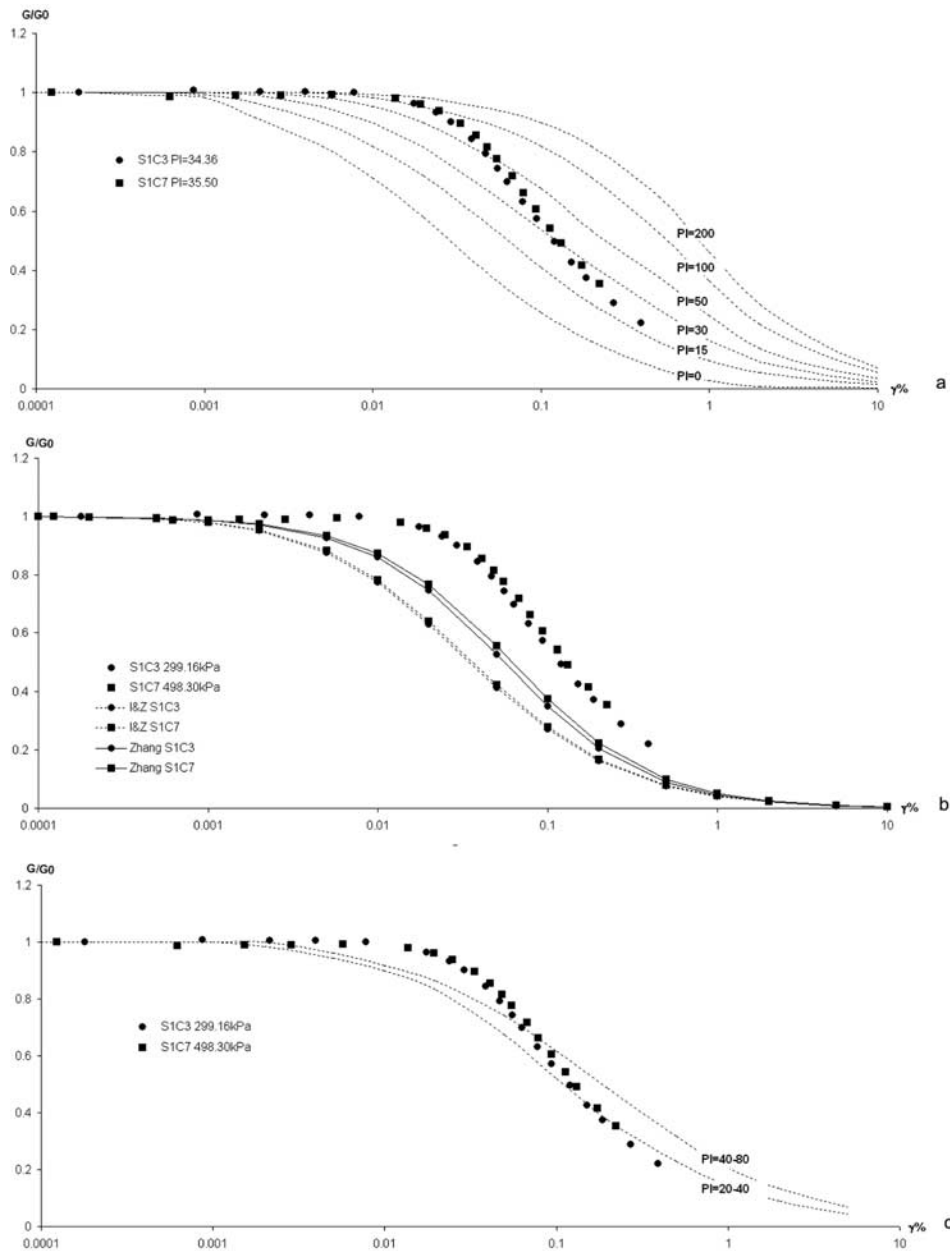
Figure 11. Decay curves $G/G_0(\gamma)$ for level C samples (S1C3 ed S1C7) compared with: a) *Vucetic and Dobry* [1991] curves; b) *Ishibashi and Zhang* [1993] and *Zhang et al.* [2005] curves; c) *Sun et al.* [1988] curves.

the two levels. This aspect is particularly evident in the normalized shear modulus decay curves (samples S1C3 and S1C7), which perfectly match, even beyond the linearity threshold; this finding confirms the homogeneity of level C deposits, which is indirectly demonstrated by the equality between site-measured and lab-obtained dynamic values.

6. Seismic Noise Data

[47] An array of seismic noise recording stations was designed for further validating the velocity values from down-hole and lab tests on the undisturbed samples collected from borehole S1 at Valco S. Paolo. This investigation was expected to compare the experimental vertical velocity profile with the one obtained from the noise field.

[48] Use was made of seven REFTEK-130 stations, equipped with Lennartz LE-3D 1/s sensors; the sampling rate was 200 samples/s. The array was installed around the borehole S1 at Valco S. Paolo, i.e., in a central position with respect to the main Tiber valley (Figure 4).

[49] The array had a double equilateral triangle geometry with the central station located near borehole S1. The external triangle (side of about 100 m) was used to reach higher depths and to sample smaller wave numbers. The internal triangle was instead used to prevent spatial aliasing due to high wave numbers otherwise sampled as low
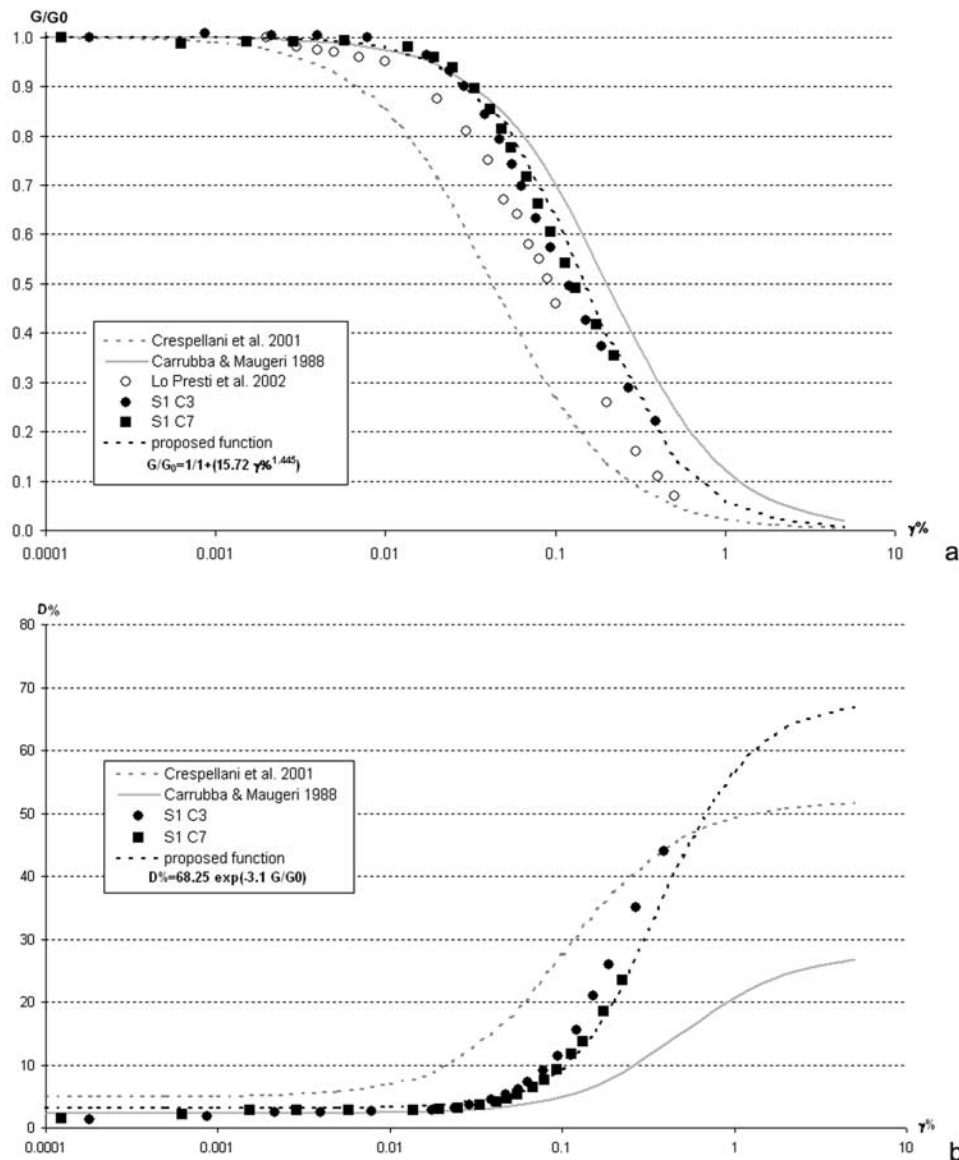
Figure 12. Comparison between decay curves $G/G_0(\gamma)$ (a) and damping curves $D/D_0(\gamma)$ (b) obtained from resonant column tests for level C samples of Valco S. Paolo and normalized decay curves obtained by various authors for Holocene alluvial clay using the *Hardin and Drnevich* [1972] relations.

[*Wathelet et al.*, 2004]. Considering that, in a circular array, the depth of investigation is 2–6 times the radius of the array [*Tokimatsu*, 1995] and that the layer of interest in this case study was equal to about 80m, the Valco S. Paolo array made it possible to investigate the entire vertical velocity profile of the site.

[50] In order to quantify, in the (K_x, K_y) wave number domain, the dependence of the spatial aliasing on the azimuth, the array transfer function (ATF) was computed for the array geometry (Figure 14); ATF was used to estimate the array performance [*Woods and Lintz*, 1973; *Asten and Henstridge*, 1984]. Following *Di Giulio et al.* [2006], K_{max} was defined as the wave number distance between the main peak and the closest side lobe exceeding 50% of main lobe magnitude (Figure 14).

[51] The maximum wave number resolution of the array has been chosen as $K_{max/2}$, while the radius of the main peak taken at its mid height provides the lowest wave number, K_{min}, that can be resolved [*Di Giulio et al.*, 2006] (Figure 14). Such a choice is to avoid, as much as possible, alias effects. The so obtained definitions of K_{min} and $K_{max/2}$ were within the range of the empirical indication of *Tokimatsu* [1995].

[52] For data analysis, resort was made to the SESAR-RAY software package, which was developed as part of the European SESAME project (Site EffectS Assessment using Ambient Excitations, Project EVG1-CT-2000-00026, available under GPL licence; see www.geopsy.org).

[53] At first, for each station, the spectral ratios of the horizontal and vertical components of the noise field (H/V ratios, *Nogoshi and Igarashi* [1971]; *Nakamura* [1989, 2000]) were computed with a view to identify the fundamental frequencies around which energy would concentrate [*Lermo and Chavez-Garcia*, 1993]. The graph of Figure 15a exemplifies the H/V ratio of one of the stations. All
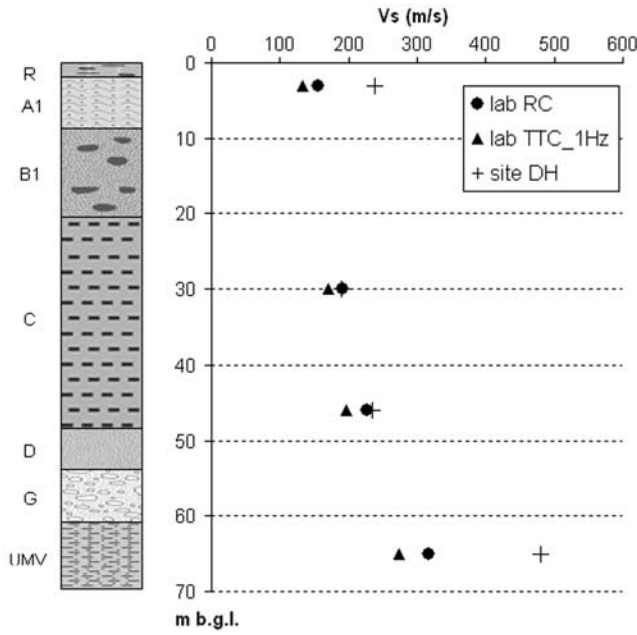
Figure 13. Vs values measured at Valco S. Paolo by downhole tests vs. those obtained from dynamic lab tests on samples collected from borehole S1 (Figures 4 and 5).

H/V spectral ratios have been computed through an anti-trigger software implemented within the SESAME project (SESAME deliverable no. D09.03, http://sesame-fp5.obs.ujf-grenoble.fr/SES_TechnicalDoc.htm). All the stations in the array have peaks around 1 Hz, in agreement with literature data [*Rovelli et al.*, 1995; *Boschi et al.*, 1995; *Olsen et al.*, 2006]. According to the SESAME deliverables D18.06-Wp, D19.06-Wp and D24.13-Wp (see http://sesame-fp5.obs.ujf-grenoble.fr/SES_TechnicalDoc.htm for details), such peaks may be regarded as representative, since spectral ratios are in the range of 3–4 and constant throughout the array; additionally, for all the stations, the standard deviation is less than 3. On the basis of these findings, the near-surface geology of the Valco S. Paolo site can be approximated to a model consisting of plane and parallel layers, which can be more easily run with the SESARRAY software.

[54] Under the assumption that both the noise wavefield is mainly composed of surface waves and the Rayleigh waves are predominant (compared to body waves) in the vertical motion [*Tokimatsu*, 1995], the Rayleigh wave dispersion curve was built using 60 minutes of noise array recording of the vertical components.

[55] The so obtained Rayleigh dispersion curve corresponds to the theoretical one computed by using the Valco S.Paolo velocity profile (Figure 15a). The frequency-wave number (f-k) method of *Capon* [1969] has been adopted to
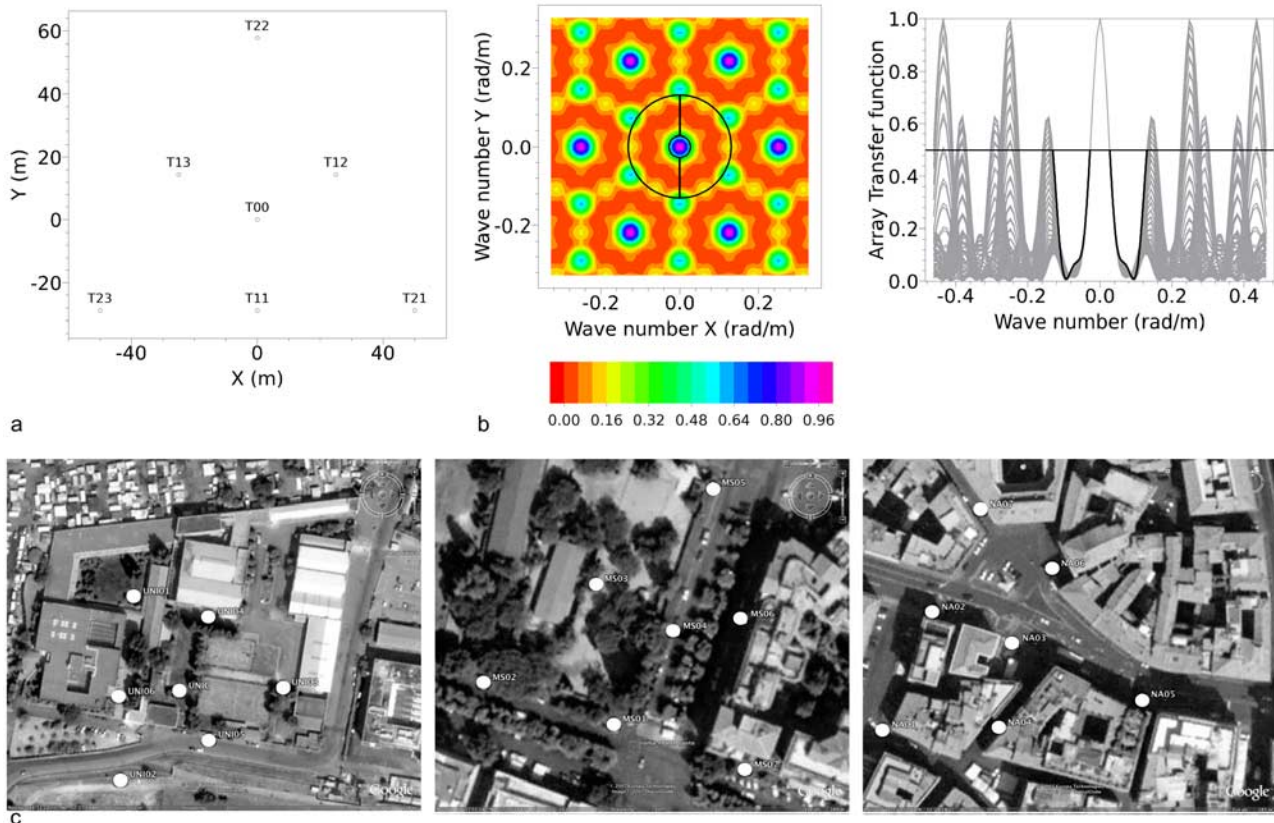

Figure 14. a) Array geometry; b) Array Transfer Function (ATF); the black circle and the black lines in the (K_x, K_y) plane show the alias-lobe position. ATF magnitude reaches the value of 0.5 ($K_{max/2}$) along the direction shown in the (K_x, K_y) plane; c) aerial view of the three array locations (from the left: Valco S.Paolo, Monte Santo, Corso Vittorio). The array geometry is the same for all three sites investigated.
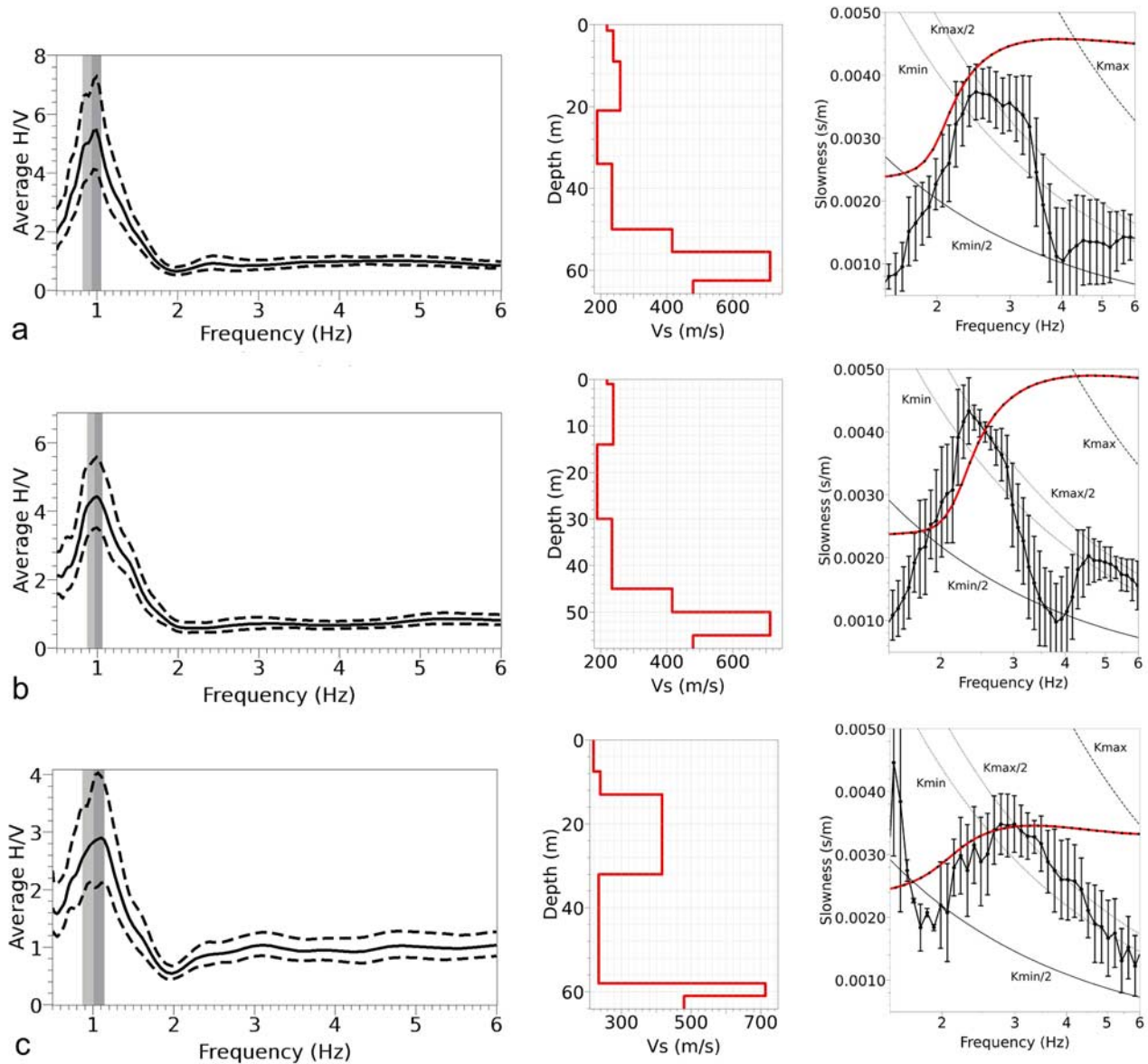
Figure 15. Columns, from the left: H/V spectral ratio ± standard deviation; vertical velocity profile of S waves; theoretical dispersion curve (solid line) and experimental dispersion curve (stippled line), the vertical bars are ± standard deviation. Row: a) Valco S. Paolo test site; b) Monte Santo test site; c) Corso Vittorio test site.

compute the Rayleigh wave dispersion curves, whereas its numerical implementation that we used, comes from SES-AME project [*Ohrnberger*, 2004a; *Ohrnberger et al.*, 2004b]. In Figure 15a, the spatial aliasing curves due to the array geometry are also plotted. The comparison theoretical/experimental Rayleigh dispersion curves holds in the frequency range where the dispersion curve is reliable, i.e., between the minimum and maximum resolvable wavelengths. With reference to Figure 15a, the upper frequency limit was chosen as the intercept of the dispersion curves with the aliasing curve corresponding to $K_{max/2}$ defined from ATF [*Scherbaum et al.*, 2003; *Wathelet et al.*, 2004]. Even though the lower limit is usually fixed around the local resonance frequency of the sites [*Di Giulio et al.*, 2006], due

to the used array geometry, it was necessary to fix such a lower frequency limit as the intercept of the dispersion curves with the aliasing curve corresponding to $K_{min/2}$.

[56] The suitable agreement between the theoretical and experimental dispersion curves for the Valco S. Paolo test site (Figure 15a), made it possible to use the same ambient noise analysis in other two test sites, named L1 and L2 in Figures 2 and 3; L1 is in Via Monte Santo (MS) and L2 in Corso Vittorio (CV). The sites are located in the historical center of the city, in zones of the Tiber valley where stratigraphic settings very similar to the one of Valco S. Paolo test site were reconstructed (Figures 3 and 4) by means of some deep borehole data. This allowed for the extrapolation of the velocity values found for the Valco S.

Table 3. Geophysical Stratigraphy and Dynamic Characteristics Measured in Borehole S1 by Down-hole Tests

Level	Group	Lithology	Height, m	Vs, m/s	Density, kg/m³	G_0, MPa	Damping, %
I	R	silty-sands	1.5	220	1800	87	5
II	A	silty-sands	7.5	239	1840	105	5
III	B	silty-sands	12.0	260	1830	124	5
IV	C1	clayey-silts	13.0	190	1830	66	5
V	C2	clayey-silts	16.0	235	1830	101	5
VI	D	sands	5.5	417	1920	334	5
VII	G	gravel	7.0	713	2100	1068	5
Bedrock	UMV	clayey-silts		480	2000	461	1

Paolo site, to the L1 and L2 test sites where the velocity profiles are not available.

[57] The array geometry of seismic noise recording stations depicted in Figure 14 was used. The corresponding Vs profiles were assumed applying the Vs values measured at Valco S. Paolo test site to the same lithotypes recognized along the stratigraphic logs of MS and CV test sites (Figure 5). Also in these cases, a good agreement between the theoretical and the experimental dispersion curves was obtained (Figures 15b, 15c) and an indirect proof of the validity of the dynamic parameters extrapolation, based on engineering-geology criterion, is then obtained.

7. 1D Modeling of Local Seismic Response

[58] Local seismic response at Valco S. Paolo was 1D-modelled via the SHAKE1D software code. The 1D approach to the Valco S. Paolo site is validated by the features of its near-surface geology (plane and parallel layer model) obtained from seismic noise data.

[59] The stratigraphy for the 1D model was obtained from boreholes and the parameters for the simulation (Table 3) were derived from the DH test. The resulting 1D model consists of 7 layers resting on the bedrock and characterized by two main velocity inversions: the first one at the top of the clay silt of level C and the second one at the top of the Marne Vaticane.

[60] In spite of historical reports of major seismic events in the entire the Roman area [Ambrosini et al., 1986; Cifelli et al., 2000], records of strong motion have been so far scarce, making it impossible to estimate the ensuing felt shaking.

[61] Consequently, the estimation of possible seismic inputs in Rome's area stems from probabilistic and stochastic approaches taking into account the mechanisms of the seismic source and the propagation of the seismic pulse to large distances from the epicenter.

[62] Reports of seismic events in Rome's urban area until about 1000 AD do not permit to identify possible seismic sources, whereas subsequent historical documents suggest that seismicity in this area is due to two sources: a) the Colli Albani hills and b) the central Apennines.

[63] The first source area is responsible for the earthquakes of 1812 and 1899 (VII and VI degree of the Mercalli scale). Conversely, the earthquakes which occurred in 801 (VII–VIII), 1349 (VII–VIII), 1703 (VII) and 1915 (VI–VII), whose macroseismic intensity felt in Rome is shown between parentheses, can be all traced to the source area of the central Apennines. The last 1997 Umbria-Marche earthquake (III MCS) also originates from the latter source.

[64] Inside the source area of the Colli Albani, two sub-areas can be distinguished. The first one, located SE of Rome and corresponding to the sector with the most recent volcanic activity (0.3 Ma or more recent), is responsible for the most frequent earthquakes. The second one, corresponding to the northern sector of the Colli Albani, has more sporadic seismicity. In both source sub-areas of the Colli Albani, the hypocentral depths range from 3 to 6 km and the maximum expected magnitude is equal to 5.2.

[65] Conversely, the source area of the central Apennines gives rise to earthquakes whose hypocentral depths are comprised between 10 and 20 km with more or less normal mechanisms, whereas their maximum expected magnitude is 7.

[66] The distance of the city of Rome from the two source areas of the Colli Albani and the central Apennines is about 25 km and about 100 km, respectively.

[67] With stochastic approaches, Rovelli et al. [1994] obtained the spectra of the possible ground motion in the city of Rome for the maximum magnitude earthquakes expected from the Colli Albani (distinctly for the two source sub-areas) and the central Apennines. The results show that the spectral contribution of 1 to 10 Hz for the earthquakes expected from the Colli Albani is anyway lower than the one from the central Apennines. For the Colli Albani, the frequency contribution of the felt earthquake is anyway above 5 Hz, whereas the one for the central Apennines (at higher distance) is more significant at lower frequencies, i.e., 0.5 to 5 Hz. In terms of peak ground acceleration (PGA), the values expected from an earthquake of magnitude 7 at a distance of 100 km range from roughly 0.03g to roughly 0.07g. These values are in line with the PGA probability of exceedance equal to 10% in 50 a obtained by Romeo et al. [2000]. For the city of Rome, the latter values lie in the 0.05–0.15g range and correspond to peak ground velocity values (PGV) of less than 8 cm/s, with and without site effects.

[68] With regard to the seismic inputs to be applied to the base of the Tiber alluvial succession at Valco S. Paolo, use was made of the two synthetic reference earthquakes proposed by Rovelli et al. [1994] for the central Apennines seismic source. These inputs refer to: (i) an event of magnitude Ms = 7.0 with epicenter at a distance of 80 km from Rome and having a PGA of 0.06g, which may be regarded as representative of the maximum expected seismicity in the entire urban area, and (ii) an event of magnitude Ms = 7.0 with epicenter at a distance of 100 km from Rome and having a PGA of 0.04g. In addition to the above inputs, one synthetic input for the Colli Albani
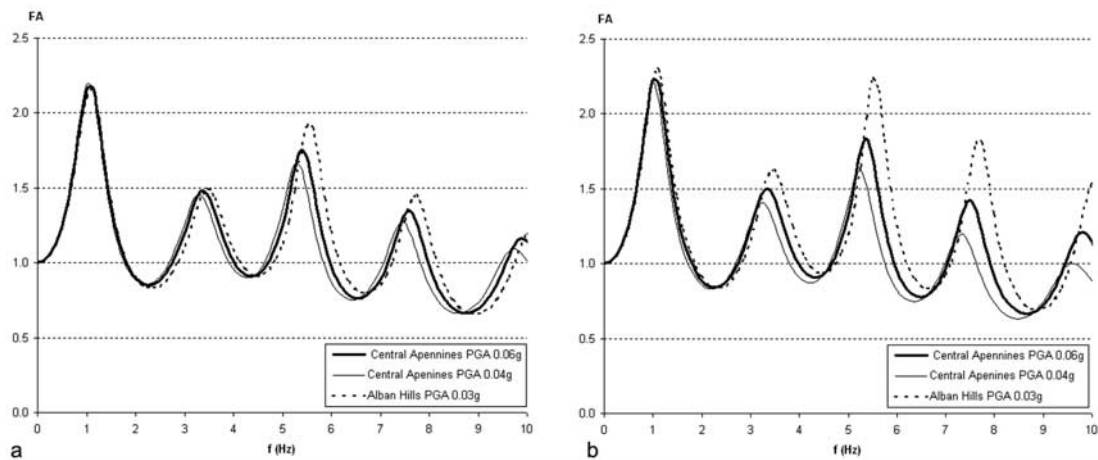
Figure 16. Amplification functions obtained with SHAKE1D for the Valco S. Paolo site, considering the maximum earthquakes expected from the seismic waves of the central Apennines and the Colli Albani hills: a) application of the decay and damping functions $G/G_0(\gamma)$ and $D/D_0(\gamma)$ proposed here to level C; b) application of the decay and damping functions $G/G_0(\gamma)$ and $D/D_0(\gamma)$ proposed by *Sun et al.* [1988] to level C.

seismic source was also obtained (PGA = 0.03 and Mw = 5.0).

[69] All the synthetic accelerograms were built by using the Strong Motion Simulation (SMSIM) [*Boore*, 2000] numerical software, which is based on random generation of white noise time series. As the spectra of these time series depend on the seismic moment and on the stress drop [*Anderson and Hough*, 1984], they can be used to derive time-history series of ground motion obeying the theoretical spectral model adopted for the earthquake under study [*Boore*, 1983; *Calderoni et al.*, 2005].

[70] The amplification function FA (obtained for the different inputs used for numerical 1D simulations) was analyzed in the 1–10 Hz frequency range. The analysis demonstrated that it exceeds the value of 2 at a frequency of about 1 Hz for both earthquakes of the central Apennines. Conversely, for the earthquakes of the Colli Albani, the FA exceeds the value of 2 even in the 5–6 Hz frequency range. Moreover, the use of the D&V function (Figure 16a), specifically obtained for level C, shows a decrease in the value of the FA vs. the one simulated with the function proposed by *Sun et al.* [1988] (Figure 16b): the higher the frequencies (those corresponding to the soil column oscillation modes following the first one), the more significant such decrease. An amplification function that is overestimated by the use of the *Sun et al.* [1988] function is observed for the Colli Albani earthquake vs. the third and fourth oscillation mode of the soil column, i.e., for the 5.5–6 Hz and 7.5–8 Hz frequency ranges (Figure 16b).

[71] Vertical deformations for the simulated seismic events were obtained by using the site-measured Vs profile (Figure 17a). The 1D simulation of local seismic response highlights that the dynamic behavior of level C clay silt, with very close linearity and volumetric thresholds, is particularly significant. Indeed, considering the ground motion due to the maximum expected PGA of 0.06g (referred to the central Apennines earthquake of M = 7.0

at a distance of 80 km), this level reaches plastic conditions by exceeding its volumetric threshold (determined via dynamic lab tests) (Figure 17c). The gradient of the maximum vertical dynamic deformation obtained on the latter assumption exhibits the strongly discontinuous deformation of level C vs. nearby levels; this finding also indicates that, when the PGA passes from 0.04 to 0.06 (considered to be reliable in the case of the maximum earthquakes expected from the central Apennines), this gradient approaches the value of 20 μstrain/m and rises by 106% at the level C/level B1 interface and by 112% at the level C/level D interface. The analysis of amplification functions obtained with the SHAKE1D software for the three simulated seismic inputs emphasizes the important role of the non-linear dynamic behavior of level C in terms of response to the frequencies corresponding to the soil column oscillation modes. Under the decay and damping laws G/G_0 (γ) and D/D_0 (γ) proposed in this study and obtained with the D&V functions, when an increase occurs in the PGA referred to the maximum inputs expected in Rome's urban area from its surrounding seismic sources, the seismic response at 1 Hz is anyway dominant over the one at higher frequencies (about 6 and 8 Hz).

[72] Conversely, in the case of the Colli Albani earthquake, the maximum deformations throughout the soil column do not exceed the linearity thresholds and the vertical deformation gradients do not exceed 5 μstrain/m (Figure 17b). Conversely, for the central Apennines earthquake of M = 7.0 at a distance of 100 km, the linearity threshold (but not the volumetric threshold) is exceeded in level C1 only.

[73] Additionally, the use of the D&V function, under the normalized decay and damping curves $G/G_0(\gamma)$ and $D/D_0(\gamma)$ and with the specific coefficients proposed here, implies a negligible underestimation of the maximum deformation of the clay silt vs. the *Sun et al.* [1988] function. Instead, the maximum deformations recorded in level A1 (historical
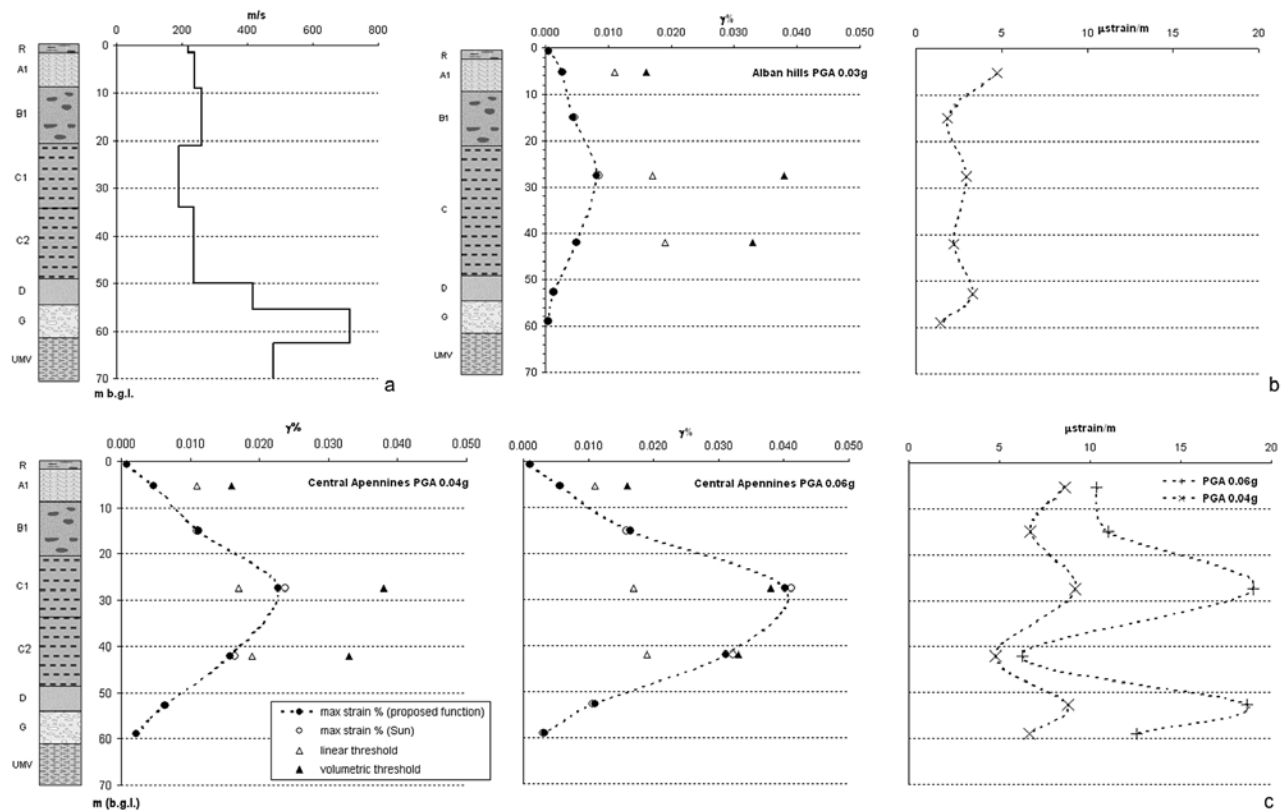
Figure 17. a) Seismic velocity profile obtained from downhole tests at Valco S. Paolo. Maximum. Co-seismic deformation and vertical gradient of the deformations obtained for the Valco S. Paolo site with SHAKE1D: b) for the maximum earthquake expected from the Colli Albani seismic source; c) for the maximum earthquakes expected from the central Apennines seismic source.

alluvia) do not exceed the linearity thresholds under any of the ground motions considered.

8. Discussion

[74] Site and lab characterization data from the investigations conducted at the Valco S. Paolo (Rome) test site demonstrate that a significant rigidity contrast occurs between the Holocene sandy and silty-clay alluvia (levels A1, B1, C, D) and the sand and gravel basal deposits (level G) that overlie the Marne Vaticane (UMV) geological substratum.

[75] This contrast, measured on site in terms of Vs, is equal to about 300 m/s; the basal gravel having a Vs >700 m/s actually represent the local seismic bedrock. On the basis of the stratigraphy of the Holocene Tiber river alluvia, as well as on the geometry of the alluvial valley, this bedrock can be extrapolated to the entire Tiber alluvial body of Rome's historical centre. This finding is in full agreement with the results (Figure 15) derived from surface noise data in three experimental test sites.

[76] Moreover, the relatively low values of Vs (<500 m/s), measured on average inside the first 10 m of the Marne Vaticane, infer that the rigidity of these marls is low in the first level which is in contact with the alluvia; this finding is consistent with the erosion and weathering processes that the stiff clay experienced upon morphogenesis of the Tiber

valley. Indeed, starting from about 500 ka, this morphogenesis involved alternating episodes of erosion of the Pliocene bedrock and filling, which culminated into the latest glacial and the deepening of the alluvial valley floor until reaching the present elevation [Bozzano et al., 2006b]. As reported by Bozzano et al. [2006a], the Pliocene clay potentially involved in these softening and weathering processes may lie in the first 20 m from the contact with the alluvia.

[77] The velocity data measured in the UMV at Valco S. Paolo do not rule out a possible gradual increase in the dynamic rigidity of the Marne Vaticane, i.e., without assuming a further contrast between their weathered and unweathered portions, but rather with a velocity-increase gradient that, in such case, would not give rise to 1D amplification effects. Furthermore, the heterogeneity of the Marne Vaticane, which is due to the occurrence of thin levels of sand and silt, makes it less easy to extrapolate the data from lab tests to the site.

[78] The analysis of the dynamic behavior of level C of the Tiber alluvia in Rome's urban area is of particular interest, since this level accounts for about 50% of the entire thickness of the alluvia in the Valco S. Paolo site and for the nearly entire thickness (up to 50 m) along the left side of the river valley between the Piazza del Popolo and Piazza Venezia squares where levels A, B and D are missing (Figures 2 and 3). The analysis of the noise records obtained for the Valco S. Paolo, Monte Santo and Corso Vittorio (very
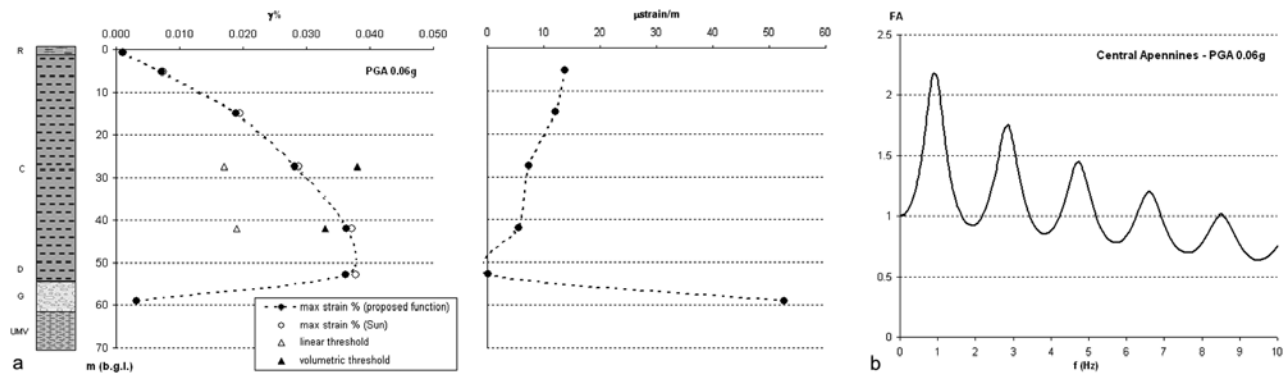
Figure 18. a) Maximum co-seismic deformation and vertical gradient of the deformations obtained for the Piazza Venezia square site with SHAKE1D for the maximum earthquake expected from the central Apennines seismic source; b) amplification function obtained with SHAKE1D for the Piazza Venezia site, considering the maximum earthquake expected from the central Apennines seismic source at a distance of 80km from Rome and applying the decay and damping functions $G/G_0(\gamma)$ and $D/D_0(\gamma)$ proposed here to level C.

close to the Piazza Venezia) test sites supports the validity of the extrapolation of the Vs values of the alluvial deposits in the considered zone of the Rome's historical center.

[79] The simulated 1D response of the Piazza Venezia area (Figure 18) to the maximum expected input (PGA = 0.06 g) fits very well the typical modal shape of a column consisting of an elastoplastic medium overlapping a rigid medium with high impedance contrast. In this instance, the simulation shows that the volumetric threshold is exceeded at the base of the silty-clay deposit (and not inside it), with a maximum vertical deformation gradient of 60 μstrain/m near its contact with the underlying gravel (Figure 18a). Therefore, where the more rigid levels A, B and D are missing and the silty-clay deposit of level C becomes thicker, deeper effects of co-seismic yielding can be expected on the basis of 1D numerical simulations. By contrast, no significant changes are observed in the amplification function, which continues to display a first mode of response of the entire alluvial deposit at about 1 Hz (Figure 18b).

9. Conclusions

[80] An engineering-geology and geophysical study was conducted at the Valco S. Paolo test site, located 2 km south of Rome's historical centre by means of laboratory and site investigations referred to the 60 m thick Tiber alluvial deposits and reaching the geological substratum.

[81] The validity of the geological criterion for the extrapolation of the dynamic properties obtained in the Valco S. Paolo test site was demonstrated by the analysis of seismic noise records obtained in two other test sites, located downtown in very similar stratigraphical setting.

[82] Based on these findings, simulations were made with the SHAKE1D software to reconstruct the vertical trends of the maximum shear deformations that could be obtained in the Tiber alluvia in response to the maximum expected earthquake for the city of Rome. The simulations, carried out for the Valco S. Paolo site and for Rome's historical centre (Piazza Venezia), infer that the major deformations occur in the silty-clay stratigraphic level (level C). This

level, which extends throughout the Tiber alluvia, has a maximum thickness of 50m. The numerical modeling also suggested that the seismic bedrock, producing the first significant impedance contrast, consists of the gravel of level G, which occur everywhere at the base of the Tiber alluvia. Moreover, the vertical deformation profiles are substantially different, depending on whether level C is directly in contact with the seismic bedrock (Piazza Venezia site) or interposed between stiffer alluvia, such as those of levels B and D (Valco S. Paolo site). Indeed, in the latter case, the maximum deformations occur within the first 30 m from ground level, at about half-way of level C, where they exceed volumetric deformation thresholds.

[83] Hence, level C of the Tiber alluvial body and its areal distribution represent non-negligible factors in assessing the local seismic response of the main Tiber valley alluvia in Rome's historical centre. Indeed, the measured dynamic behavior of level C shows close values of linear and volumetric thresholds. Therefore, upon the maximum earthquakes expected from the various seismic sources surrounding the Roman area, such thresholds are already exceeded in sectors that are distant from the valley sides, such as the considered test sites.

[84] It is worth pointing that, when lateral wave-induced 2D effects [*Bard and Bouchon*, 1995] contribute to local seismic amplification, the 1D model underestimates amplification effects at the centre of the valley, contrary to what happens at its margins. Indeed, 2D amplification effects in the main Tiber valley near Rome's historical centre were reported by previous studies [*Rovelli et al.*, 1994, 1995; *Panza et al.*, 2004] based on numerical modeling. However, these models do not take into account the heterogeneous composition and the specific dynamic deformability that the main Tiber valley alluvia proved to have in the study reported in this paper.

References

Amato, A., C. Chiarabba, M. Cocco, M. di Bona, and M. G. Selvaggi (1994), The 1989–1990 seismic swarm in the Alban Hills volcanic area, central Italy, *J. Volcanol. Geotherm. Res.*, 61, 225–237.

Ambrosini, S., S. Castenetto, F. Cevolan, E. Di Loreto, R. Funiciello, L. Liperi, and D. Molin (1986), Risposta sismica dell'area urbana di Roma in occasione del terremoto del Fucino del 13-1-1915, *Mem. Soc. Geol. It.*, 35, 445–452.

Amorosi, A., A. Lembo Fazio, and G. Scarpelli (2002), Interazione tra una struttura esistente e lo sviluppo urbano circostante: l'esempio dell'ex Vasca Navale di Roma, in *Proceedings of the XXI Convegno Nazionale di Geotecnica– Opere Geotecniche in ambiente urbano*, pp. 323–330, L'Aquila 11–14 Settembre 2002.

Anderson, J. G., and S. E. Hough (1984), A model for the shape of the Fourier amplitude spectrum of acceleration at high frequencies, *Bull. Seismol. Soc. Am.*, 74, 1969–1994.

Andrus, R. D., P. Piratheepan, J. Zhang, and S. Ellis (2002), Estimating shear-wave velocity from cone penetrating resistance and geologic age, *Seismol. Res. Lett.*, 73(3), 422.

Asten, M. W., and J. D. Henstridge (1984), Array estimators and the use of microseisms for reconnaissance of sedimentary basins, *Geophysics*, 49, 1828–1837.

Bard, P. Y., and M. Bouchon (1995), The seismic response of sediment-filled valleys. Part2. The case of P and SV waves, *Bull. Seismol. Soc. Am.*, 70, 1921–1941.

Bard, E., B. Mahelin, M. Arnold, L. Montaggioni, G. Cabioch, G. Faure, and F. Rougerie (1996), Deglacial sea-level record from Tahiti corals and the timing of global meltwater discharge, *Nature*, 382, 241–244.

Basili, A., L. Cantore, M. Cocco, A. Frepoli, L. Margheriti, C. Nostro, and G. Selvaggi (1996), The June 12, 1995 microearthquake sequence in the city of Rome, *Annali. di Geofisica*, 39(6), 1167–1175.

Boore, D. M. (1983), Stochastic simulation of high-frequency ground motion based on seismological models of radiated spectra, *Bull. Seismol. Soc. Am.*, 73, 1865–1894.

Boore, D. M. (2000), SMSIM-FORTRAN programs for simulation ground motions from earthquakes: version 2.0-A revision of OFR 96-80A, U.S. Geol. Surv. Open-file Rept. 00-509, available at http://geo-pubs.we.usgs.gov//open-file/of00-509/.

Bordoni, P., and G. Valensise (1998), Deformation of the 125 ka marine terrace in Italy: Tectonic implications, in *Coastal Tectonics*, edited by I. S. Stewart, *Geol. Soc. Spec. Pub.*, 146, 71–110.

Boschi, E., A. Caserta, C. Conti, M. Di Bona, R. Funiciello, L. Malagnini, F. Marra, G. Martines, A. Rovelli, and S. Salvi (1995), Resonance of subsurface sediments: An unforeseen complication for designers of roman columns, *Bull. Seismol. Soc. Am.*, 85, 320–324.

Bozzano, F., R. Funiciello, M. Gaeta, F. Marra, C. Rosa, and G. Valentini (1997), Recent alluvial deposit in Rome (Italy): morpho-stratigrafic, mineralogical and geomechanical characterisation, in the *Proceedings of the International Symposium of Egineering Geology and Environment, Publ 1*, 1193–1198.

Bozzano, F., A. Andreucci, M. Gaeta, and R. Salucci (2000), A geological model of the buried Tiber River valley beneath the historical centre of Rome, *Bull. Eng. Geol. Env.*, 59, 1–21.

Bozzano, F., M. Gaeta, and S. Marcoccia (2006a), Weathering of Valle Ricca stiff and jointed clay, *Eng. Geol.*, 84(3–4), 161–182.

Bozzano, F., S. Martino, and M. Priori (2006b), Natural and man-induced stress evolution o slopes: The Monte Mario hill in Rome, *Environ. Geol.*, 50, 505–524.

Calderoni, G., A. Rovelli, G. Cultrera, R. M. Azzara, and G. Di Giulio (2005), Assessment of ground motion in Palermo, Italy, during the 6 September 2002 MW 5.9 earthquake using source scaling law, *Bull. Seismol. Soc. Am.*, 95, 2342–2363.

Campanella, R. G., P. K. Robertson, D. G. Gillespie, and J. Grieg (1985), Recent developments in in-situ testing of soils, in the *Proceedings of the 11th International Conference on Soil Mechanics and Foundation Engineering 2*, pp. 849–854, San Francisco.

Capon, J. (1969), High-resolution frequency–wavenumber spectrum analysis, in the *Proc. IEEE*, 57 (8), 1408–1418.

Carrubba, P., and M. Maugeri (1988), Determinazione delle proprietà dinamiche di un'argilla mediante prove di colonna risonante, *Rivista Italiana di Geotecnica*, 22(2), 101–113.

Cifelli, F., S. Donati, F. Funiciello, and A. Tertulliani (2000), High-density macroseismic survey in urban areas. Part 2: Results for the city of Rome, Italy, *Bull. Seismol. Soc. Am.*, 90(2), 298–311.

Corazza, A., M. Lanzini, C. Rosa, and R. Salucci (1999), Caratteri stratigrafici, idrogeologici e geotecnici delle alluvioni tiberine nel settore del centro storico di Roma, *Il Quaternario*, 12, 215–235.

Crespellani, T., C. Madiai, G. Simoni, and G. Vanucchi (2001), Dynamic geotechnical testing and seismic response analyses in two sites of the Commune di Nocera Umbra, Italy, *Rivista Italiana di Geotecnica*, 35(4), 39–52.

Di Giulio, G., C. Cornou, M. Ohrnberger, M. Wathelet, and A. Rovelli (2006), Deriving wavefield characteristics and shear-velocity profiles from two-dimensional small-aperture arrays analysis of ambient vibrations in a small-size alluvial basin, Colfiorito, Italy, *Bull. Seismol. Soc. Am.*, 96(5), 1915–1933.

Douglas, B. J., and R. S. Olsen (1981), Soil classification using the electric cone penetrometer, *ASCE Geot. Div. Symp. on Cone Penetration Testing and Experience*, St. Luis (USA).

Fäh, D., C. Iodice, P. Suhadolc, and G. F. Panza (1993), A new method for the realistic estimation of seismic ground motion in megacities: The Case of Rome, *Earthquake Spectra*, 9, 643–668.

Funiciello, R., L. Lombardi, F. Marra, and M. Parotto (1995), Seismic damage and geological heterogeneity in Rome's Colosseum area: are they related?, *Annali di Geofisica*, 38(3), 267–277.

Hardin, B. O., and V. P. Drnevich (1972a), Shear modulus and damping in soil: Measurement and parameter effects, *J. Soil Mech. Foundation Eng. Div. ASCE*, 98(6), 603–624.

Hardin, B. O., and V. P. Drnevich (1972b), Shear modulus and damping in soil: Design equations and curves, *J. Soil Mech. Foundation Eng. Div. ASCE*, 98(7), 667–692.

Hearty, P. J., and G. Dai-Pra (1986), Aminostratigraphy of Quaternary marine deposits in the Lazio region of central Italy, in *Dating Mediterranean shorelines*, edited by A. Ozer and C. Vita-Finzi, pp. 131–140, *Zeitschrift fuer Geomorphologie, Supplementband 62*.

Hegazy, Y. A., and P. W. Mayne (1995), Statistical correlations between VS and cone penetration data for different soil types, in the *Proceedings of the International Symposium on Cone Penetration Testing*, pp. 173–178, Linkoping, Sweden.

Ishibashi, I., and X. Zhang (1993), Unified dynamic shear moduli and damping ratios of sand and clay, *Soils and Foundations*, 33(1), 182–191.

Karner, D. B., and F. Marra (1998), Correlation of Fluviodeltaic Aggradational Sections with Glacial Climate History: A Revision of the Classical Pleistocene Stratigraphy of Rome, *Geol. Soc. Am. Bull.*, 110, 748–758.

Karner, D. B., and P. R. Renne (1998), 40Ar/39Ar geochronology of Roman volcanic province Tephra in the Tiber River Valley: Age calibration of Middle Pleistocene sea-level changes, *Bull. Seismol. Soc. Am.*, 110, 740–747.

Karner, D. B., F. Marra, F. Florindo, and E. Boschi (2001), Pulsed uplift estimated from terrace elevations in the coast of Rome: Evidence for a new phase of volcanic activity?, *Earth Planet. Sci. Lett.*, 188, 135–148.

Lermo, J., and F. J. Chavez-Garcia (1993), Site evaluation using spectral ratios with only one station, *Bull. Seismol. Soc. Am.*, 83, 1574–1594.

Lo Presti, D., M. Jamiolkowski, and M. Pepe (2002), Geotechnical characterisation of the subsoil of Pisa Tower, in *Characterization and Engineering Properties of Natural Soils Vol. 2*, pp. 909–946, Balkema, Rotterdam.

Madiai, C., and G. Simoni (2002), Correlazioni Vs – Qc per alcuni terreni dell'alta Val Tiberina, in the *Atti dell'incontro annuale dei ricercatori di geotecnica*, IARG 2002, Napoli.

Marra, F., and C. Rosa (1995), Stratigrafia e assetto geologico dell'area romana, in "La Geologia di Roma. Il Centro Storico", *Memorie Descrittive della Carta Geologica d'Italia (special issue)*, 50, 49–118.

Marra, F., M. G. Carboni, L. De Bella, C. Faccenna, R. Funiciello, and C. Rosa (1995), Il substrato Plio-Pleistocenico dell'area Romana, *Boll. Soc. Geol. It.*, 114, 195–214.

Marra, F., F. Florindo, and D. B. Karner (1998), Paleomagnetism and geochronology of early Middle Pleistocene depositional sequences near Rome: Comparison with the deep sea 18O climate record, *Earth Planet. Sci. Lett.*, 159, 147–164.

Mayne, P. W., and G. J. Rix (1993), G_{max}-Qc, relationships for c1ays, *ASTM Geotechnical Testing J.*, 16(l), 54–60.

Molin, D., and E. Guidoboni (1989), Effetto fonti, effetto monumenti a Roma: i terremoti dell'antichità a oggi, in *I Terremoti prima del Mille in Italia e nell'Area Mediterranea*, Edited by E. Guidoboni, pp. 194–223, S. G. A., Bologna.

Molin, D., S. Ambrosini, S. Castenetto, E. Di Loreto, L. Liperi, and A. Paciello (1986), Aspetti della sismicità storica di Roma, *Mem. Soc. Geol. It.*, 35, 439–448.

Nakamura, Y. (1989), A method for dynamic characteristics estimation of subsurface using microtremor on the ground surface, *Q. Rep. Railway Tech. Res. Inst.*, 30(1), 25–33.

Nakamura, Y. (2000), Clear identification of fundamental idea of Nakamura's technique and its applications, in *Proc. 12th World Conference on the Earthquake Engineering*, Auckland, New Zealand.

Nogoshi, M., and T. Igarashi (1971), On the amplitude characteristic of microtremor (part 2) (in Japanese with English abstract), *J. Seismol. Soc. Jpn.*, 24, 26–40.

Ohrnberger, M. (2004a), User manual for software package CAP—a continuous array processing toolkit for ambient vibration array analysis, SESAME report D18.06, http://sesame-fp5.obs.ujfgrenoble.fr.

Ohrnberger, M., E. Schissele', C. Cornou, S. Bonnefoy-Claudet, M. Wathelet, A. Savvaidis, F. Scherbaum, and D. Jongmans (2004b), Frequency wavenumber and spatial autocorrelation methods for dispersion curve determination from ambient vibration recordings. In *Proc. 13th World Conference on Earthquake Engineering, Vancouver, B.C.*, Canada, 1–6 August 2004, paper no. 0946.

Olsen, K. B., A. Akinci, A. Rovelli, F. Marra, and L. Malagnini (2006), 3D ground-motion estimation in Rome, Italy, *Bull. Seismol. Soc. Am.*, 96(1), 133–146.

Panza, G. F., et al. (2004), Realistic modeling of seismic input for megacities and large urban areas, *J. Tech. Environ. Geol.*, 1(2004), 6–42.

Riguzzi, F., and A. Tertulliani (1993), Re-evaluation of minor events: The examples of the 1895 and 1909 Rome earthquakes, *Natural Hazards*, 7, 219–235.

Romeo, R., A. Paciello, and D. Rinaldis (2000), Seismic hazard maps of Italy including site effects, *Soil Dyn. Earth. Eng.*, 20, 85–92.

Rovelli, A., A. Caserta, L. Malagnini, and F. Marra (1994), Assessment of potential strong motions in the city of Rome, *Annali di Geofisica*, 37, 1745–1769.

Rovelli, A., L. Malagnini, A. Caserta, and F. Marra (1995), Using 1-D and 2-D modelling of ground motion for seismic zonation criteria: results for the city of Rome, *Annali di Geofisica*, 38(5–6), 591–605.

Salvi, S., E. Boschi, M. Di Bona, R. Funiciello, L. Malagnini, F. Marra, and A. Rovelli (1991), Subsurface geology and variations of seismic response in the city of Rome. In the *Proceedings of the 4th Int. Cong. on Seismic Zonation* (*Vol. II*), pp. 115–122, EERI, Stanford, California.

Scherbaum, F., K.-G. Hinzen, and M. Ohrnberger (2003), Determination of shallow shear wave velocity profiles in the Cologne, Germany area using ambient vibrations, *Geophys. J. Int.*, 152(3), 597–612.

Sun, J. I., R. Golesorkhi, and H. B. Seed (1988), Dynamic moduli and damping ratios for cohesive soils, *Report No. EERC-88/15*, Earthquake Engineering Research Centre, Univ. of California, Berkeley.

Tatsuoka, F., and S. Shibuya (1992), Deformation characteristics of soils and rocks from field and laboratory tests. *Report of the Institute of Industrial Science 37* (l), *Serial No. 235*, The Univ. of Tokio, pp. 136.

Tertulliani, A., P. Tosi, and V. De Rubeis (1996), Local seismicity in Rome (Italy): recent results from macroseismic evidences, *Annali di Geofisica*, 39(6), 1235–1240.

Tokimatsu, K. (1995), Geotechnical site characterization using surface waves, in the *Proceedings of the 1st Intl. Conf. Earthquake Geotechnical Engineering*, edited by K. Ishihara, pp. 1333–1368, Balkema, Leiden.

Vucetic, M., and R. Dobry (1991), Effect of soil plasticity on cyclic response, *J. Geotech. Eng. ASCE*, 117(1), 89–107.

Wathelet, M., D. Jongmans, and M. Ohrnberger (2004), Surface-wave inversion using a direct search algorithm and its application to ambient vibration measurements, *Near Surface Geophys.*, 211–221.

Wathelet, M., D. Jongmans, and M. Ohrnberger (2005), Direct inversion of spatial autocorrelation curves with the neighborhood algorithm, *Bull. Seismol. Soc. Am.*, 95(5), 1787–1800.

Woods, J. W., and P. R. Lintz (1973), Plane waves at small arrays, *Geophysics*, 38(6), 1023–1041.

Zhang, J., R. D. Andrus, and C. H. Juang (2005), Normalized shear modulus and material damping ratio relationships, *J. Geotech. Geoenviron. Eng. ASCE*, 131(4), 453–464.

––––––––––––––––––

F. Bozzano and S. Martino, Università di Roma "La Sapienza"-Dipartimento di Scienze della Terra, P.le A., Moro 5, 00185, Rome Italy. (salvatore.martino@uniromal.it)

A. Caserta and F. Marra, INGV-Via di Vigna Murata 605, 00143 Rome Italy.

A. Govoni, Instituto Nazionale di Oceanografia e di Geofisica Sperimentale - OGS, Udine, Italy.

Corresponding Author: Salvatore Martino, PhD

Corresponding Author's Institution: University of Rome Sapienza

First Author: Arrigo Caserta, PhD

Order of Authors: Arrigo Caserta, PhD;Salvatore Martino, PhD;Francesca Bozzano, Prof.;Aladino Govoni, Dr.;Fabrizio Marra, Dr.

Abstract: The presence of peats and high compressibility inorganic clays within alluvial fills on the left-side tributaries of the Tiber River, close to Rome's historic center in Italy, is well documented in literature. Nevertheless, dynamic properties of these deposits have rarely been characterised by undisturbed bore-hole samples up until now. The Galba test-site was set up to characterise dynamic properties of the alluvial deposits by using lab-tests as well as to derive velocity profiles by seismic noise measurements. This was performed in the Giustiniano Imperatore area located in the Grottaperfetta valley, about 2 km south of Rome's historic centre. The alluvial deposits filled a paleovalley excavated in the bedrock during the Würm glacial (18-20 ka). The stratigraphic setting of the alluvial body was reconstructed along three geological cross-section by means of the available logs; seven lithotecnical horizons can be distinguished within the alluvial body, some tens of meters thick, based on both log-stratigraphic data and in-site geotechnical characterisations. These horizons include peaty layers (T) and high compressibility inorganic clays (AGI), which characterise the alluvial deposits in the Grottaperfetta valley. They do not have direct correlation with the alluvial horizons which constitute the alluvial body of the main Tiber valley in Rome's historical centre. These alluvial horizons which are distinguished and characterised at the Galba test-site can be regarded as typical of other lateral valleys of the Tiber River in Southern Rome and characterised by the presence of similar high compressibility clayey deposits as well as peaty layers up to some meters thick. Undisturbed samples were also obtained at the Galba test-site for dynamic testing via resonant column and cyclical torsional shear tests. In order to attribute dynamic properties to the alluvial body at the Grottaperfetta valley, an extrapolation process was performed based on a detailed engineering-geology model of the alluvial body which was reconstructed along three transversal geological sections of the valleyusing bore-hole data.
Three soil columns, considered representative of the geological setting along the three reconstructed transversal cross sections, were analysed by seismic noise measurements performed specifically to derive S-waves velocity profiles. The results obtained show a very low velocity (<180 m/) for the layers T and AGI.
1D modelling of seismic shaking was performed for each considered column by the code SHAKE1D, in order to evaluate the influence of the low-velocity strata on maximum shear strains induced within the alluvial deposits under the maximum expected seismic action. The results of the numerical modelling

indicate that the AGI and the T layers play a key role in: i) concentrating the maximum shear strain along the soil columns, even though the volumetric threshold is never exceeded; ii) increasing the maximum shear strain along the soil columns; iii) causing the resonance frequency of the alluvial fill to assume an almost constant value (about 1Hz) which is quite similar to that measured in the main Tiber River valley, despite a significant change in thickness of the alluvial body along the Grottaperfetta valley.

1   **DYNAMIC PROPERTIES OF LOW VELOCITY ALLUVIAL DEPOSITS**

2   **INFLUENCING SEISMICALLY-INDUCED SHEAR STRAINS: THE**

3   **GROTTAPERFETTA VALLEY TEST-SITE (ROME - Italy)**

4

5

6   **Caserta A. [1], Martino S. [2], Bozzano F.[2], Govoni A. [3], Marra F. [3]**

7

8   [1] INGV - Via di Vigna Murata 605 , 00143 Roma; Charles University, Faculty of Mathematics and Physics,

9   Prague, Czech Republic.

10   [2] Università di Roma "La Sapienza" - Dipartimento di Scienze della Terra, P.le A. Moro 5, 00185, Roma.

11   [3] INGV - Via di Vigna Murata 605 , 00143 Roma.

12

13

14   **ABSTRACT**

15

16   The presence of peats and high compressibility inorganic clays within alluvial fills on the left-

17   side tributaries of the Tiber River, close to Rome's historic center in Italy, is well documented

18   in literature. Nevertheless, dynamic properties of these deposits have rarely been

19   characterised by undisturbed bore-hole samples up until now. The Galba test-site was set up

20   to characterise dynamic properties of the alluvial deposits by using lab-tests as well as to

21   derive velocity profiles by seismic noise measurements. This was performed in the

22   Giustiniano Imperatore area located in the Grottaperfetta valley, about 2 km south of Rome's

23   historic centre. The alluvial deposits filled a paleovalley excavated in the bedrock during the

24   Würm glacial (18-20 ka). The stratigraphic setting of the alluvial body was reconstructed

25   along three geological cross-section by means of the available logs; seven lithotecnical

26   horizons can be distinguished within the alluvial body, some tens of meters thick, based on

27   both log-stratigraphic data and in-site geotechnical characterisations. These horizons include

28   peaty layers (T) and high compressibility inorganic clays (AGI), which characterise the

29   alluvial deposits in the Grottaperfetta valley. They do not have direct correlation with the

30   alluvial horizons which constitute the alluvial body of the main Tiber valley in Rome's

31   historical centre. These alluvial horizons which are distinguished and characterised at the

32   Galba test-site can be regarded as typical of other lateral valleys of the Tiber River in

33   Southern Rome and characterised by the presence of similar high compressibility clayey

34   deposits as well as peaty layers up to some meters thick. Undisturbed samples were also

obtained at the Galba test-site for dynamic testing via resonant column and cyclical torsional shear tests. In order to attribute dynamic properties to the alluvial body at the Grottaperfetta valley, an extrapolation process was performed based on a detailed engineering-geology model of the alluvial body which was reconstructed along three transversal geological sections of the valley using bore-hole data.

Three soil columns, considered representative of the geological setting along the three reconstructed transversal cross sections, were analysed by seismic noise measurements performed specifically to derive S-waves velocity profiles. The results obtained show a very low velocity (<180 m/) for the layers T and AGI.

1D modelling of seismic shaking was performed for each considered column by the code SHAKE1D, in order to evaluate the influence of the low-velocity strata on maximum shear strains induced within the alluvial deposits under the maximum expected seismic action. The results of the numerical modelling indicate that the AGI and the T layers play a key role in: i) concentrating the maximum shear strain along the soil columns, even though the volumetric threshold is never exceeded; ii) increasing the maximum shear strain along the soil columns; iii) causing the resonance frequency of the alluvial fill to assume an almost constant value (about 1Hz) which is quite similar to that measured in the main Tiber River valley, despite a significant change in thickness of the alluvial body along the Grottaperfetta valley.

KEYWORDS

local seismic response, alluvial valley, low-velocity deposits, seismic noise measurements, numerical modelling, Rome

1. INTRODUCTION

Rome is located some tens of kilometres away from the central Apennines seismogenic zone (Basili et al., 2008; DISS3 catalogue, 2009), where earthquakes of a tectonic origin reaching magnitudes of up to 7.0 can be expected. This was recently proved on the 6th April 2009 during the L'Aquila earthquake. A study by Ambrosini et al. (1986) reported that the 1915 earthquake caused severe damage to buildings located on the Holocene alluvial fill of the Tiber valley (Fig. 1), thereby stressing the role of local geology by amplifying ground shaking. Even smaller and local earthquakes (in 1812 and 1895) induced damage to architectural heritage (Molin et al., 1986; Molin and Guidoboni, 1989). Similarly, Boschi et al., (1995) and Funiciello et al. (1995) showed the close relationship that exists between damage to monuments and the presence of underlying soft alluvial sediments.

Since then, several studies have been conducted to quantify the expected site effects within the city of Rome, including simulations via the finite-difference technique applied to 2D and 3D models (Rovelli et al., 1994; 1995; Olsen et al., 2006), as well as a hybrid technique based on mode summation and finite differences (Fah et al., 1993). However, all of these studies relied on theoretical values from the scientific literature for the dynamic geomechanical properties of geological materials and were not supported by *in situ* measurements and specific engineering-geology studies in the city of Rome.

Our recent paper (Bozzano et al., 2008b) attempts to fill the gap of the lack of research for in direct measurements of the dynamic geomechanical parameters attributed to the alluvial deposits, filling the Tiber River valley. These properties cannot be applied to characterise alluvial fills of the Tiber lateral valleys, due to the presence of different geological deposits (Campolunghi et al., 2007) which are responsible for the high settlement phenomena as found in the Giustiniano Imperatore area (Stramondo et al., 2008) as well as for peculiar local seismic response effects (Moczo et al., 1995).

This prompted us to select the left side of the Grottaperfetta valley, with respect to the main Tiber valley (Fig.1), as a site test to dynamically characterise the high compressibility clays and the peats within the alluvial fill by lab-tests and to derive S-waves velocity profiles performing specific seismic noise measurements.

Seismic array for noise measurements was installed for this project and a detailed classification of the physical and mechanical properties of the rocks constituting the geological subsoil of the selected site under dynamic conditions was performed.

As the dynamic behaviour of recent clay deposits may disagree with widespread empirical relations used in numerical modelling, the dynamic properties of the Holocene alluvial deposits in the Grottaperfetta valley were compared to results obtained by other authors for different Holocene Italian deposits (Carubba and Maugeri, 1988; Crespellani et al., 2001, Lo Presti et al., 2002) . A comparison was also made to the Tiber River valley close Rome's center (Bozzano et al., 2008b).

In order to highlight the possible role of high compressibility inorganic clays and peats, a 1D numerical modelling was performed for the Grottaperfetta valley under a strong motion seismic action (PGA of up to 0.06g) on the vertical distribution of the maximum shear strains as well as on the first resonance mode of the alluvial deposits.

2. SEISMICITY OF THE AREA OF ROME

103 Rome has extensive records of felt earthquakes and a detailed study of historical sources

104 allowed Molin and Guidoboni (1989) to produce a catalogue, which was renewed with the

105 assessment of additional minor events (Riguzzi and Tertulliani, 1993). Reports of seismic

106 events in Rome's urban area since 1000 AD suggest that seismicity in this area is due to two

107 sources (Tertulliani et al., 1996): a) the Colli Albani hills and b) the central Apennines

108 (Fig.1).

109 The Colli Albani hills are responsible for the 1812 and 1899 earthquakes (VII and VI degree

110 of the Mercalli scale). Conversely, the earthquakes which occurred in 801 (VII-VIII), 1349

111 (VII-VIII), 1703 (VII) in 1915 (VI-VII), whose macroseismic intensity was felt in Rome

112 (shown between brackets), can all be traced to the source area of the central Apennines. The

113 most recent 2009 L'Aquila earthquake (IV-V MCS) also originates from the latter source.

114 Two sub-areas can be distinguished in the Colli Albani source area , (Amato et al., 1994). The

115 first one, located SE of Rome corresponds to the sector with the most recent volcanic activity

116 (0.3 Ma or more recent) and is responsible for the most frequent earthquakes. The second one

117 has a more sporadic seismicity and corresponds to the northern sector of the Colli Albani

118 hills. In both source sub-areas of the Colli Albani hills, the hypocentral depths range from 3

119 to 6km and the maximum expected magnitude is equal to 5.2. These smaller events expect to

120 produce a maximum I_{felt} = VI-VII in Rome.

121 On the other hand, the central Apennines source area gives rise to earthquakes whose

122 hypocentral depths comprise between 10 and 20km with more or less normal mechanisms

123 and their maximum expected magnitude is 7.0.

124 The Colli Albani hills are 25km away from Rome whereas the central Apennines are about

125 100km.

126 The last seismic sequence in L'Aquila started on 6th April 2009 with the mainshock (Mw

127 6.3), whose epicentre was located near Roio, about 5 km southwest of L'Aquila town (for the

128 location see the upper part of Fig.1) in seismogenic zone of the central Apennines. The focal

129 mechanisms of the sequence clearly define a NW-SE trending normal faulting mechanism

130 and the focal depths are generally within 10-12 km.

131 The L'Aquila mainshock was felt in Rome with an intensity up to V MCS (INGV, 2009) and

132 it was recorded with a PGA of about 0.01g by a 3D seismic array installed by the INGV in

133 the Tiber alluvial valley (Caserta et al., 2009). This ground motion cannot be regarded as the

134 maximum expected for a 10% of excedance in 50 years since this last one corresponds to

135 0.132g, according to INGV (2006).

136

3. GEOLOGICAL SETTING

Similarly to the Tiber valley and other tributaries, the Grottaperfetta Valley originated during the Würm glacial (18-20 ka). During this glacial era the fall of the sea level (more than 120 m) caused a deep erosion of the fluvial valleys in Rome, cutting the bedrock from bottom to top composed of high consistent clays (Pl) , sandy-gravelly (G_{Pl}, D_{Pl},) and clayey-sandy (A_{Pl}) paleo-alluvial deposits down to 60 m below sea level (Marra and Rosa, 1995) (Fig.2). The change in climatic conditions provoked the glaciers to melt, and the sea level to rise at a relatively fast pace, (Bard *et alii*, 1996) consequently filling of fluvial valleys. The sediments deposited during Holocene within the valleys are generally characterized by a fining-upward succession, with a relatively thin horizon of gravel at the base, grading upward into a thick pack of sand and clay (Bozzano et al., 2000). Within this sedimentary body the intercalations of organic material such as carbonized plants and peat horizons are frequent. Therefore, the alluvial deposits are generally characterised as low consistency fine-grained soils, saturated in water, from normally consolidated to weakly over consolidated in the superficial part and generally characterized by low stiffness parameter values (Bozzano et al., 2000).

A detailed stratigraphic reconstruction and geochronologic study of the alluvial fill corresponding to the intermediate portion of the Grottaperfetta Valley is given in Cinti et al. (2008). Stratigraphic logs were used for 7 boreholes, drilled in the Galba test site in 2004-2005 (Fig.3, 4), up to 50 m b.g.l. (S1), 43 m b.g.l. (S2), 36 m b.g.l. (S3), 31 m b.g.l. (S4), 29 m b.g.l. (S7), 26 m b.g.l. (S5) and 20 m b.g.l. (S6) respectively. The boreholes are aligned along a N45 trace within 150 m of distance (from NW to SE) according to the above reported order (Fig.3). Here we extend the stratigraphic analyses to the higher portion of the valley (Giardinetti site, Fig. 5) and to its confluence to the Tiber River valley (Leonardo site, Fig.5). The study of the Giardinetti section is notably performed through the analysis of unpublished stratigraphic logs performed for civil engineering purposes, while the stratigraphy of the Leonardo section is extrapolated from the intermediate portion of the valley.

The geological reconstruction gives us the results of the geological substratum of the alluvial deposits at Grottaperfetta valley and is composed from the bottom to the top by high consistency clays referred to the Marne Vaticane unit (UMV) of Pliocene age, Paleotiber alluvial deposits, downward passing from clayey sand (A_{Pl}) to sandy gravels (G_{Pl} and D_{Pl}).

The thickness of the alluvial fill increases from ~35 m at Giardinetti site, up to ~50 m at the Leonardo site and the bottom of the incision deepens from -20 m a.s.l. to -40 m a.s.l. (Fig.2).

171 Taking into account the lithologic features, five main sedimentary horizons (layers ALS,

172 AGI, T, ATG, D; Fig. 4) can be identified within the alluvial body. A relatively thin layer (1-

173 2 m) of loose, coarse, prevalently carbonatic gravel (layer G) is present only in

174 correspondence of the deeper central axis of the valley. It is followed by a coarse sand layer

175 about 6 m in thickness (layer D), with intercalations of decimetric, generally volcanic, fine

176 gravel layers. It grades upward into the ATG layer, constituted by grey clayey-sandy silt with

177 abundant organic matter. A 2 to 4 m thick peat layer (layer T) extends throughout the

178 investigated territory of the Grottaperfetta valley at depths ranging between 20 m (Giardinetti

179 site) and 30 m (Leonardo site) below the ground surface (Fig.5). The T layer characterises the

180 alluvial deposits of Grottaperfetta valley and marks the transition between layer ATG and

181 layer AGI; the latter is a 6 m thick pack of low consistency, high plasticity, light grey silt and

182 clay (CH and MH in the Unified Soil Classification System), grading upwards to a 2-3 m

183 thick horizon of light brown, sandy silt. The AGI layer represents the other marker layer

184 within the Grottaperfetta alluvia and distinguishes it from the ones in the main valley of the

185 Tiber river, where such thick horizons of homogeneous and very low-consistency sediments

186 is absent (Stramondo et al., 2008). The upper alluvial unit ALS shows a significantly diverse

187 feature with respect to the previous ones, testifying a reversal of the overall grain size. It is a

188 light brown sandy fine grained deposit with abundant reworked pyroclastic material and

189 sparse vegetal remains. Two peat layers occur locally in the lower portion of this unit at the

190 Galba site within the ALS horizon. It has been hypothesized that their presence may be

191 linked to a recent tectonic deformation of the alluvial sediment (Cinti et al., 2008). Finally, a

192 man-made fill stratum (R in Fig. 4), up to 8 m thick, and related to the urbanization of the

193 area over the past 50 years, represents the top of the succession; it is characterised by various

194 sizes of brick fragments and blocks of tuff embedded in a reddish silty-sandy matrix (Fig. 4)

195

4. GEOMECHANICAL PROPERTIES OF THE ALLUVIAL DEPOSITS DERIVED AT THE GALBA TEST-SITE

The new engineering-geology data collected at the Galba test-site at the Grottaperfetta valley derive from the above mentioned 7 boreholes drilled on 2004-2005 (cfr. par. 3). In particular, 17 undisturbed samples were obtained from the S1 and S2 boreholes (Figs. 3, 4) by using Shelby tubes for performing geomechanical lab-tests as well as dynamic characterisation by resonant column and cyclic torsional devices, in particular on the AGI, T and UMV layers; CPTU (electrical piezocone penetrometer measurements) were also performed along the same boreholes.

Several lithotechnical groups were associated to the corresponding stratigraphic horizons (R, ALS, AGI, T, ATG, D, G) within the alluvial fill (Fig.4) as well as to the geological substratum corresponding to the UMV high consistency clays of the Marne Vaticane formation. Physical and mechanical parameter values (Table 1) were attributed to all the distinguished lithotechnical groups.

The value of electrical piezocone penetrometer resistance (qc) measured with CPTU along boreholes S1 and S2, down to about 41.5 m b.g.l. and 42 m b.g.l. respectively, does not exceed 4 MPa in layer R, 2 MPa in layer ALS and AGI, 1.5 MPa in T layer, while the resistance qc reaches 8 MPa within layers ATG and D. In the first 40 m b.g.l., the resistance ratio (Fr%=local lateral resistance/point resistance %) is up to 6 only within layer R while its average value is generally close to 4 in the remnant part of the soil column.

Taking into account the results of the CPTU tests, layers T, AGI and ATG are classified (Robertson, 1986; Robertson and Fear, 1995) as clay and silty clays with organic matter while layers R and ALS are classified as silty sands and clayey silt respectively (Fig.6). Moreover, according to the empirical relation by Baligh (1975) the undrained cohesion resulting for the distinguished lithotechnical groups were also derived (Table 1).

Three undisturbed samples were collected at the Galba test-site from the S2 borehole and were tested at the Laboratorio di Geotecnica (Torino Polytechnic laboratory) via resonant column (RC); only two of them were also tested via cyclical torsional shear at 1Hz (TTC_1Hz). Standard procedures were taken into account to select the TTC test frequency as well the results obtained by Rovelli et al. (1995) and by Bozzano et al. (2008b) in previous numerical modelling of the seismic response of the main Tiber valley. The confining

228 pressures for dynamic tests were estimated on the basis of a vertical propagation of shear
229 wave model, i.e. they were computed for a saturated soil along the vertical direction.

230 The tested samples were collected as follows: one from the high compressibility inorganic
231 silty clay AGI layer (19.50 – 20.20 m from ground level, S2 C2), one from the peat T layer
232 (25.50 – 26.20 m from ground level, S2 C4) and one from the high consistency clay of the
233 UMV (49.00 – 49.30 m from ground level, S2 C5).

234 According to the results obtained by Bozzano et al. (2008b) for the main Tiber valley, the
235 dynamic deformability properties of the tested samples (Fig.7) reveal an accentuated
236 distinction between the alluvial covers and the Pliocene clay bedrock, corresponding to a
237 shear modulus difference of about 100 MPa. On the contrary, a smaller difference (lower than
238 20 MPa) was measured between the T and the AGI alluvial deposits (Fig.7a).

239 The linearity threshold (γ_l) corresponds to shear strains within range 0.003-0.007% for the
240 UMV and within the range 0.004%-0.01% for the tested alluvial deposits (i.e. T and AGI
241 layers) (Fig.7a). The plasticity threshold (γ_v) (Fig.7c) ranges from 0.04% to 0.14% for the
242 alluvial horizons (samples S2 C2 –AGI – and S2 C4 – T – respectively) while the same
243 threshold is about 0.02% for the UMV.

244 The normalised shear modulus decay curves (G/G$_0$ vs γ) proposed in the paper Sun et al.,
245 1988; Vucetic and Dobry, 1991, Ishibashi and Zang, 1993, Zhang et al. 2005 are generally in
246 disagreement with the laboratory results reported here for the inorganic silty clays of AGI
247 layer (Fig.8). These results are very similar to the ones obtained by Bozzano et al. (2008b) for
248 the silty clays of the C layer in the main Tiber valley. The observed differences with the ones
249 proposed by the studies do not only concern the shape of the curves, but also the values of the
250 linearity threshold. A marked inconsistency (curve shape and threshold values) is noted with
251 respect to the curves proposed by Vucetic and Dobry (1991) for the corresponding plasticity
252 index (PI) of 50% (Fig.8a). On the other hand the decay curves $G/G_0(\gamma)$ resulting in the peat T
253 layer are very similar to the curves proposed by Vucetic and Dobry (1991) for the high
254 plasticity soils (PI of about 100%) while, on the contrary, the effective PI for the peat layer T
255 is lower than 15%. These results are in very good agreement with the data by Stokoe et al.
256 (1996) and by Boulanger et al. (1998), derived by dynamic characterisation via cyclic
257 laboratory tests performed on peaty organic soils.

258 However, sample S2 C2 (AGI) responded to dynamic tests with decay curves $G/G_0(\gamma)$ that
259 are very similar to those reported by Ishibashi and Zhang (1993) (Fig.8b). The experimental

curves proposed in this paper are very different to the ones reported in the studies. Moreover, strong differences are evident whilst comparing the curves proposed by Sun et al. (1988) and largely used in software codes for modelling local seismic response and decay of NC clay (Fig.8c).

The normalised decay curves obtained for the AGI samples of the Grottaperfetta alluvia fill are included within the variability-range of the experimental decay curves obtained for the Holocene alluvial clay in Nocera Umbra by Crespellani et al. (2001), for the Catania alluvial clay by Carruba and Maugeri (1988), for the Pisa clay (layer B) by Lo Presti et al. (2002) and for the C layer of the main Tiber valley by Bozzano et al. (2008b) (Fig.9). Moreover, the obtained decay curves fit the relation proposed by Hardin and Drnevich (1972a,b) well. In particular, for the tested clay (layer AGI) the interpolation function according to the Hardin and Drnevich (1972) relation is (Fig.9a):

$$G/G_0 = 1/(1+(14.50 \, \gamma\%^{1.248}))$$

For all the tested samples, damping values (D%) remain in the 5% range, below the plasticity threshold.

On the basis of the same Hardin and Drnevich (1972a,b) function, the damping decay curves obtained for the layer AGI may be expressed by the relation (Fig.9b):

$$D\% = 21 \exp(-2.57 \, G/G_0)$$

The comparison of the physical and mechanical properties of the 7 lithotecnical groups distinguished in the Grottaperfetta valley at Galba test-site as well as the lithotecnical groups defined in the main Tiber valley by Bozzano et al. (2000), whose dynamic properties were obtained by Bozzano et al. (2008b), supports the attribution of $G/G_0(\gamma)$ decay curves to the other layers of the alluvial deposits and are not specifically characterised by laboratory tests at Giustiniano Imperatore (Fig.10). In particular, the dynamic behaviour of the ATG layer at Galba test site has been assimilated to the dynamic behaviour of the C layer derived at Valco S.Paolo by the means of in site and laboratory tests.

The dynamic properties derived from RC tests for the Grottaperfetta peaty T layer, are in good agreement with the findings obtained by other Authors (Boulanger et al., 1998; Boulanger et al., 2001) on similar deposits (Sherman Island peaty organic soil). Therefore, it is worth noting that the $G/G_0(\gamma)$ decay curves obtained for the Grottaperfetta peats (T layer) are very close to the same curves derived for the Sherman Island peats, sampled below a 10 m

thick layer of levee fill (Fig. 10). These conditions can be regarded as very similar to the ones referred to the Grottaperfetta peaty layers since they are involved in an ongoing consolidation processes due mainly to the man-made fill loads (Stramondo et al., 2008). On the contrary, the same peaty deposits, sampled in free field conditions (i.e. at similar depth but far from levee fill) show a quite different behaviour. They are characterised by a further continuous reduction of the dynamic shear modulus with increasing shear strain beginning at the smallest strain (about 0.001%). The same comparison shows relevant differences between dynamic behaviour of Grottaperfetta inorganic clays (AGI layer) and the Sherman Island peaty organic deposits.

Based on the obtained geomechanical properties as well as on the log-stratigraphic borehole data, only layer R and G can be directly related to the corresponding deposits in the Tiber River alluvial valley according to Bozzano et al. (2000), Corazza et al. (1999) and Amorosi et al. (2002). On the other hand, layer ATG can be laterally extended toward the layer C of the main Tiber River valley while layer ALS can be laterally extended towards layers A, B and C of the main Tiber River valley. Layers AGI and T, on the contrary, have no lateral continuity within the alluvial body of the main Tiber River valley and, for this reason, they can be regarded as peculiar for the Grottaperfetta lateral valley.

6. S-WAVE VELOCITY PROFILES FROM SEISMIC NOISE DATA

Arrays of seismic noise recording stations were designed to obtain S-wave velocity (Vs) profiles located along the axis of the Grottaperfetta valley (Fig.2c), i.e. Leonardo, Galba and Giardinetti sites. Nevertheless, since no down-hole or cross-hole data are available for the Grottaperfetta valley, in order to obtain reference Vs-stratigraphy to better fit the seismic noise measurements, use was made of unpublished data referring to both to another lateral valley (Vallerano valley in Fig. 18, left tributary of the Tiber river and located south of the Grottaperfetta one), as well as of the down-hole data from the of Valco San Paolo test site referred to the Tiber river valley (Bozzano et al., 2008b). The attribution of the Vs values were initially based on engineering - geology criteria due to the similarity of the lithotechnical units as well as the possible correlation between the considered alluvial deposits both in the lateral and in the main Tiber river valley.

The success of these criteria in order to extrapolate Vs profiles for alluvial deposits was previously demonstrated by the Authors (Bozzano et al. 2008b) by using the inversion of ambient noise tests as a validation of the extrapolation of the Vs profiles.

The derived S-wave velocity (Vs) profiles (Fig. 11) show a maximum value (713 m/s) in correspondence with the gravels (layer G), while the slowest layer (140 m/s) corresponds to the peats (layers T). Nevertheless, in agreement with the deepening of the geological substratum, which is a result of the contouring reported in Fig.2, the Vs value of 713 m/s is reached at different depths, these last ones increasing from section A (Giardinetti site) to section C (Leonardo site) of Fig.5 (i.e. toward the Tiber River alluvial valley). In particular, in correspondence with the soil column A (along section A – Giardinetti site) the maximum Vs value is reached at 26 m b.g.l. while in correspondence with the soil column C (along section C – Leonardo site) the same value occurs at 53 m b.g.l.. Moreover, it's worth noticing that all along section B and section C (i.e in correspondence with the related soil columns) the sandy layer D overlays the gravels (G layers) and, as a consequence, the Vs values sharply increases to about 300 m/s. On the other hand, all along section A (i.e. columns A and A1) the same value is of about 500 m/s, since the ATG level directly overlays the G level.

In order to perform the seismic noise measurements, we used ten REFTEK-130 stations, equipped with Lennartz LE-3D 5/s sensors; the sampling rate was 1000 samples/s. The arrays have a triple equilateral triangle geometry with the central station located in the middle of the basin (Fig. 13). The external triangle (a side of about 100 m) was used to reach higher depths and to sample smaller wave numbers. The intermediate internal triangle was used instead to prevent spatial aliasing due to high wave numbers otherwise sampled as low (Wathelet et al., 2004). A further internal triangle was added to improve and account for high frequencies.

In the case of the array performed at the Galba site, two stations were removed from the analysis: TR13 and TR22. The former did not record due to malfunctioning whereas the latter was too close to a wide underground car park. This cavity adversely affected the data analysis so much that we were forced to remove it from the database.

In the case of the arrays performed at the Leonardo and Giardinetti sites, stations three and one (Fig.14), were removed from the dataset. In both sites such stations were located very close to the edge of the Grottaperfetta valley where the near-surface geology is far from a model of plane and parallel layers. This is why their H/V spectral ratios were very different from the spectral ratios of the other stations. Considering that, in a circular array, the depth of investigation is 2 – 6 times the radius of the array (Tokimatsu, 1995) and the layer of interest

354   in this case study was equal to about 50 m, the arrays made it possible to investigate the entire

355   vertical velocity profile of the site.

356   In order to quantify, the dependence of the spatial aliasing on the azimuth in the (K_x, K_y)

357   wave number domain, the array transfer function (ATF) was computed for the array geometry

358   (Fig. 14); ATF was used to estimate the array performance (Woods and Lintz, 1973; Asten

359   and Henstridge, 1984). As in Bozzano et al. (2008), K_{max} was defined as the wave number

360   distance between the main peak and the closest side lobe exceeding 50% of main lobe

361   magnitude (Fig. 14).

362   The maximum wave number resolution of the array was chosen as $K_{max/2}$, while the radius of

363   the main peak taken at its mid height provides the lowest wave number, K_{min}, that can be

364   resolved (Di Giulio et al., 2006; Bozzano et al., 2008b). This choice was made to avoid alias

365   effects as much as possible.. The obtained definitions of K_{min} and $K_{max/2}$ were within the

366   range of the empirical indication of Tokimatsu (1995). For data analysis, we resorted to the

367   SESARRAY software package, which was developed as part of the European SESAME

368   project (Site Effects Assessment using Ambient Excitations, Project EVG1-CT 2000-00026,

369   available under GPL license; see www.geopsy.org).

370   At first, the spectral ratios of the horizontal and vertical components of the noise field (H/V

371   ratios, Nogoshi and Igarashi (1971); Nakamura (1989, 2000) were computed, at all the

372   stations, with a view to identify the fundamental frequencies around which energy would

373   concentrate (Lermo and Chavez-Garcia, 1993). The graphs of Fig. 14 exemplifies, for each

374   array, the H/V ratio of one of the stations. All H/V spectral ratios were computed through an

375   anti-trigger software implemented within the SESAME project (SESAME deliverable no.

376   D09.03, http://sesame-fp5.obs.ujf-grenoble.fr/SES_TechnicalDoc.htm). According to the

377   SESAME deliverables D18.06-Wp, D19.06-Wp and D24.13-Wp (see http://sesame-

378   fp5.obs.ujf-grenoble.fr/SES_TechnicalDoc.htm for details), the peaks of the H/V curves may

379   be regarded as representative, since spectral ratios are in the range of $3 - 4$ and constant

380   throughout the array. In addition, the standard deviation is less than 3 for all the stations.

381   Based on these findings, the near-surface geology of the three sites can be approximated to

382   a model consisting of plane and parallel layers, which can be more easily run with the

383   SESARRAY software.

384   Under the assumption that both the noise wavefield are mainly composed of surface waves

385   and the Rayleigh waves are predominant (compared to body waves) in the vertical motion

386   (Tokimatsu, 1995), the Rayleigh wave dispersion curve was built using 30 minutes of noise

387   array recording of the vertical components.

The Rayleigh dispersion curve obtained (red curves in the right panel in Fig.15) corresponds to the theoretical ones, computed by using the Galba site velocity profile (Fig.15). The frequency-wave number (f-k) method of Capon (1969) has been adopted to compute the Rayleigh wave dispersion curves, whereas the numerical implementation that we used, comes from SESAME project (Ohrnberger, 2004a; Ohrnberger et al., 2004b). In Figure 13, due to the array geometry, the spatial aliasing curves are also plotted. The comparison theoretical/experimental Rayleigh dispersion curves holds in the frequency range where the dispersion curve is reliable, i.e. between the minimum and maximum resolvable wave-lengths.

With reference to Fig.15, the upper frequency limit was chosen as the intercept of the dispersion curves with the aliasing curve corresponding to $K_{max}/2$ defined from ATF (Scherbaum et al., 2003; Wathelet et al., 2004). Even though the lower limit is usually fixed around the local resonance frequency of the sites (Di Giulio et al., 2006), due to the used array geometry, it was necessary to fix such a lower frequency limit as the intercept of the dispersion curves with the aliasing curve corresponding to $K_{min}/2$. Good compatibility was obtained between the theoretical and the experimental dispersion curves (Fig. 15) at the three test sites, confirming the validity of the Vs profiles which have been reconstructed by means of engineering-geology criteria.

7. 1D NUMERICAL MODELLING OF SEISMIC SHAKING

A 1D numerical modelling was performed by using the software SHAKE1D in order to obtain the shear strains, expected as an effect of a strong motion shaking. The 1D models were derived for the three different columns whose stratigraphies are described in the previous paragraph 4 (Fig.11) and which were obtained from the geological cross sections (Fig. 5) located along the Grottaperfetta valley: at its upper part (column A – Giardinetti site, Fig.2), in its middle part (column B – Galba site, Fig.2) and close to its confluence with the main Tiber valley (column C – Leonardo site, Fig.2).

Nevertheless, one more stratigraphic log has been considered along the Giardinetti site section to take into account the changes of depth and composition of the geological substratum, which result along the section, moving from north to south. For this reason, a first stratigraphic log is referred to the southern portion of the Giardinetti site cross section (column A) where the geological substratum is characterised by Paleotiber deposits while a second stratigraphic log is obtained moving northward along the same section, where the

421 Paleotiber deposits seem to be eroded and the UMV formation directly underlies the alluvial
422 fill (column A1).

423 Except for columns A and A1, which are respectively composed of 8 and 6 layers above the
424 bedrock, both columns B and C are composed of 7 layers above the bedrock (Fig.11).

425 The values of both the physical properties and the dynamic parameters for all the modelled
426 layers (Table 1, Fig. 12) were attributed on the basis of both the performed lab-test and the in-
427 site derived Vs profiles. These values, which are plotted in Fig.11 along the corresponding
428 stratigraphic logs, point out that the basal coarsely grained G layer produces a significant
429 inversion of values within the vertical Vs profile (up to about 200 m/s) with respect to the
430 high consistency UMV clays. A minor inversion of Vs values (lower than 100 m/s) results in
431 correspondence of the T layer (i.e., in the range 20 – 25 m b.g.l.) along all the considered
432 logs . Another significant inversion of the Vs values results at about 30 m b.g.l. along column
433 A (i.e., Giardinetti site cross section, southern portion), within the Paleotiber sandy gravels
434 (layers G_{Pl} and D_{Pl}).

435 Despite historical reports of major seismic events in the entire the Roman area (Ambrosini et
436 al., 1986; Cifelli et al., 2000), records of strong motion have so far been scarce, making it
437 impossible to estimate the ensuing felt shaking.

438 The spectra of the possible ground motion in the city of Rome stochastically derived by
439 Rovelli et al. (1994) show that the spectral contribution of 1 to 10 Hz for the earthquakes
440 expected from the Colli Albani hills is lower than the one from the central Apennines. For the
441 Colli Albani hills, the frequency contribution of felt earthquakes is above 5 Hz, whereas the
442 one for the central Apennines (at higher distance) is more significant at lower frequencies, i.e.
443 0.5 to 5 Hz. In terms of peak ground acceleration (PGA), the values expected from an
444 earthquake of magnitude 7 at a distance of 100km range roughly from 0.03g to 0.13g. These
445 values are in line with the PGA recurrence for 475 years according to the most recent Italian
446 hazard maps (INGV, 2006).

447 Based on the previously discussed considerations the two synthetic reference earthquakes for
448 1D numerical modelling have been derived according to Rovelli et al. [1994] and with
449 reference to the central Apennines seismic source, i.e.: i) to an event of magnitude Ms=7.0
450 with epicentre at a distance of 80km from Rome and having a PGA of 0.06g, which may be
451 regarded as representative of the maximum expected seismicity in the entire urban area, and
452 ii) to an event of magnitude Ms=7.0 with epicentre at a distance of 100km from Rome and
453 having a PGA of 0.04g.

The two synthetic accelerograms were built by using the Strong Motion SIMulation (SMSIM) (Boore, 2000) numerical software, which is based on a random generation of white noise time series. As the spectra of these time series depend on the seismic moment and on the stress drop (Anderson and Hough, 1984), they can be used to derive time-history series of ground motion obeying the theoretical spectral model adopted for the earthquake under study (Boore, 1983; Calderoni et al., 2005).

The transfer function A(f) was analysed in the 1-10 Hz frequency range both in linear and linear-equivalent solutions (Fig. 16). For all the considered columns, the 1D-modeled first resonance frequency shows a very good fit with the HVSRs from the seismic noise measurements, according to the Nakamura technique. Here it is worth noting that the results by numerical modelling obtained for the soil column A were compared with the noise measurements performed at the only station of the seismic noise array which is distinguished in Fig.18 by an empty circle, since its response can be considered representative for the southern portion of the Grottaperfetta valley along section A of Fig. 2 (Giardinetti site). Moreover, since the ambient noise records have a good fit with the simulated effects, this allows neglecting possible 2D resonance effects, *sensu* Bard and Bouchon (1985). Nevertheless, no reliable comparison can be done between the HVSRs from the seismic noise array and the A(f) numerical modelled frequency peaks, referred to the higher mode of resonance of the soil column (Thomson et al., 2009).

The maximum values of the A(f) function result equal to about 3.5 result from the numerical modelling within the very close frequency range 1 – 1.5 Hz.. Nevertheless, if both the high compressibility T and AGI layers are not considered and substituted by the ATG silty clay layer, the A(f) maximum values are equal to about 2.5 and they result slightly shifted within the frequency range 2 – 1 Hz, moving from the head of the Grottaperfetta valley toward its confluence with the main Tiber valley. On the basis of these findings it's worth highlighting that the low velocity layers (corresponding to AGI and T alluvial horizons) stretch the amplified frequency down to 1 Hz all along the considered valley without a significant increase of the maximum resulting A(f) values.

The effect due to the presence of T and AGI layers within the alluvial fill of the Grottaperfetta lateral valley was also highlighted by computing the theoretical Haskell-Thomson transfer functions (HT), for four soil columns obtained along a geological section that cuts transversally a part of the Tiber valley and longitudinally the Grottaperfetta tributary valley (Fig.17). Among these columns, three correspond to those previously considered at the

487 Giardinetti (A1), Galba (B) and Leonardo (C) sites, while the last one corresponds to the

488 Valco S.Paolo test-site (Bozzano et al., 2008b).

489 A three-layer model was adopted for each soil column by distinguishing soft alluvial deposits

490 (i.e. silty clays or silty sands) with an average Vs of 260 m/s, a basal layer of stiff gravels

491 with a Vs of 713 m/s and a geological bedrock composed of high consistency stiff clays with

492 a Vs of 461 m/s. The obtained theoretical HT functions (HT_{th}) were compared to the

493 normalised HT functions (HT_{rl}) obtained for the effective stratigrafic logs. The comparison

494 (Fig.17) showed that the HT_{rl} functions show a constant value of the first resonance mode at

495 about 1Hz moving from the Tiber valley (i.e. Valco S.Paolo) toward the head of the

496 Grottaperfetta Valley (i.e. Giardinetti) while, on the contrary, the HT_{th} functions show a shift

497 of the first resonance mode up to 2 Hz, moving in the same direction. As a consequence, the

498 low velocity layers T and AGI, which are inter-layered within the alluvial fill of the

499 Grottaperfetta valley, can be regarded as responsible for equalizing the first resonance mode

500 of the alluvia. A gradual increase of the Vs value within the UMV was also taken into

501 account in the 1D numerical solutions, performed under linear equivalent conditions, in order

502 to consider the effects due to the previously described geological evolution of the area, i.e.

503 UMV erosion as a consequence of the strong fluvial incision of the valley during the Würm

504 glacial period. This fluvial erosion and the associated processes of releasing (Bozzano et al.

505 2006b) and weathering involved the UMV, producing a layer of softened clays below the

506 present bottom of the alluvial fill, which can be estimated about 15m thick softened stratum

507 of UMV clays can be considered (Tommasi et al., 1996; Bozzano et al., 2006a; 2006b;

508 Bozzano et al., 2008a). In particular, the softening of UMV clays has been reproduced by

509 assuming a multilayer composed of 5 sub-layers, each one 3 m thick and with Vs values

510 linearly increasing from 480 m/s up to 900 m/s. Under these conditions, the numerical

511 modelling outputs no so relevant increase of the maximum A(f) values as well as of the first

512 resonance value of the frequency, related to the first resonance mode (Fig.16).

513 The role of the T and of the AGI layers within the alluvial fill of the Grottaperfetta valley was

514 also analysed in terms of maximum shear strain, expected along the considered columns

515 under the modelled seismic shaking (Fig. 18). The results highlight that the layers highest

516 values of shear strain (up to 0.1%) is reached within the peaty layer (T); nevertheless,

517 plasticity conditions are not reached within this layer due to the very wide dynamic plasticity

518 field (γ_l-γ_v) which characterize its $G/G_0(\gamma)$ decay curve. On the contrary, plasticity conditions

519 are reached within both the AGI and the ATG layers due to their significantly closer dynamic

plasticity field layers. If the AGI and the T layers are not considered in the stratigraphic logs and substituted with the ATG layer, the maximum shear strain within the alluvial deposits do not exceed the value of 0.03% and no plasticity deformations occur during the seismic shaking.

Since the above mentioned AGI and T layers which typify the alluvial deposit of the Grottaperfetta lateral valley with respect to the Tiber valley, are also present within the alluvial deposits which fill the lateral valleys of the left side tributaries of the Tiber (Campolunghi et al., 2007) in the southern portion of the Rome urban area (Fig.19), our obtained results highlight that all these lateral valleys can be characterised by proper seismic strain effects, strictly related to the mechanical properties of the low velocity alluvial layers. On the other hand, the same AGI and T layers have been considered by some Authors (Stramondo et al., 2008; Ascani et al., 2008) to be responsible for the ongoing settlements within the alluvial fill of the valley; as a consequence, some peculiar features of the lateral valleys, in terms of mechanical behaviour, can be recognised under both static and dynamic conditions.

8. CONCLUSIONS

Engineering-geology and geophysical studies based on seismic array noise measurements were carried out at the Galba test-site, located 2 km south of Rome's historical centre. This study refers to the 40m thick alluvial fills of the Grottaperfetta valley (hosting the Giustiniano Imperatore area), located on the left-side with respect to the main Tiber valley. The present reconstructed engineering–geology model of the alluvial deposits which fill the Grottaperfetta valley demonstrates that: i) based on homogeneous lithotechnical features, seven horizons (R, ALS, AGI, T, ATG, D, G) can be identified within the alluvial body, respectively constituted by man-made fill, low-consistency sandy-silty clays, very low consistency inorganic clays, peats, low consistency clays, coarse grained sands and gravel; ii) a significant velocity contrast (equal to about 200 m/s) occurs between the alluvial body of the valley (including the layers R, ALS, AGI, T, ATG) and the basal sandy gravel deposits (layers D and G) that overlie the Marne Vaticane (UMV) geological substratum; ii) a minor velocity contrast (up to about 100 m/s) is found within the alluvial deposits in correspondence with the organic peaty deposits (T layer).

Very low S-wave velocities (<180 m/s) characterise the organic T layer as well as the high compressibility inorganic AGI layer. Based on these findings, a 1D numerical modelling was performed by the software SHAKE1D to reconstruct the vertical maximum shear strain distribution that could be obtained in response to the maximum expected earthquake for the city of Rome (i.e. M=7 earthquake for the Central Apennine seismic sources). The modelling results infer that the major shear strains occur in the low consistency layer of inorganic clays (AGI layer) but, above all, within the organic clays including peats (T layer). In particular, the lab-derived dynamic behaviour of the peaty T layer, which is characterised by a plastic field significantly wider that the one related to the adjacent inorganic clay layers (AGI and ATG), justifies that no plasticity conditions are reached within the peats, even if shaking due to strong motion is considered (i.e., M=7 earthquake from Central Apennines). Moreover, the performed numerical simulations do not point to any relevant variations of the first resonance frequency along the Grottaperfetta valley . This is also true for the maximum value of the numerical transfer function A(f) under different modelling conditions (i.e. gradual increase of Vs within the UMV geological substratum; absence of both T and AGI layer, linear and linear-equivalent simulation solutions).

On the other hand, the AGI and the T layers are responsible for equalizing the local seismic amplification since a constant frequency peak of about 1 Hz characterises the Grottaperfetta valley moving from the head of the valley towards its confluence with the Tiber valley, instead of expecting a slight decrease (i.e. from 2 to 1 Hz) along the same direction of the theoretically expected first resonance frequency .

Since low velocity deposits, such as inorganic clays and peats of the layers T and AGI sampled in the Grottaperfetta valley are generally included within the alluvial fills of many lateral valleys, the present results in terms of dynamic behaviour, seismically-induced shear strains and local seismic amplification can be reliably extrapolated to other contexts in the urban area of Rome as they are characterised by very similar geological features (such as Caffarella, Tre Fontane, Cecchignola, Fioranello, Vallerano, Tor di Valle alluvial valleys), where low consistency deposits with high compressibility inorganic clays or peats are present.

REFERENCES

Amato A, Chiarabba C, Cocco M, Di Bona M, Selvaggi G (1994) The 1989-1990 seismic swarm in the Alban Hills volcanic area, central Italy. Jour. of Volc. and Geoth. Res. 61: 225-237.

Ambrosini S, Castenetto S, Cevolan F, Di Loreto E, Funiciello R, Liperi L, Molin D. (1986) Risposta sismica dell'area urbana di Roma in occasione del terremoto del Fucino del 13-1-1915. Mem. Soc. Geol. It. 35:445-452.

Amorosi A, Lembo Fazio A, Scarpelli G (2002) Interazione tra una struttura esistente e lo sviluppo urbano circostante: l'esempio dell'ex Vasca Navale di Roma. In Proceedings of the XXI Convegno Nazionale di Geotecnica–Opere Geotecniche in ambiente urbano, L'Aquila 11-14 Settembre 2002, 323-330.

Anderson, J. G. and S. E. Hough (1984), A model for the shape of the Fourier amplitude spectrum of acceleration at high frequencies. Bull. Seism. Soc. Am., 74, 1969-1994.

Ascani F, Bozzano F, Buccellato A, Del Monte M, Matteucci R, Vergari F. (2008) Evoluzione del paesaggio e antiche vie di drenaggio nell'area de "Il Castellaccio" (Roma) da indagini geologiche, geomorfologiche e archeologiche. Geologica Romana 41:93-116.

Asten MW, Henstridge JD (1984) Array estimators and use of microseisms for reconnaissance of sedimentary basins. Geophysics 49:1828-1837.

Baligh MM (1975) Theory of deep site Static Cone Penetration Resistance. Research Rep. R75-56. Dept. of Civ. Engng. MIT; Cambridge – Mass. (USA).

Bard PY, Bouchon M (1995) The seismic response of sediment-filled valleys. Part2. The case of P and SV waves. Bull. Seism. Soc. Am. 70:1921-1941.

Basili R, Valensise G, Vannoli P, Burrato P, Fracassi U, Mariano S, Tiberti MM, Boschi E (2008) The Database of Individual Seismogenic Sources (DISS), version 3: summarizing 20 years of research on Italy's earthquake geology. Tectonophysics doi:10.1016/j.tecto.2007.04.014

Boore DM (2000) SMSIM-FORTRAN programs for simulation ground motions from earthquakes: version 2.0-A revision of OFR 96-80A, U.S. Geol. Surv. Open-file Rept. 00-509, available at http://geo-pubs.we.usgs.gov//open-file/of00-509/.

Boschi E, Caserta A, Conti C, Di Bona M, Funiciello R, Malagnini L, Marra F, Martines G, Rovelli A, Salvi S (1995) Resonance of subsurface sediments: an unforeseen complication for designers of roman columns. Bull. Seism. Soc. Am. 85:320-324.

Boulanger RW, Arulnathan R, Harder LF, Torres RA, Driller MW (1998) Dynamic properties of Sherman Island Peat. Journal of Geotechnical and Geoenvironmental Engineering 1998:12-20

Boulanger RW, Harder LF, Driller MW, Wehling TM (2001) Confinement and disturbance effects on dynamic properties of fibrous organic soil. Proc. XV ICSMGE satellite Conference on "Lessons learned from recent strong earthquakes", 25 August 2001, Istanbul, Turkey, 211-217.

Bozzano F, Andreucci A, Gaeta M, Salucci R (2000) A geological model of the buried Tiber River valley beneath the historical centre of Rome. Bull. Eng. Geol. Env. 59:1-21.

Bozzano F, Gaeta M, Marcoccia S. (2006a) Weathering of Valle Ricca stiff and jointed clay, Engineering Geology 84(3-4):161-182.

Bozzano F, Martino S, Priori M. (2006b) Natural and man-induced stress evolution o slopes: the Monte Mario hill in Rome, Environmental Geology 50:505-524.

Bozzano F, Bretschneider A, Martino S (2008a) Stress-strain history from the geological evolution of the Orvieto and Radicofani cliff slopes (Italy). Landslides 5(4):351-366.

Bozzano F, Caserta A, Govoni A, Marra F, Martino S (2008b) Static and dynamic characterization of alluvial deposits in the Tiber River Valley: new data for assessing potential ground motion in the city of Rome. Journal of Geophysical Research 113: B01303, doi: 10.1029/2006JB004873.

Calderoni G, Rovelli A, Cultrera G, Azzara R M, Di Giulio G (2005) Assessement of ground motion in Palermo, Italy, during the 6 September 2002 MW 5.9 earthquake using source scaling law. Bull. Seism. Soc. Am. 95:2342-2363.

Campanella RG, Robertson PK, Gillespie DG, Grieg J (1985) Recent developments in in-situ testing of soils. In the Proceedings of the 11th International Conference on Soil Mechanics and Foundation Engineering, San Francisco 2:849-854.

Campolunghi MP, Capelli G, Funiciello R, Lanzini M (2007) Geotechnical studies for foundation settlement in Holocenic alluvial deposits in the City of Rome (Italy). Engineering Geology 89:9–35

Carrubba P, Maugeri M (1988) Determinazione delle proprietà dinamiche di un'argilla mediante prove di colonna risonante. Rivista Italiana di Geotecnica 22(2):101-113.

Cifelli F, Donati S, Funiciello F, Tertulliani A. (2000) High-Density Macroseismic Survey in Urban Areas. Part 2: Results for the City of Rome, Italy. Bulletin of the Seismological Society of America 90(2):298-311.

Cinti FR, Marra F, Bozzano F, Cara F, Di Giulio G, Boschi E (2008) Chronostratigraphic study of the Grottaperfetta alluvial valley in the city of Rome (Italy): investigating possible interaction between sedimentary and tectonic processes. Annals of Geophysics, 51(5-6):849-868.

Corazza A, Lanzini M, Rosa C, Salucci R (1999) Caratteri stratigrafici, idrogeologici e geotecnici delle alluvioni tiberine nel settore del centro storico di Roma. Il Quaternario 12:215-235.

Crespellani T. Madiai C, Simoni G, Vanucchi G (2001) Dynamic geotechnical testing and seismic response analyses in two sites of the Commune of Nocera Umbra, Italy. Rivista Italiana di Geotecnica 35(4):39-52.

Di Giulio G, Cornou C, Ohrnberger M, Wathelet M, Rovelli A (2006) Deriving wavefield characteristics and shear-velocity profiles from two-dimensional small-aperture arrays analysis of ambient vibrations in a small-size alluvial basin, Colfiorito, Italy. Bull. Seism. Soc. Am. 96(5):1915-1933.

DISS Working Group (2009). Database of Individual Seismogenic Sources (DISS), Version 3.1.0: A compilation of potential sources for earthquakes larger than M 5.5 in Italy and surrounding areas. http://diss.rm.ingv.it/diss/, © INGV 2009 - Istituto Nazionale di Geofisica e Vulcanologia - All rights reserved.

Fäh D, Iodice C, Suhadolc P, Panza GF (1993) A new method for the realistic estimation of seismic ground motion in megacities: the Case of Rome. Earthquake Spectra 9:643-668.

Funiciello R, Lombardi L, Marra F, Parotto M (1995) Seismic damage and geological heterogeneity in Rome's Colosseum area: are they related? Annali di Geofisica 38(3): 267-277.

Hardin BO, Drnevich VP (1972a) Shear modulus and damping in soil: measurement and parameter effects. Journal of the Soil mechanics and Foundation Engineering Division - ASCE 98(6):603-624.

Hardin BO, Drnevich VP (1972b) Shear modulus and damping in soil: design equations and curves. Journal of the Soil mechanics and Foundation Engineering Division - ASCE 98(7):667-692.

Ishibashi I, Zhang X (1993) Unified dynamic shear moduli and damping ratios of sand and clay. Soils and Foundations 33(1):182-191.

INGV (2006), Mappa di pericolosita` sismica del territorio nazionale. Available at http://zonesismiche.mi.ingv.it/mappa_ps_apr04/italia.html

INGV (2009), Mappa sul risentimento macrosismico del terremoto del 6 Aprile 2009. http//terremoto.rm.ingv.it

Lermo J, Chavez-Garcia FJ (1993) Site evaluation using spectral ratios with only one station. Bull. Seism. Soc. Am. 83:1574–1594.

Lo Presti D, Jamiolkowski M, Pepe M (2002) Geotechnical characterisation of the subsoil of Pisa Tower. In Characterization and Engineering Properties of Natural Soils Balkema, Rotterdam, 2:909-946,.

Marra F, Rosa C (1995) Stratigrafia e assetto geologico dell'area romana, in "La Geologia di Roma. Il Centro Storico", Memorie Descrittive della Carta Geologica d'Italia (special issue) 50:49-118.

Moczo P, Rovelli A, Labak P, Malagnini L (1995) Seismic response of the geologic structure underlying the Roman Colosseum and a 2-D resonance of a sediment valley. Annali di Geofisica 38(5-6): 939-956.

Molin D, Guidoboni E (1989) Effetto fonti, effetto monumenti a Roma: i terremoti dell'antichità a oggi, in I Terremoti prima del Mille in Italia e nell'Area Mediterranea, Edited by E. Guidoboni, S.G.A., Bologna, 194-223.

Molin D, Ambrosini S, Castenetto S, Di Loreto E, Liperi L, Paciello A (1986) Aspetti della sismicità storica di Roma. Mem. Soc. Geol. It. 35:439-448.

Nakamura Y (1989) A method for dynamic characteristics estimation of subsurface using microtremor on the ground surface. Q. Rep. Railway Tech. Res. Inst. 30(1):25–33.

NakamuraY (2000) Clear identification of fundamental idea of Nakamura's technique and its applications. In Proc. 12th World Conference on the Earthquake Engineering, Auckland, New Zealand.

Olsen KB, Akinci A, Rovelli A, Marra F, Malagnini L (2006) 3D ground-motion estimation in Rome, Italy. Bull. Seism. Soc. Am. 96(1):133-146.

Ohrnberger M (2004a) User manual for software package CAP—a continuous array processing toolkit for ambient vibration array analysis, SESAME report D18.06, http://sesame-fp5.obs.ujfgrenoble.fr.

Ohrnberger M, Schissele E, Cornou C, Bonnefoy-Claudet S, Wathelet M, Savvaidis A, Scherbaum F, Jongmans D (2004b) Frequency wavenumber and spatial autocorrelation methods for dispersion curve determination from ambient vibration recordings. In Proc. 13th World Conference on Earthquake Engineering, Vancouver, B.C., Canada, 1–6 August 2004, paper no. 0946.

Riguzzi F,Tertulliani A (1993) Re-Evaluation of Minor Events: The Examples of the 1895 and 1909 Rome Earthquakes. Natural Hazards 7:219-235.

Robertson PK, Campanella RG, Gillespie D, Greig J (1986) Use of Piezometer Cone Data. Proc. Int. Symp. IN SITU '86, Blacksburg USA.

Robertson PK, Fear CE (1995) Liquefaction of sands and its evaluation, IS TOKYO 95, First International Conference on Earthquake Geotechnical Engineering, Keynote Lecture, November 1995.

Romeo R, Paciello A, Rinaldis D (2000) Seismic hazard maps of Italy including site effects. Soil Dyn. and Earth. Eng. 20:85–92.

Rovelli A, Caserta A, Malagnini L, Marra F (1994) Assessment of potential strong motions in the city of Rome, Annali di Geofisica 37:1745-1769.

Rovelli A, Malagnini L, Caserta A, Marra F (1995) Using 1-D and 2-D modelling of ground motion for seismic zonation criteria: results for the city of Rome, Annali di Geofisica 38(5-6):591-605.

Scherbaum F, Hinzen KG, Ohrnberger M (2003) Determination of shallow shear wave velocity profiles in the Cologne, Germany area using ambient vibrations. Geophys. J. Int. 152(3):597–612.

Semblat JF, Pecker A (2009) Waves and vibrations in soils: earthquakes, traffic, shocks, construction works. IUSS Press (Pavia, Italy), 499.

Stokoe KH, Bay JA, Rosenbald BL, Hwang SK, Twede MR (1970) In situ seismic and dynamic measurements of geotechnical materials at Queensboro Brisge and Roosevelt Island. Geotechnical Engineering Report, GR94-5, Civil Engineering Dept., University of texas at Austin, June.

Stramondo S, Bozzano F, Marra F, Wegmuller U, Cinti FR, Moro M and Saroli M (2008) Subsidence induced by urbanisation in the city of Rome detected by advanced InSAR technique and geotechnical investigations. Remote Sensing of Environment 112:3160–3172

Sun JI, Golesorkhi R, Seed HB (1988) Dynamic moduli and damping ratios for cohesive soils, Report No. EERC-88/15, Earthquake Engineering Research Centre, University of Califorbia, Berkeley.

Tertulliani A, Tosi P, De Rubeis V (1996) Local seismicity in Rome (Italy): recent results from macroseismic evidences. Annali di Geofisica 39(6):1235-1240.

Thompson EM, Baise LG,Kayen RE, Guzina BB (2009) Impediments to Predicting Site Response: Seismic Property Estimation and Modeling Simplifications. Bull. Seism. Soc. Am., 99:2927-2949.

Tommasi P, Ribacchi R, Sciotti M (1996) Geotechnical aspects in the preservation of the historical town of Orvieto. In Proceedings of the Arrigo Croce Memorial Symposium on Geotechnical Engineering for the Preservation of Monuments and Historic Sites, Napoli, Italy, 3-4 October 1996. Edited by C. Viggiani. A.A. Balkema, Rotterdam, The Netherlands, 849-858

Tokimatsu K (1995) Geotechnical site characterization using surface waves, in the Proceedings of the 1st Intl. Conf. Earthquake Geotechincal Engineering, edited by K. Ishihara, Balkema, Leiden, 1333-1368.

Vucetic M, Dobry R (1991) Effect of soil plasticity on cyclic response, Journal of Geotechnical Engineering - ASCE 117(1):89-107.

Wathelet M, Jongmans D, Ohrnberger M (2004) Surface-wave inversion using a direct search algorithm and its application to ambient vibration measurements. Near Surface Geophysics 2004:211-221.

Woods JW, Lintz PL (1973) Plane waves at small arrays. Geophysics 38:1023-1041.

Zhang J, Andrus RD, Juang CH (2005) Normalized Shear Modulus and Material Damping Ratio Relationships, Journal of Geotechnical and Geoenvironmental Engineering - ASCE 131(4):453-464.

CAPTIONS

Fig.1 – a) Geological sketch of central Apennines: 1) Meso-Cenozoic limestones, 2) Meso-Cenozoic marly-limestones, 3) Tortonian flysch, 4) Messinian flysch, 5) Pleistocene volcanic deposits, 6) recent alluvial deposits. b) Tiber valley near the city of Rome: the box identifies the areas of Grottaperfetta valley (Figures 2 and 5). The star shows the epicentral location of the 6th April 2009 L'Aquila earthquake.

Fig.2 – Location of the Grottaperfetta valley and the city of Rome. a) Satellite view of the valley: the white line bounds the alluvial deposits, the three sections (A – Giardinetti; B – Galba; C – Leonardo) are also shown and the white ellipses indicate the location of the seismic noise array along the sections. b) Contour of the top of the Plio-Pleistocene deposits all along the Grottaperfetta valley and the adjacent Tiber valley: the traces of the transversal geological sections of Fig.5 and of the longitudinal geological section of Fig.17 are also shown. c) Detailed contour of the top of the Plio-Pleistocene deposits all along the Grottaperfetta valley: the location of the three seismic noise arrays is also shown by triangles.

Fig.3 – Location of the boreholes drilled in 2004-2005 along section B of Figure 5. The thin white line bound the alluvial deposits of the Grottaperfetta valley.

Fig.4 – Geological section of the Grottaperfetta valley derived along the section B of Figure 3 by the use of the boreholes data: 1) manmade fill (R layer); 2) brown sandy-silty clay (ALS layer); 3) silty clay with organic matter (AGI layer);; 5) peat (T layer); 6) dark grey silty clay with organic matter and gravelly sand intercalations (ATG layer); 7) gravelly sands (D layer); 8) gravel (G); 8) Plio-Pleistocenic deposits (Pl) (including the high consistency clays of the marne Vaticane formation – UMV and the Paleotiber alluvial deposits – G_{Pl} and D_{Pl}; 9) boreholes drilled on 2004-2005 along section B of Fifure 2; 10) boreholes drilled before 2004.

Fig.5 – Geological section A-Leonardo, B-Galba and C-Giardinetti (see Figure 2 for location): R) manmade fill; ALS) brown sandy-silty clay; AGI) silty clay with organic matter; T) peat; ATG) dark grey silty clay with organic matter and gravelly sand intercalations; D) gravelly sands; G) gravel; UMV) high consistency clays of the Marne Vaticane formation; A_{Pl}) clayey-sandy Paleotiber alluvial deposits ; gravelly-sandy Paleotiber alluvial deposits (G_{Pl} - D_{Pl}).

816　Fig.6 – Soil classification of the lithotecnical units distinguished in the alluvial deposits of

817　　the Grottaperfetta valley, according to Robertson et al. (1986) and based on the CPTU

818　　tests performed in the S1 and S2 boreholes of Figures 3 and 4.

819　Fig.7 – Decay curves $G(\gamma)$ (a) and damping curves $D(\gamma)$ (b) obtained for undisturbed samples

820　　collected from the S2 borehole of Figure 4 and 5 and undergoing resonant column (RC)

821　　tests and cyclical torsional shear (TTC) tests at 1 Hz; the position of the linearity

822　　thresholds γ_l is shown. (c) Variations of water overpressures (Δu) normalised during

823　　resonant column tests on samples S1C3 ed S1C7; volumetric thresholds (γ_v) are shown.

824　Fig.8 – Decay curves $G/G_0(\gamma)$ for samples from AGI and T layers (S2 C2 and S2 C4) of

825　　Grottaperfetta valley compared with: a) Vucetic & Dobry (1991) curves referred to

826　　different values of the plasticity index (PI); b) Ishibashi and Zang (1993) and Zhang et

827　　al. (2005) curves; c) Sun et al. (1988) curves.

828　Fig.9 – Comparison between decay curves $G/G_0(\gamma)$ (a) and damping curves $D/D_0(\gamma)$ (b)

829　　obtained from resonant colum tests for samples from AGI and T layers of

830　　Grottaperfetta valley and normalised decay curves obtained by various authors for

831　　Holocene alluvial clays using the Hardin & Drnevich (1972) relations and the Hardin &

832　　Drnevich function specifically obtained for C layer sampled at Valco S.Paolo test site

833　　(see Figure 2 for location).

834　Fig.10 – Comparison between normalised decay curves $G/G_0(\gamma)$ obtained by Boulanger et al.,

835　　2001 from resonant colum tests for samples of peats from Sherman Island (California)

836　　and decay curves $G/G_0(\gamma)$ obtained at Grottaperfetta valley for peats of T layer.

837　Fig.11 – Seismic Vs-velocity profile used for the 1D numerical modelling of shaking of the

838　　three soil columns derived along section A, B and C of Figure 5 at Grottaperfetta

839　　valley.

840　Fig.12 – $G/G_0(\gamma)$ decay curves used for 1D numerical modelling by SHAKE1D in linear

841　　equivalent conditions for all the lithotecnic group which compose the alluvial fill of the

842　　Grottaperfeta valley.

843　Fig.13 – Satellite views of the Grottaperfetta valley showing the location of the three

844　　performed seismic noise arrays. All the white circles indicate the record points while

845　　the empty circles correspond to the stations which were not taken into account for

846　　fitting the 1D velocity models.

847　Fig.14 – Columns, from left: Array geometry, removed stations are also shown, Array

848　　Transfer Function (ATF) middle and right panels; black circles and black lines in the

849 $\left(K_X, K_Y\right)$ plane show the alias lobe position. ATF magnitude reaches the value of 0.5

850 $(K_{max/2})$ along the azimuth shown in the $\left(K_X, K_Y\right)$ plane. Rows: a) Leonardo site; b)

851 Galba site; c) Giardinetti site.

852 Fig.15 – Columns, from left: H/V spectral ratios $\pm$ 1 standard deviation; vertical velocity

853 profiles for S waves; comparison between theoretical dispersion curves (solid red lines)

854 and experimental dispersion curves for the Rayleigh waves (strippled lines), the vertical

855 bars are $\pm$ 1 standard deviation. Rows: a) Leonardo site; b) Galba site; c) Giardinetti

856 site.

857 Fig.16 – Amplification function (A(f)) obtained by the 1D numerical modelling of the soil

858 columns in Figure 11, compared with the HVSRs resulting from the seismic noise

859 arrays of Figure 2 and 13.

860 Fig.17 – Geological section along the section D of Fig.2 and normalized HT functions

861 obatined for four soil columns (corresonding to Valco S.Paolo, Leonardo, Galba and

862 Giardinetti locations) under theoretical and effective hypoteses of Vs profile.

863 Fig.18 –Vertical distribution of the maximum shear strain resulting by the 1D numerical

864 modelling of the soil columns in Figure 11.

865 Fig.19 – Satellite image of the southern portion of Rome's urban area showing the

866 boundaries (white lines) of the left-side lateral alluvial valleys due to some of the

867 tributaries of the Tiber River.

868

869 Table 1 – Physical and mechanical parameters derived from site and laboratory test for the

870 lithotecnic group composing the alluvial fill of the Grottaperfeta valley.

871
872

Fig1
Click here to download high resolution image
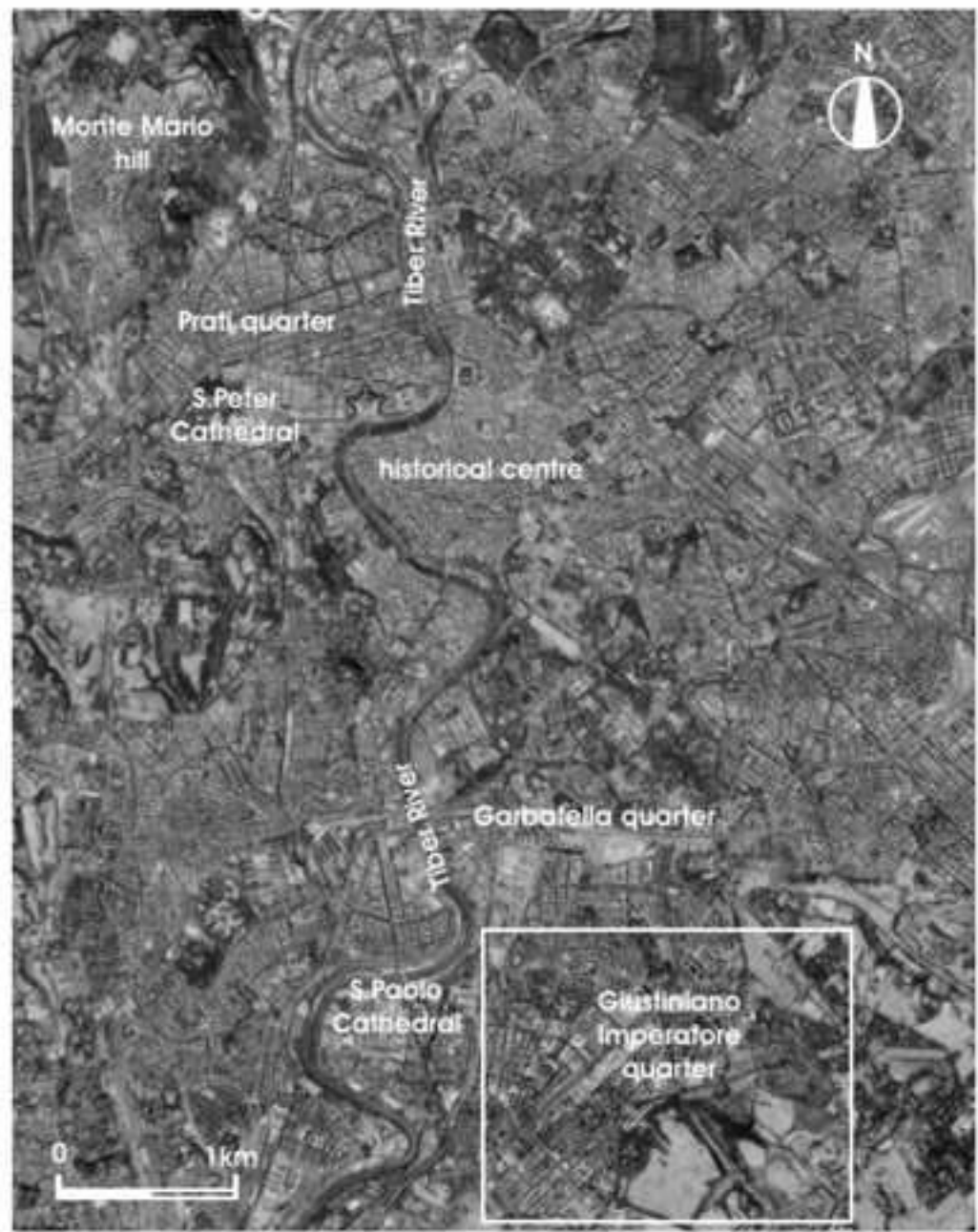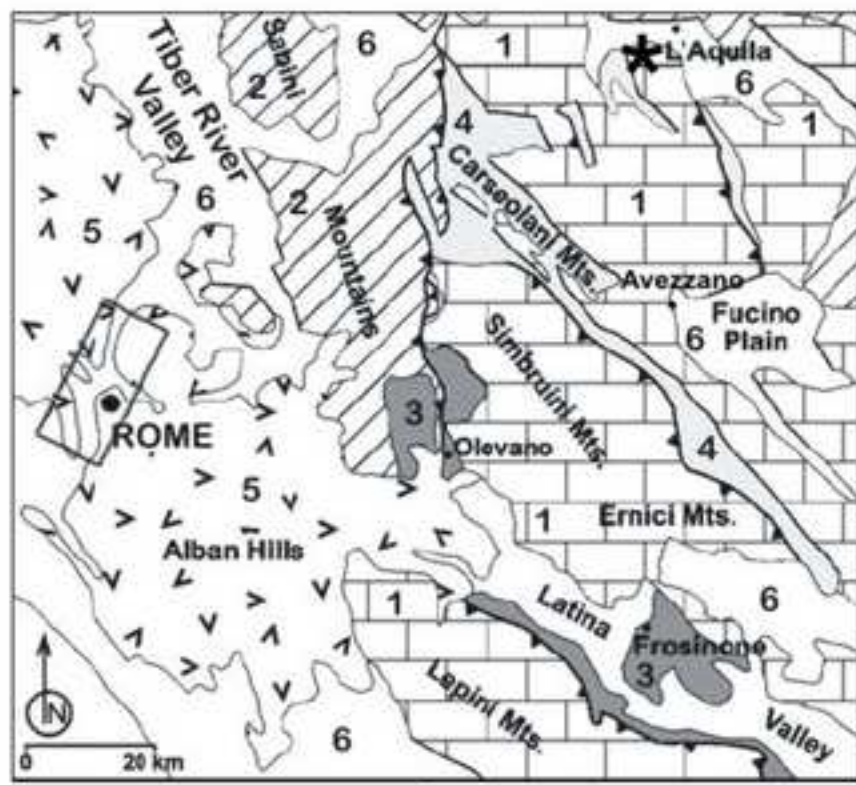
a

b

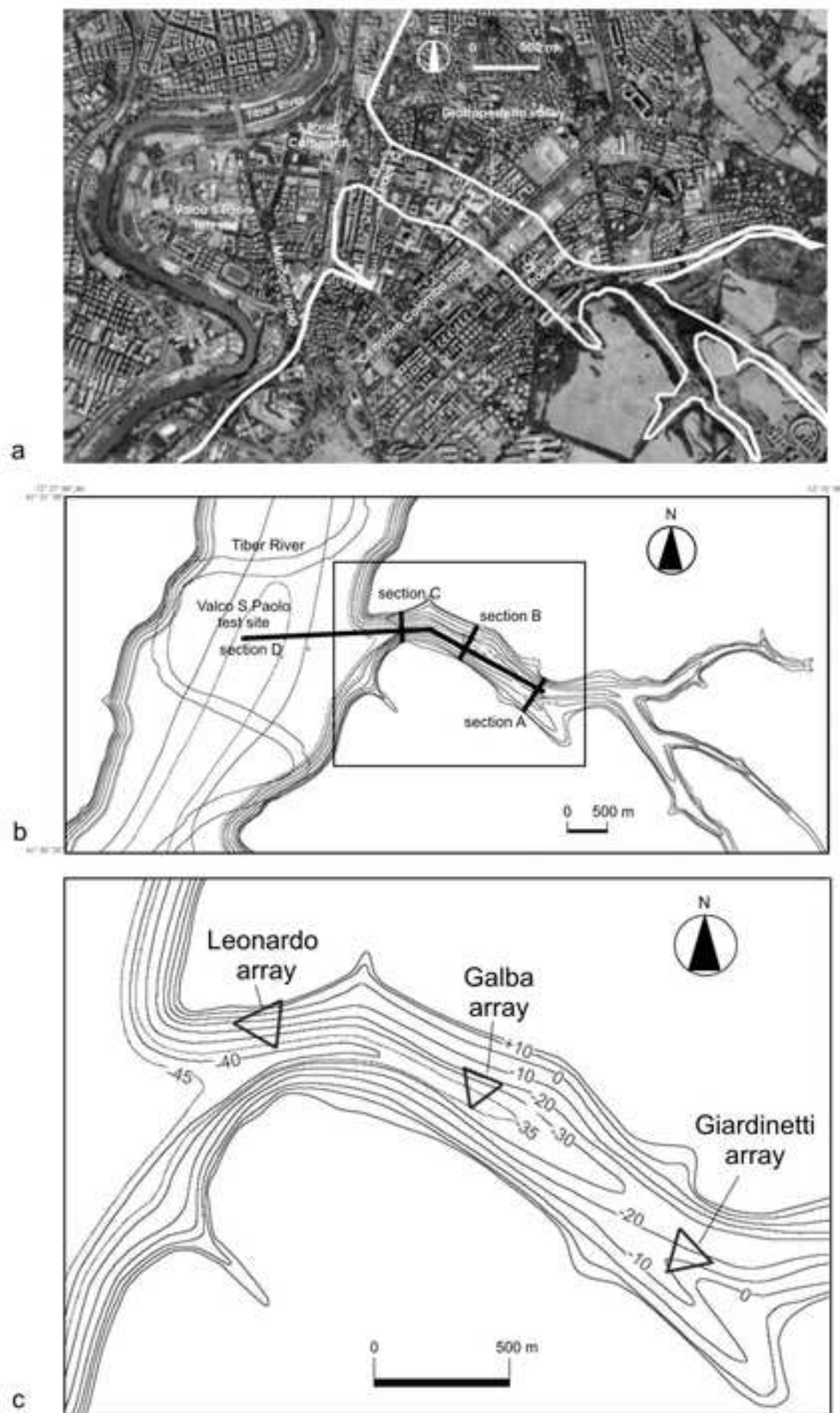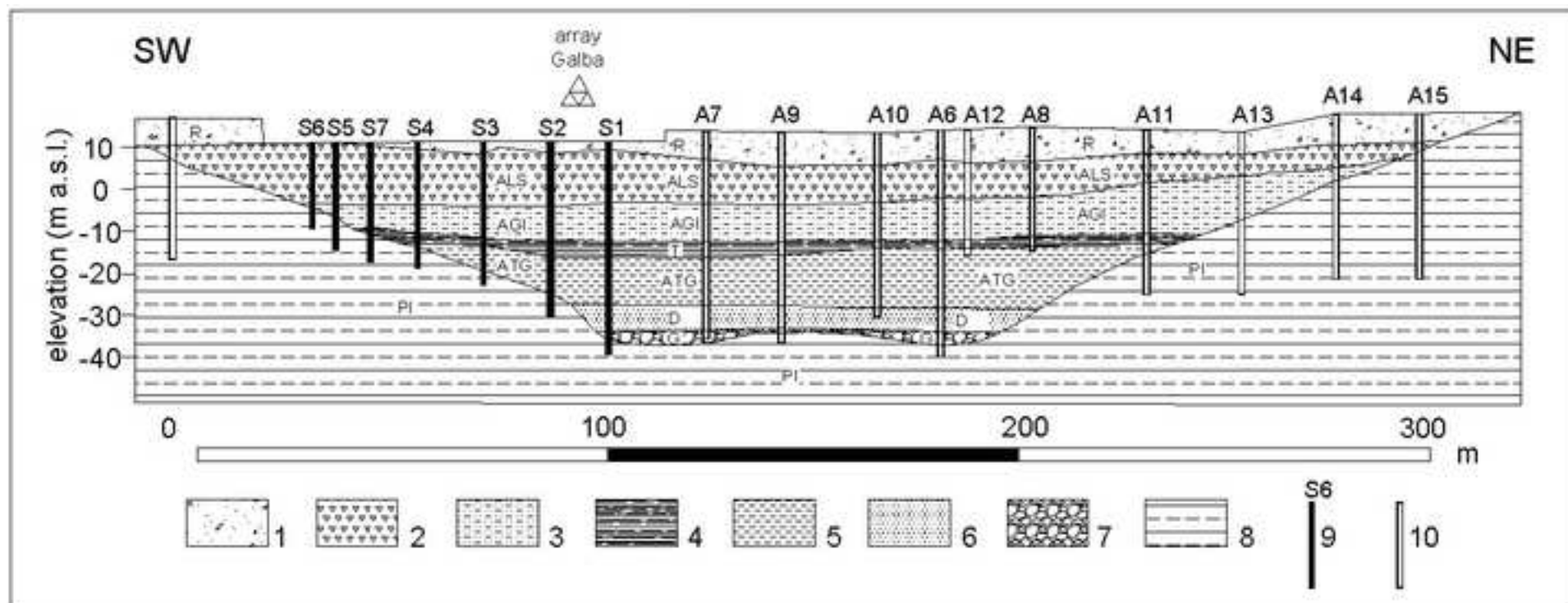

c

Fig3
Click here to download high resolution image

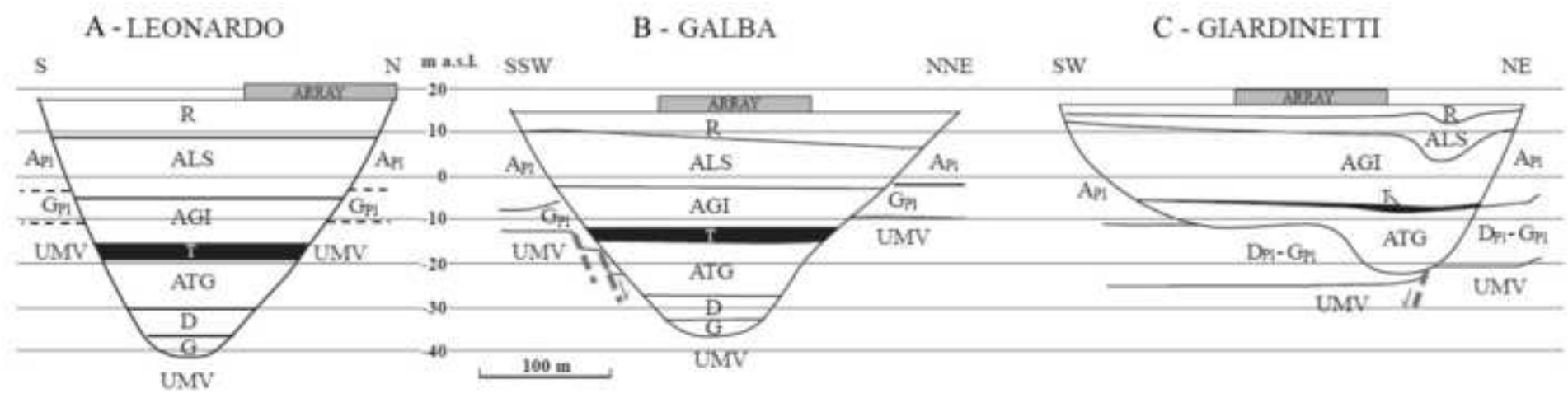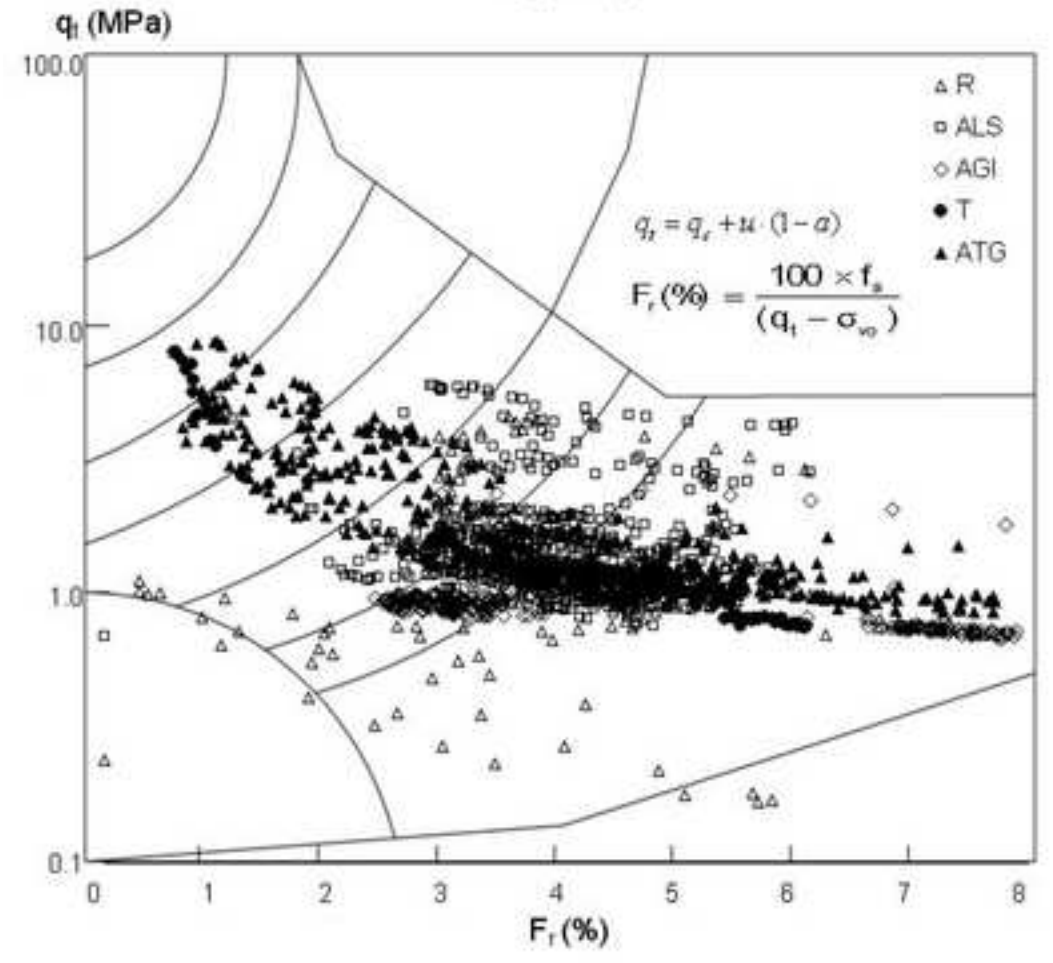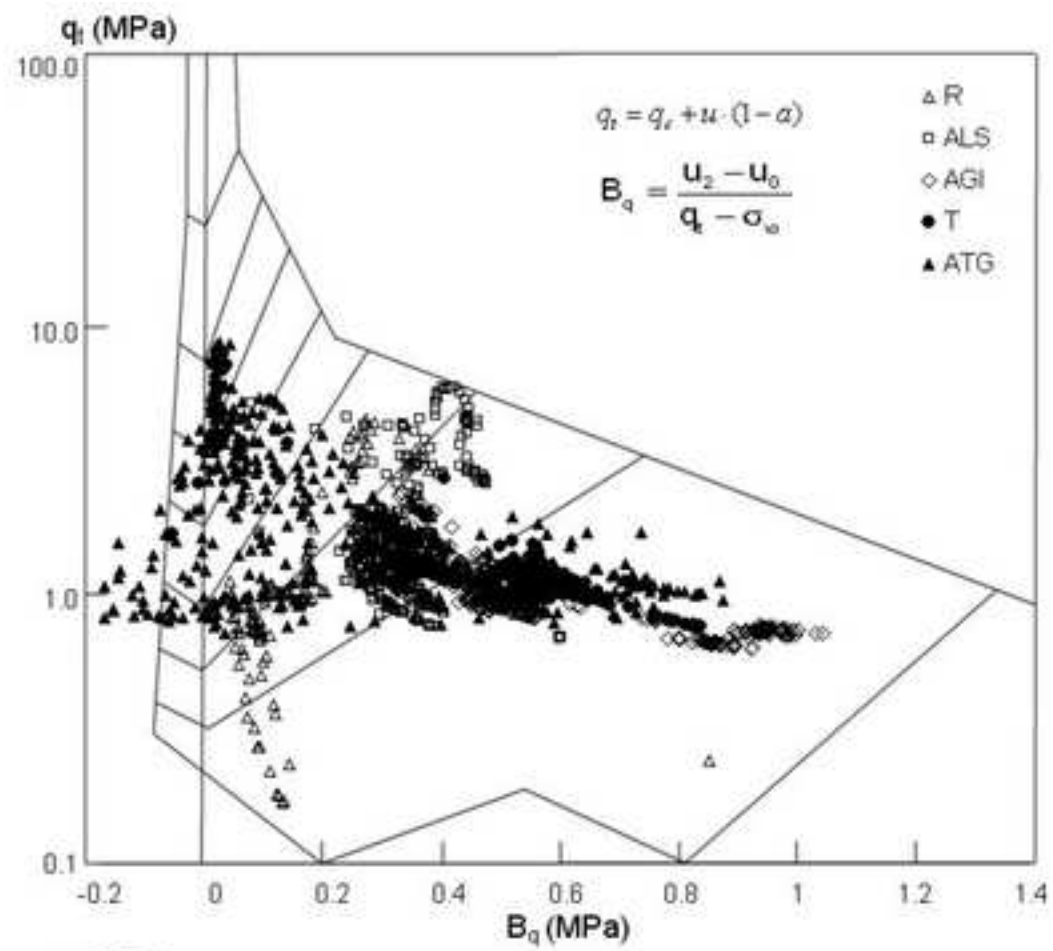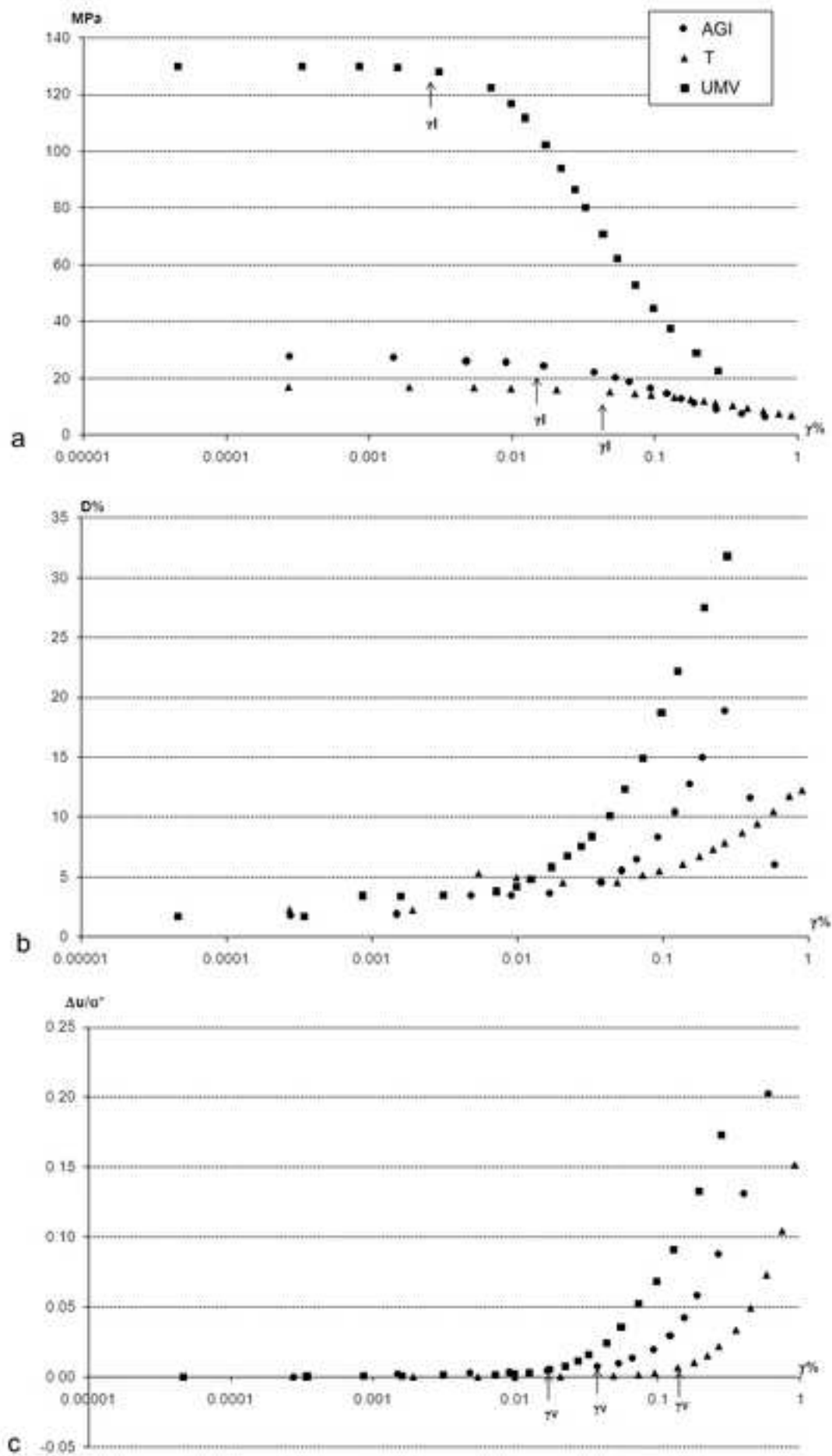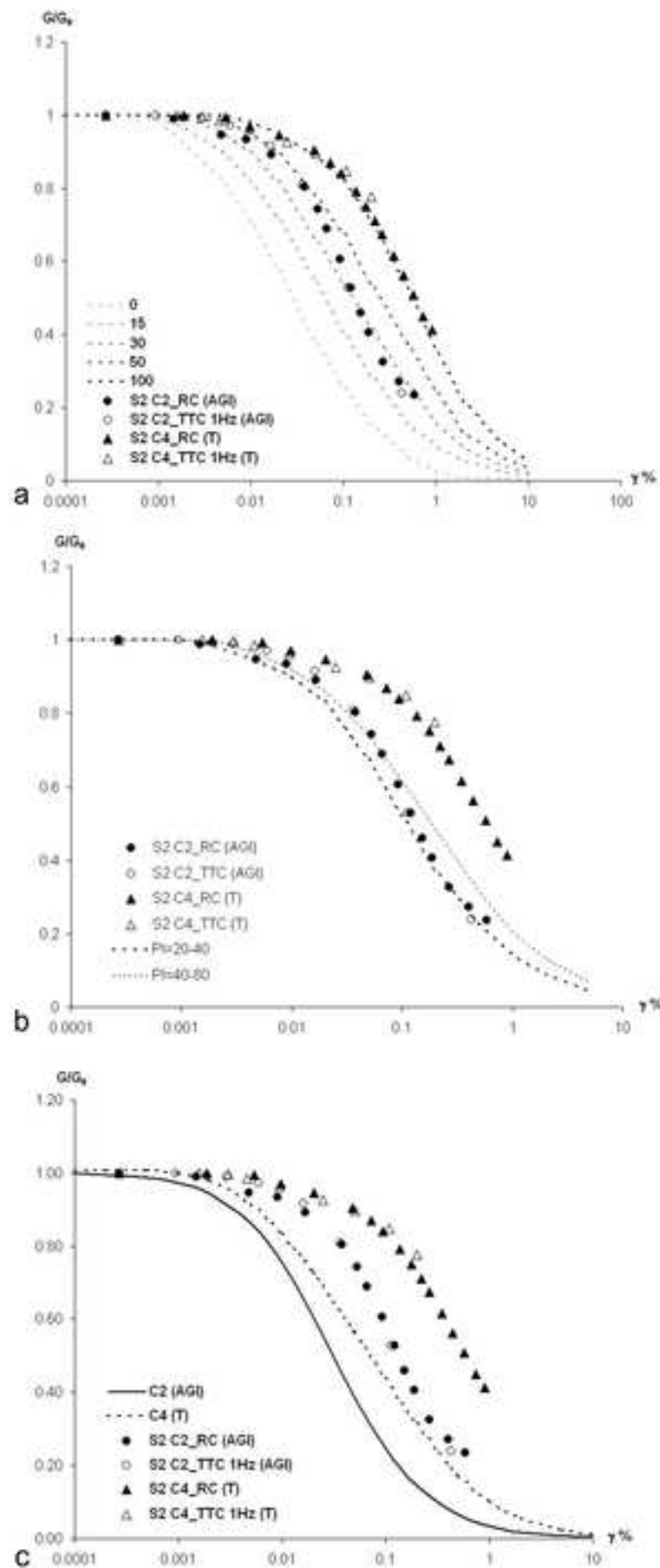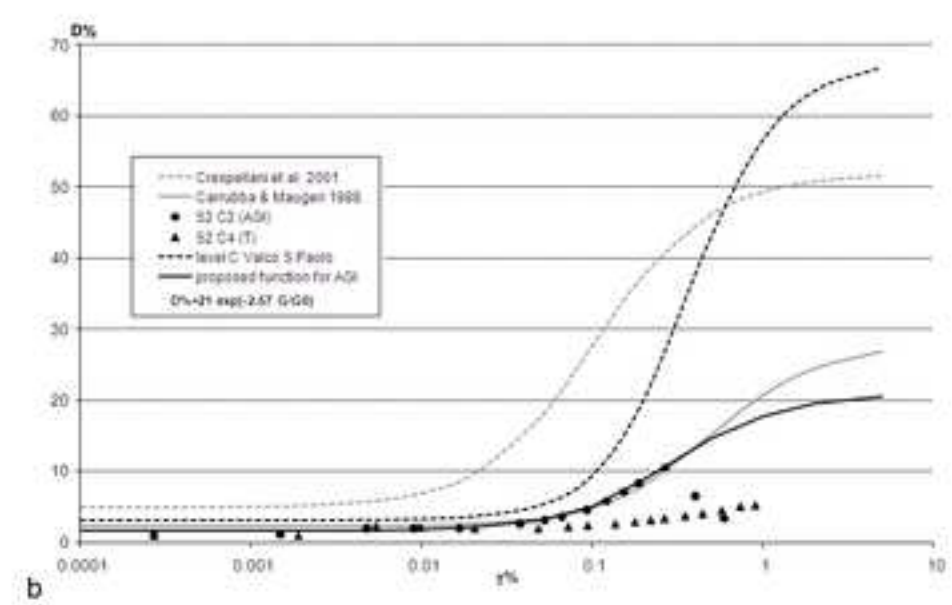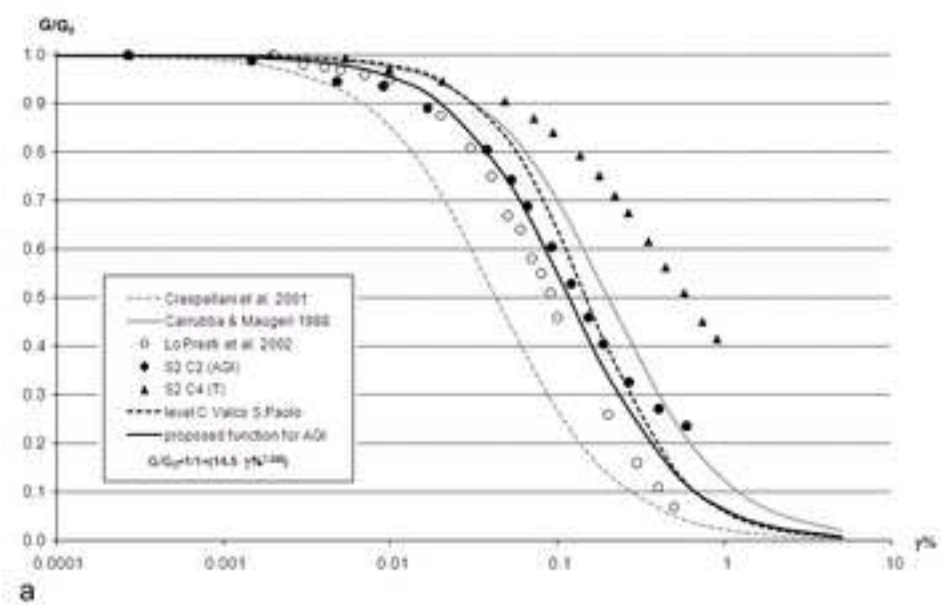**Fig5**
Click here to download high resolution image

q_t (MPa)

$$q_t = q_c + u \cdot (1-a)$$

$$B_q = \frac{u_2 - u_0}{q_t - \sigma_{vo}}$$

△ R
□ ALS
◇ AGI
● T
▲ ATG

B_q (MPa)

q_t (MPa)

$$q_t = q_c + u \cdot (1-a)$$

$$F_r (\%) = \frac{100 \times f_s}{(q_t - \sigma_{vo})}$$
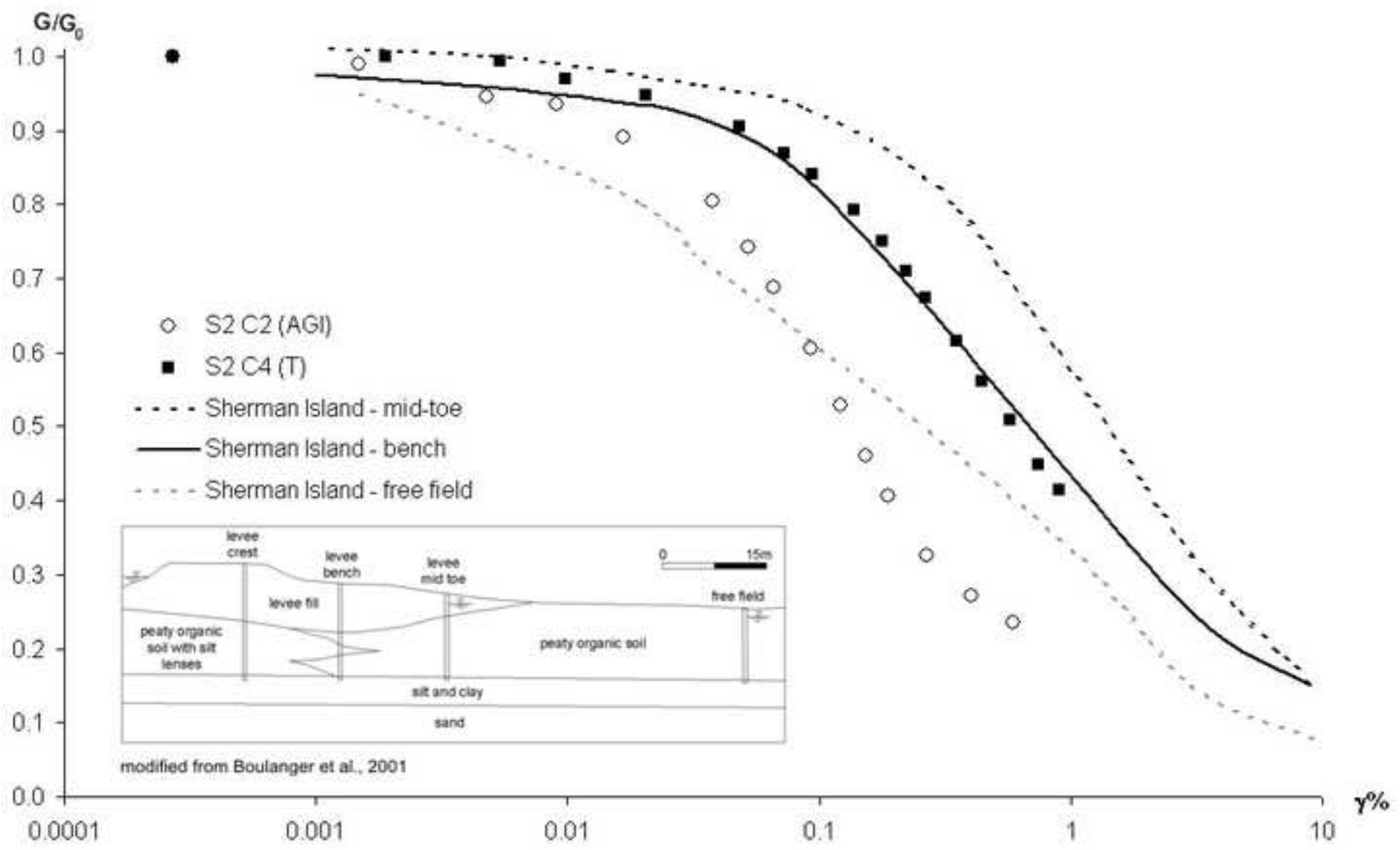
△ R
□ ALS
◇ AGI
● T
▲ ATG

F_r (%)

Fig8
Click here to download high resolution image

Fig9
Click here to download high resolution image
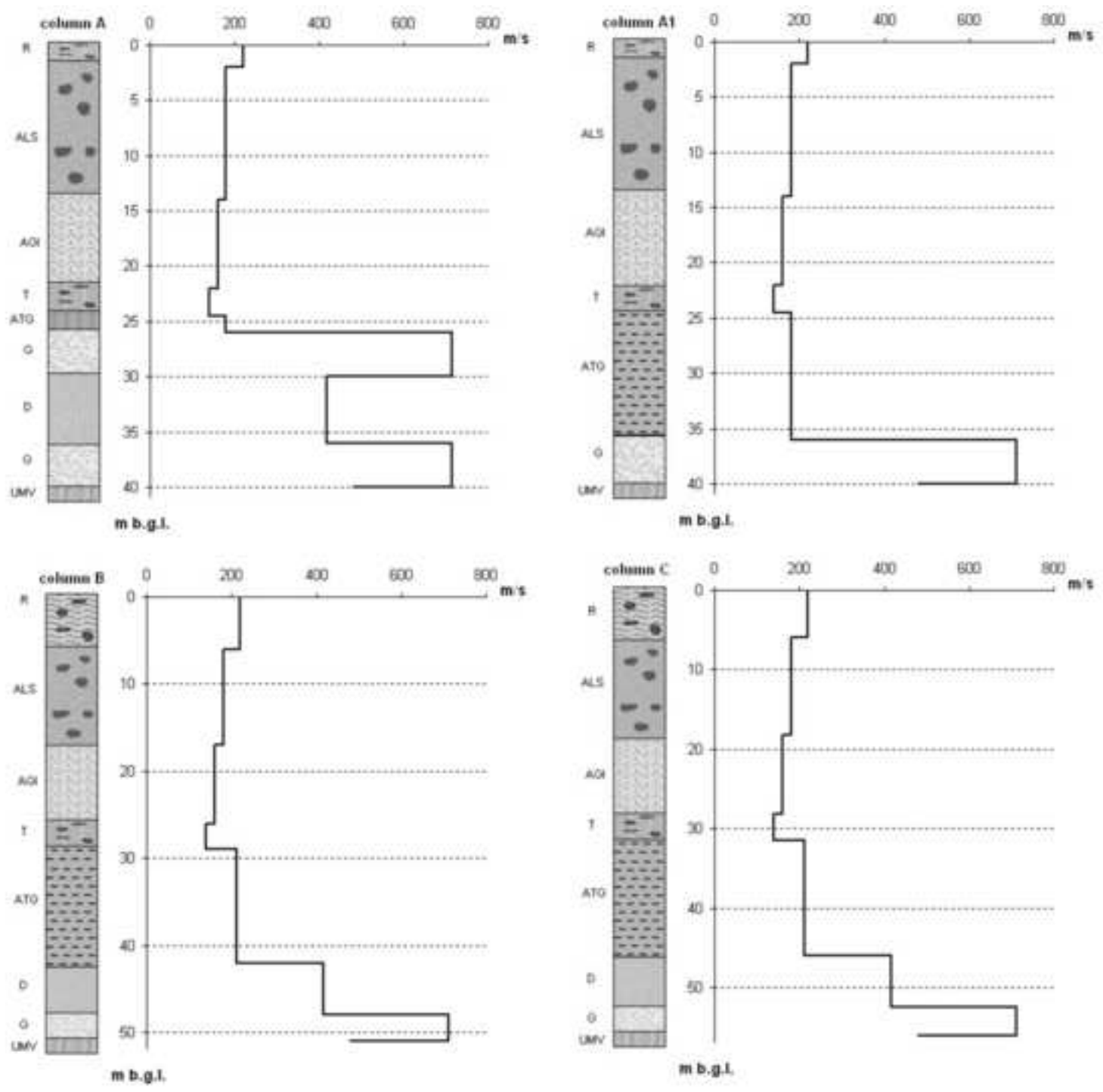
Fig10
Click here to download high resolution image

Legend:
- ◇ S2 C2 (AGI)
- ■ S2 C4 (T)
- ···· Sherman Island - mid-toe
- —— Sherman Island - bench
- ···· Sherman Island - free field

modified from Boulanger et al., 2001

Fig11
Click here to download high resolution image

Fig12
Click here to download high resolution image
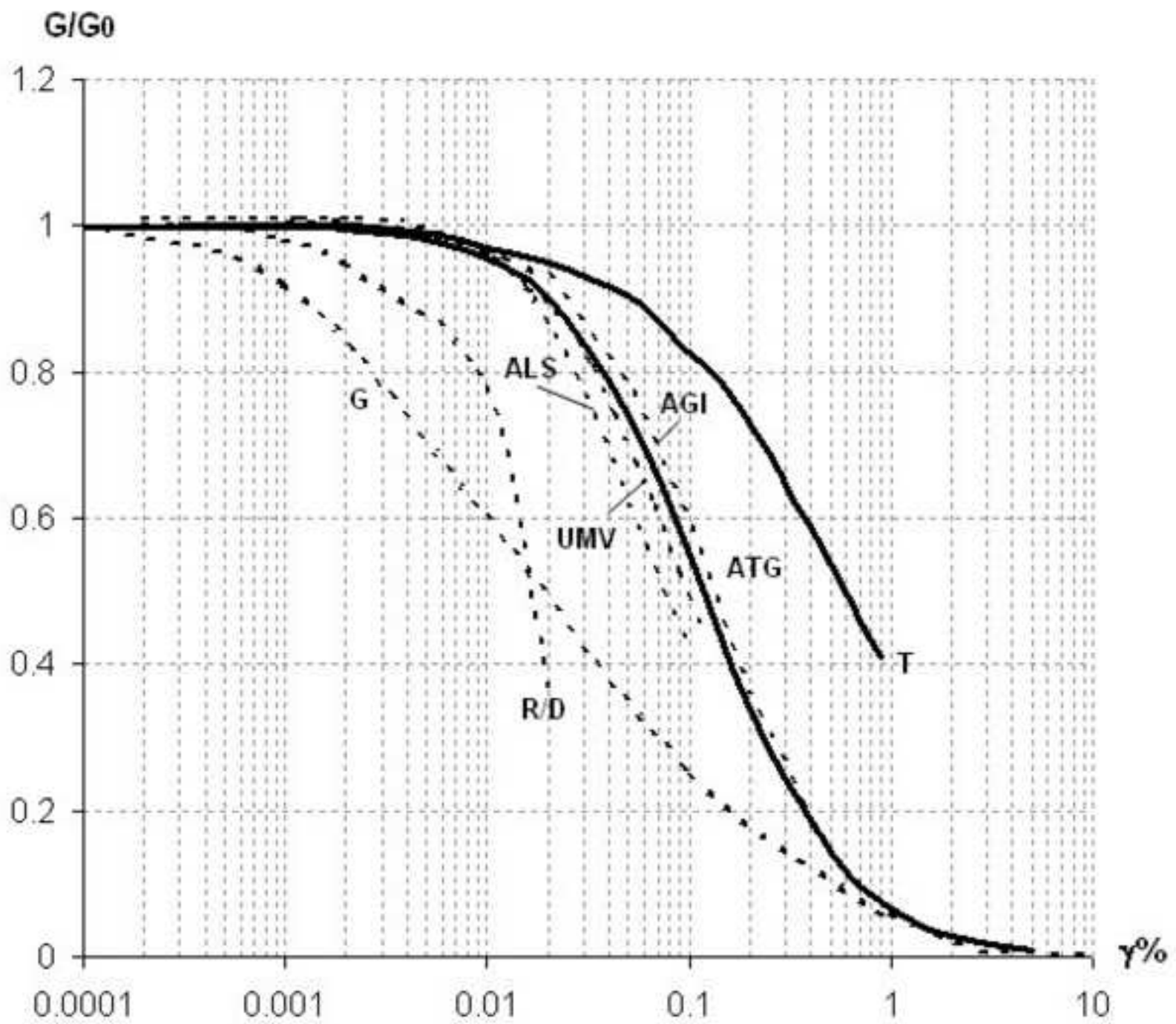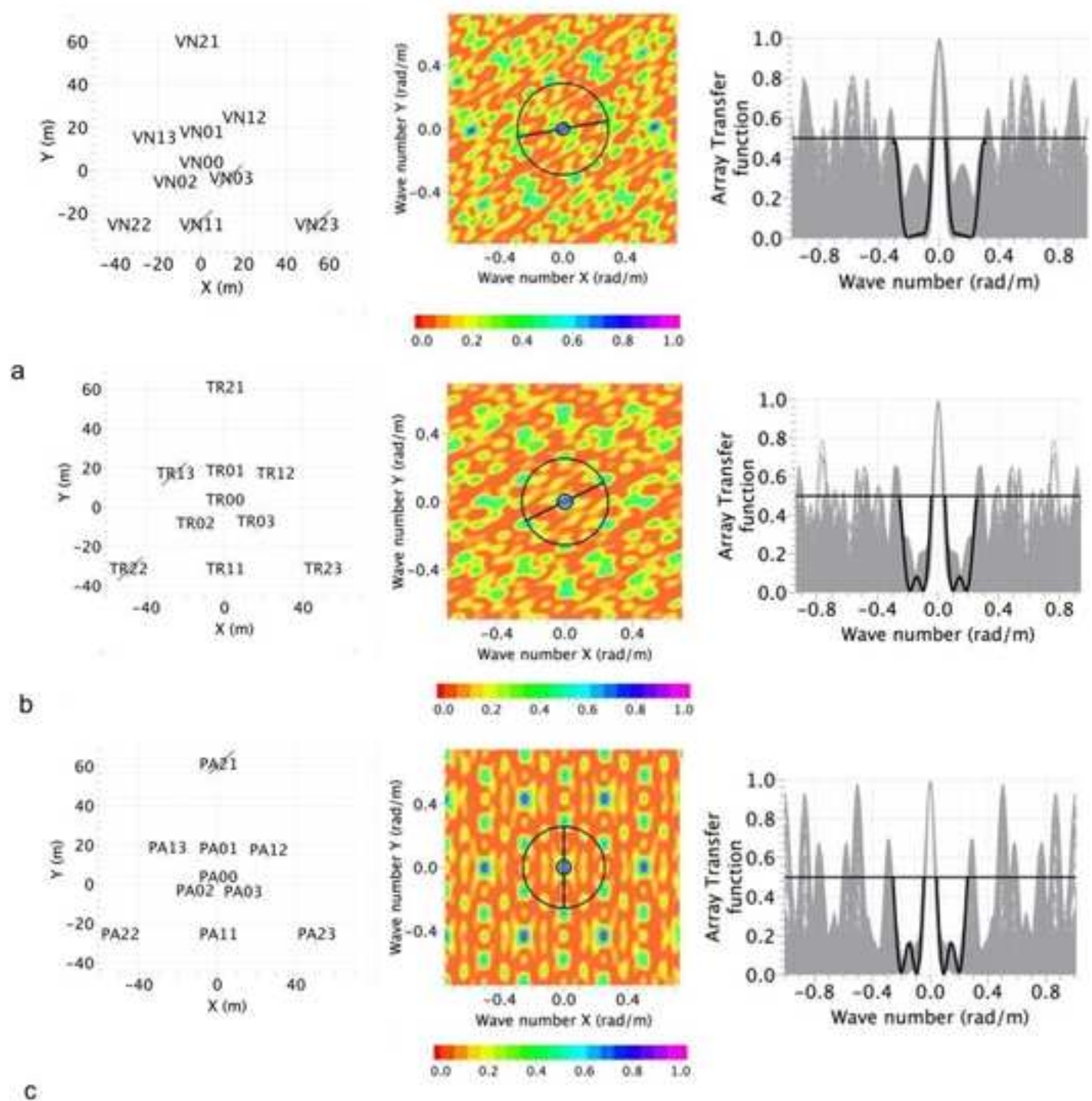
Fig14
Click here to download high resolution image

a

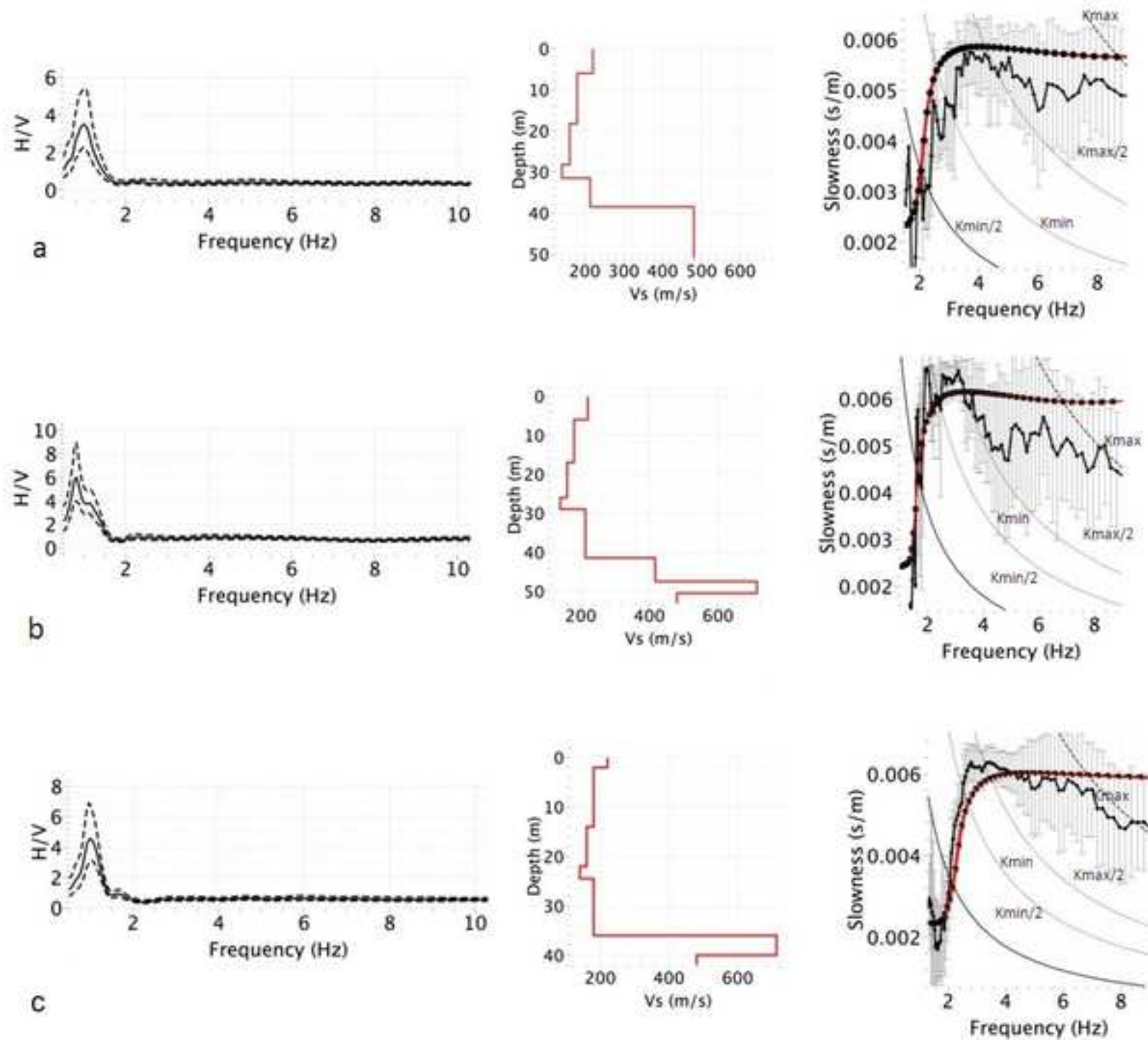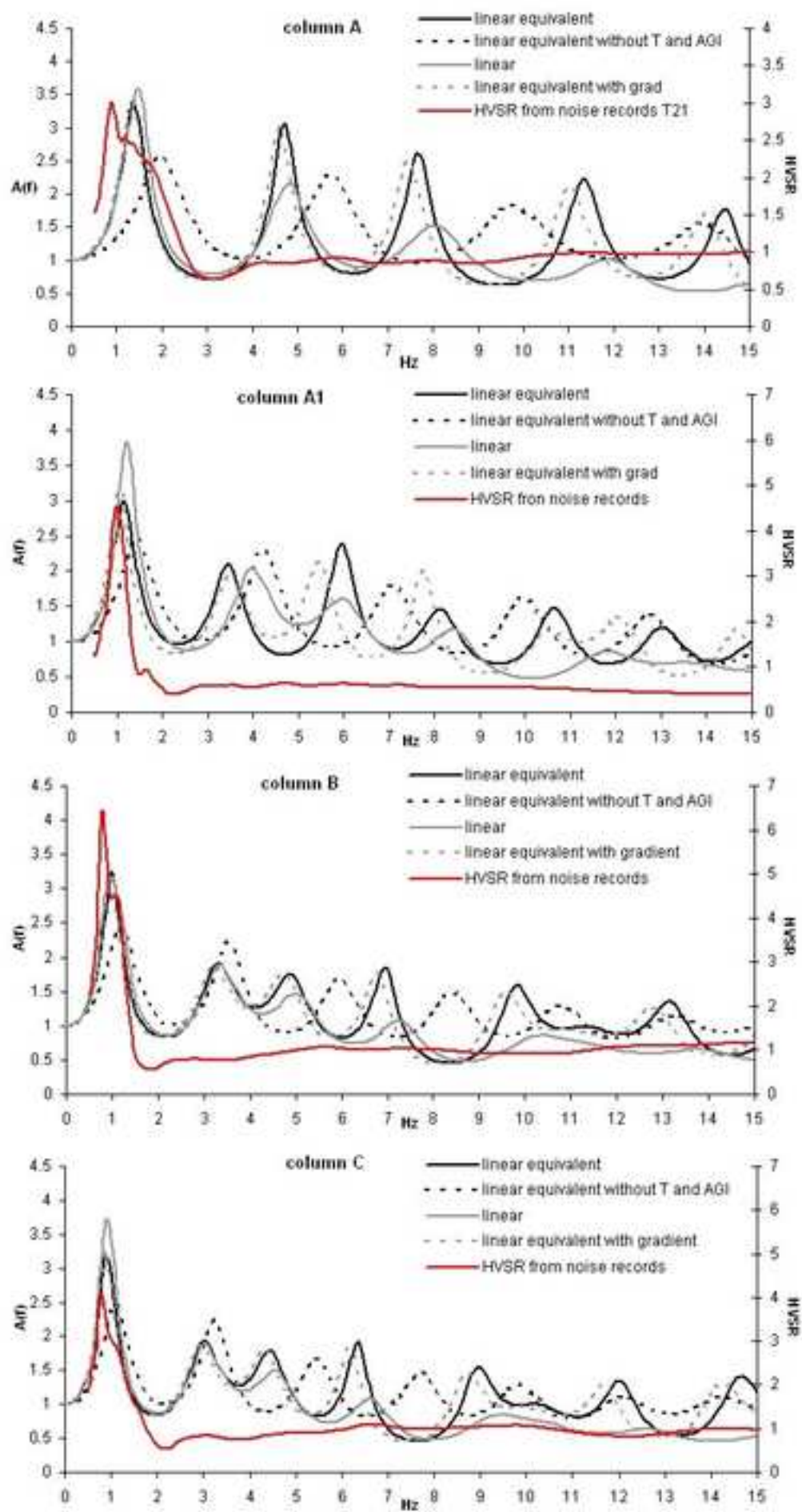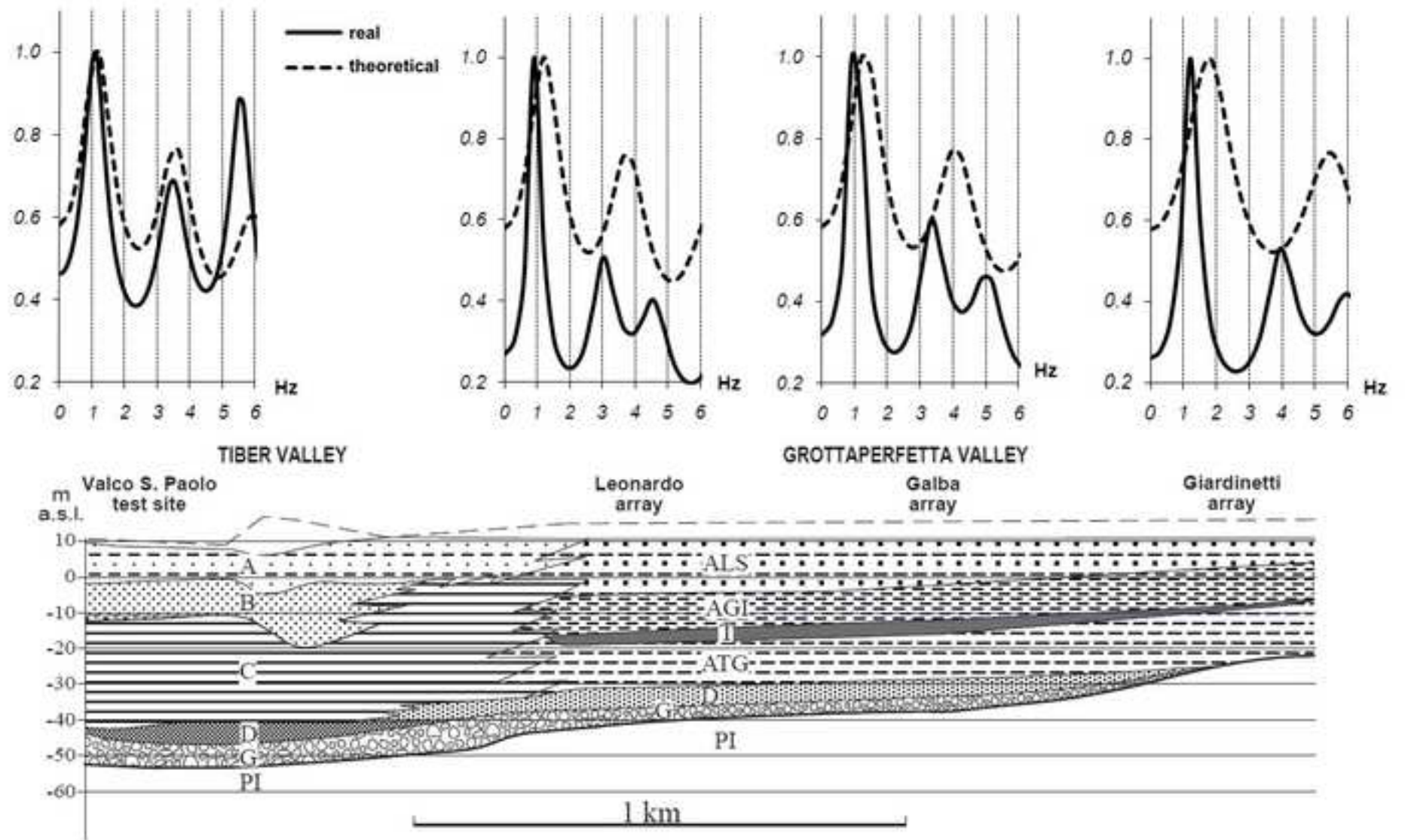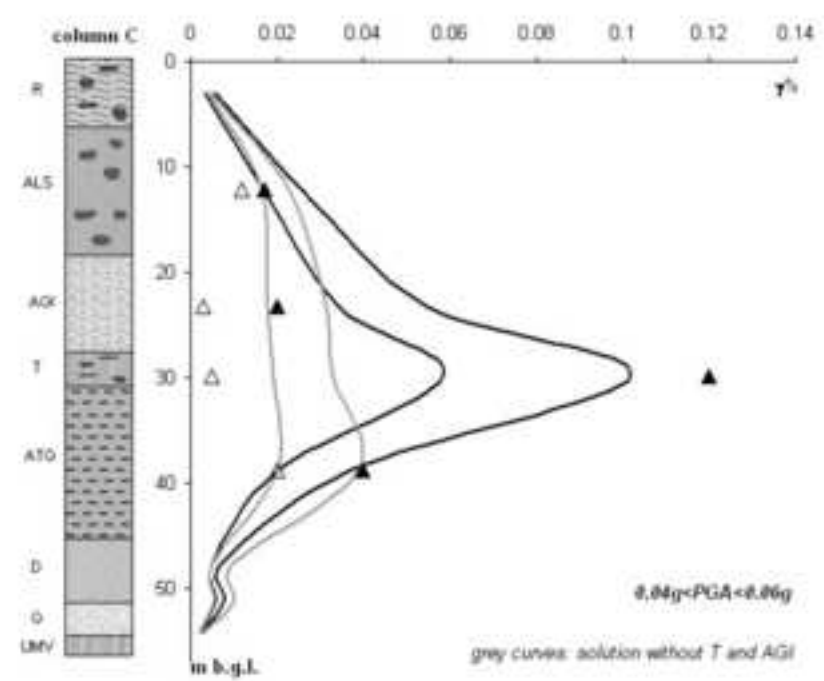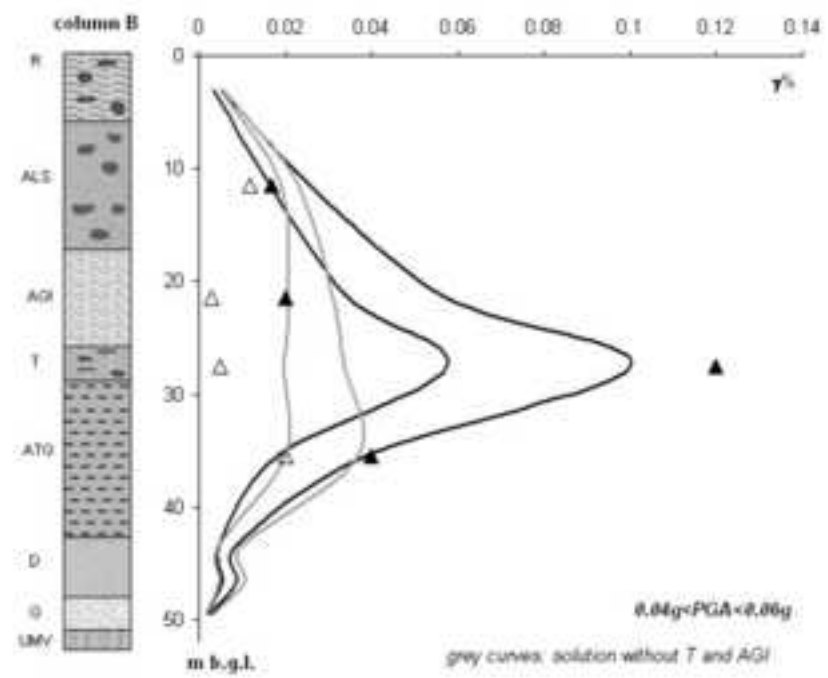b

c

Fig15
Click here to download high resolution image

Fig16
Click here to download high resolution image

TIBER VALLEY

GROTTAPERFETTA VALLEY

Fig18
Click here to download high resolution image

Table1

	age	w_{LL}	w_{LP}	PI	A	w_n	CI	γ_n	Cc	s_u	q_c	Vs	Vp	G_e
	years	%	%	%		%		kN/m^3		kPa	MPa	m/s	m/s	MPa
R	50	n.d.	n.d.	n.d.	n.d.	n.d.	n.d.	17.0	n.d.	77	1.2	220	523	82
ALS	2000	78	42	36	0.9	56	0.6	16.5±0.4	0.32±0.1	82.5±35	1.9	180	1400	53
AGI	7500	88	36	52	0.9	67	0.5	15.7±1.3	0.57±0.2	28±18	0.8	160	1100	40
T	8600	84	74	11	11.0	126	-3.8	12.7	1.50	34±10	0.9	140	800	25
ATG	9000	113	45	68	2.6	66	0.5	16.6±2.9	0.63±0.3	74.5±52	2.9	180-213	1000-1230	54-75
D	n.d.	n.d.	n.d.	n.d.	n.d.	n.d.	n.d.	19.2	n.d.	n.d.	n.d.	417	1760	334
G	n.d.	n.d.	n.d.	n.d.	n.d.	n.d.	n.d.	21.0	n.d.	n.d.	n.d.	713	2560	1068
UMV	Pliocene	56	22	35	1.0	20	1.0	20.9	0.11	n.d.	n.d.	480	1880	461

13th January 2011, Rome

To Whom It May Concern:
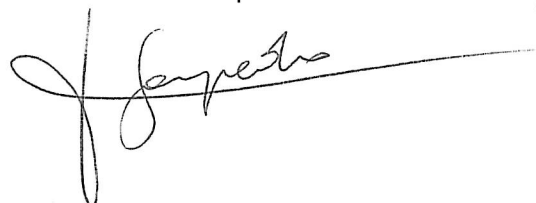
I, the undersigned, Laura Sampedro (B.A Hons Degree in modern languages at the University of Westminster), born in London, England on 2nd of August 1971 of English mother tongue declare that I have satisfactory skills and competences to have reviewed the paper:

DYNAMIC PROPERTIES OF LOW VELOCITY ALLUVIAL DEPOSITS INFLUENCING SEISMICALLY-INDUCED SHEAR STRAINS: THE GROTTAPERFETTA VALLEY TEST-SITE (ROME - ITALY)

by Caserta A, Martino S, Bozzano , Govoni A. and Marra F.

Yours sincerely,

Laura Sampedro

Parallelisation Technique for Serial 3D Seismic Codes: SMS Approach

Arrigo Caserta ([1])([2])**, Vittorio Ruggiero** ([3])**, Maria Pia Busico** ([3]) **and Ivo Opršal** ([2])

([1]) *Istituto Nazionale di Geofisica e Vulcanologia, Roma, Italy*
([2]) *Charles University, Prague, Czech Republic*
([3]) *C.A.S.P.U.R., Roma, Italy*

Abstract
We investigate a fast and easy way to parallelise seismological serial codes mainly oriented for simulating the seismic wave propagation through anelastic dissipative media. Having an efficient modelling tool is important in both assessing strong ground motion and mitigation of seismic hazard when the site effects are considered, and in crustal propagation when the crustal geological structures are of interest. Our chosen case study is representative of a set of such seismological 3D problems. The Scalable Modelling System (SMS) tool for parallelization is considered. The IBM SP5 native compiler has been used. Results such as Speed-Up and Efficiency are shown and discussed. SMS can run both in shared and distributed memory environments. The greater advantages of using SMS in such environments become apparent with the utilisation of a higher number of multiprocessor machines arranged in a cluster. We also demonstrate how successful porting from serial to parallel codes is realised by way of minimal instructions (6% of the serial original code only) provided that an ad hoc profiling analysis of the serial code is first performed.

1. Introduction

An important contribution to assessing interaction between near-surface geology and seismic radiation arises from studies involving the so called *site effects* P.-Y. Bard, 1995; 1998; Panza *et al.,* 2001; S. Bonnefoy-Claudet *et al.,* 2006, amongst others). These latter are related to seismic wave propagation phenomena (Aki, 1988; 1993) with important implications for seismic hazard mitigation.

Site effects can be studied using an instrumental approach during earthquakes recording soil shaking on specific stations located on suitable chosen sites (Caserta *et al.,* 2000; Di Giulio *et al.,* 2002; Cultrera *et al.,* 2003; Cara *et al.*, 2005). Nevertheless, it would be more useful to know the site characteristics of the ground motion before an earthquake occurs, in this respect numerical modelling is a powerful approach (Caserta and Lanucara, 2000; Moczo *et al.,* 2001) also for estimating parameters commonly used for earthquake engineering purposes (Fäh *et al.,* 1993; Rovelli *et al.,* 1994). This is particularly true in urban areas where the instrumental approach may not always be used because of the high level of anthropogenic noise (Olsen *et al.,* 2006).

The great drawback to modelling more realistic site dynamics is the impressive computational requirements needed for numerical simulations such as: gigabytes of memory, performances at gigaflops rate, days of computational time to simulate a minute's soil shaking, etc. (Sáncez-Sesma and Luzon, 1995; Graves, 1998). Seismologists have been addressing these issues through the use of parallel computers (Olsen and Archuleta, 1996) coupled with

Mailing address: Dr. Arrigo Caserta, Istituto Nazionale di Geofisica e Vulcanologia, via di Vigna Murata 605, 00143 Roma, Italy; e-mail: arrigo.caserta@ingv.it

optimization techniques such as the use of un-
structured grids to reduce the number of com-
putational nodes (Bao *et al.,* 1996).

During the last 20 years a considerable
amount of work has been done in numerically
modelling the interaction between both near-
surface and inner geological heterogeneities
and seismic radiation (see the review of Bard,
1998; Bielak *et al.,* 1998, Panza *et al.,* 2001;
Moczo *et al.,* 2007, and references therein). The
results are huge serial codes able to numerical-
ly simulate the process. It would be useful to re-
convert such serial codes into parallel ones, to
have more powerful simulations that realistical-
ly represent the dynamics of such interaction.

On the other hand, the conversion of a seri-
al code to a parallel one requires typically
rewriting only choice available is to rewrite
from the beginning a new 3D code, and this is
not an easy task as well as being energy de-
manding. Not to mention that writing a 3D code
from the scratch, on the basis of our experience,
is more time demanding than paralleling an ex-
isting serial 3D code. This paper is aimed at in-
vestigating a more simple and efficient way to
parallelise a 3D serial code, more specifically
codes for simulating the seismic wave propaga-
tion through viscoelastic dissipative 3D media.

For the purposes of our study, we adopted
the serial code of Opr?al and Zahradnik (2002),
which contains general aspects that make it rep-
resentative of the dynamics that we want to
simulate. Based on a finite-difference technique
on a Cartesian mesh (Opr?al and Zahradnik,
2002; Opr?al *et al.,* 2004, 2005), it computes
the full 3D seismic wave-field. Null normal
stress boundary condition on the topographic
surface is realized by the so-called *vacuum for-
malism* (Opr?al and Zahardnik, 2002). Its sta-
bility conditions are represented by the classical
C.F.L. criterion for explicit methods (Mitchel
and Griffits, 1980).

These features are similarly adopted in
many of the serial codes developed in the last
years dealing with the seismic wave propaga-
tion problem, used to assess strong ground mo-
tion (Zahradnik *et al.,* 1993; Graves, 1998;
Opr?al and Zahradnik, 1999; Pitarka, 1999;
Moczo *et al*., 2001; amongst others).

2. Study case: serial 3D wave propagation code

The main guidelines for the previously-ref-
erenced program by Opr?al and Zahradnik
(2002) are based on the formulation of an initial
boundary value problem that represents the vis-
coelastic dynamics driving the full 3D wave-
field propagation. The medium is dissipative
with arbitrary 3D shape and topography.

Source energy nucleation and its crustal
propagation can be numerically modelled
through a discrete wave-number method (DW),
as well as ray theory or even an analytical solu-
tion; the resulting wave-field represents the
seismic radiation ready to light up the site un-
der study. The finite-difference (FD) technique
is adopted to model the interaction between the
site and the seismic radiation previously com-
puted yielding the site response. In such a way
we are able to study the combined source – path
– site response of the medium under the action
of input radiation as it arises from the seismic
source and propagated through the crust be-
neath the site.

The DW-FD coupling used here is realized
by extending hybrid technique developed first
for the 2D case by Zahradnik and Moczo
(1996) and generalized by Opr?al *et al*. (2009)
to the 3D case.

The main advantage of such a hybrid tech-
nique is fast evaluation of site effects and seis-
mic hazard because it needs less computer
memory and time than all-in-one source-path-
site computational methods. Computations are
made in the time domain. The results are syn-
thetic seismograms on the free surface and
snapshots of the wave amplitude inside a 3D
profile (for further details see Opr?al and
Zahradnik, 2002). Furthermore, this hybrid
technique allows us to study the source-crustal
propagation in case we are interested in the
crustal propagation only.

Our test case deals with a real geological
structure (Fäh *et al.,* 2006), representing the
stratigraphy underlying the Roman city Augus-
ta Raurica (fig. 1), located east of Basel,
Switzerland. The 3D structure of the area was
retrieved through array investigations (H/V, am-
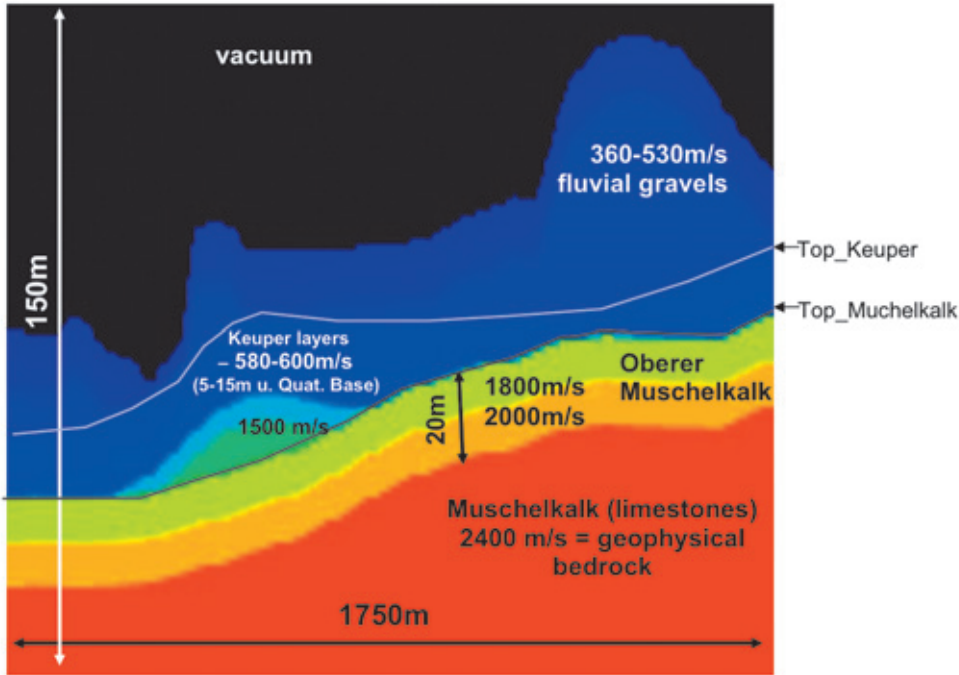bient vibrations) and borehole data (Fäh *et al.,*

Fig. 1. Geological model at Augusta Raurica. The EW vertical slice is a 3D FD computational model extraction. See also fig. 2.

2006; Opršal and Fäh, 2007), and the topmost structure (namely so-called Top_Muschelkalk interface), was refined in terms of fundamental frequencies fit by modifying the shape of the interface limiting the upper geology from below (see fig. 2). The geological model was converted into a computational one according to the stability conditions of the numerical scheme (fig. 1).

According to Fäh *et al.* (2006), the section of interest is 1552 m (WE) x 1696 m (SN) large rectangular area with constant spatial sampling of 4 m. The computational domain covers the wave dumping area around, resulting in 442 x 480 grid points corresponding to 1764 m x 1916 m of computational model, respectively. The vertical extent of the computational model is 115 grid points corresponding to ~793 m depth while the geological structure differing from bedrock up to topography peaks is less

then 150 m. The vertical grid step is not constant, being scaled with respect to the vertical velocity profile.

This study also used the same time-step, 0.00023 s and these parameters guarantee the accuracy of the FD computation up to a frequency of 12 Hz with a usable range up to 10 Hz. We simulate 5 s ground shaking for a total of 21740 time-steps. A problem of near 73 million unknowns is solved at each time-step. Although the Augusta Raurica site was chosen for the purpose of this test case, our study code can be applied to any 3D stratigraphy, as it depends on neither the shape nor the geological details of the site. Indeed, other recent real case studies (Opr?al and Fäh, 2007; Sorensen *et al.,* 2006; Opr?al *et al.*, 2004; 2005), have used this study code to simulate wave-field time evolution and its interaction with the geological structure.
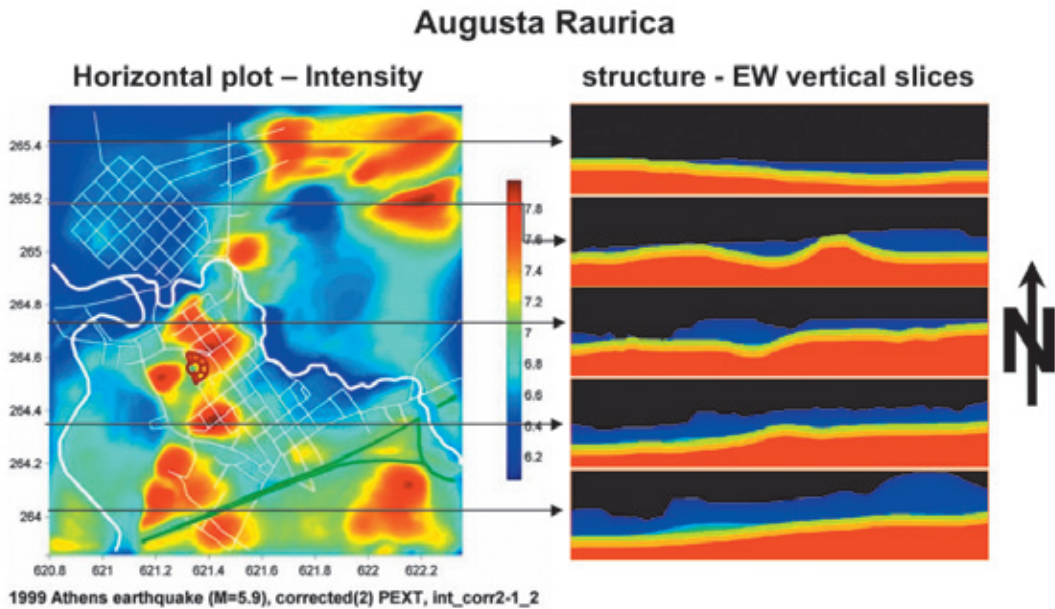
505

Augusta Raurica

Fig. 2. Intensities for Mw=5.9 1999 Athens-like earthquake simulation in Augusta Raurica (left panel); for details see Fäh *et al*. (2006) and Opr?al and Fäh (2007). Thick white lines are rivers Ergolz (left) and Violenbach (right), red semi-ring denotes the amphitheatre, and the green lines in the southern part are for present-time highway. The thin white lines are historically re-mapped streets of the upper and lower city of Augusta Raurica. The right panel depicts vertical slices of computational model realization of the geology structure; vacuum shown as black color. Black arrows connect the surface traces of the vertical geology slices.

3. Parallelisation

Tools to parallelise a code can be divided into high-level and low-level programming. Parallel virtual machine (PVM) and message passing interface (MPI) belong to low-level programming, where the parallelisation scheme is planned, designed and realized by the user. In more detail, the management of information exchanged among processors (*e.g*., message passing, synchronisations, etc.) is realised by the user adding code segments. Although efficient on shared and distributed memory architectures, low-level techniques will not be considered in this study as, on the basis of our experience, too much effort (and time) must be spent to convert a serial code into an MPI (or PVM) parallel one (Caserta *et al.,* 2002). To parallelise our serial code we chose tools based on a high level technique where all low level parallel machinery (creation, communications and maintenance of processes) is realised by directives to the compiler in a user-hiding mode.

The best candidates for such an approach are High Performance Fortran (HPF), OpenMP and Scalable Modelling System (SMS). It must be noted that while OpenMP is only available on shared memory architectures, both HPF and SMS can be used in shared as well as distributed memory environments. Contrary to Caserta *et al*. (2002), we have avoided adopting OpenMP for several reasons. First of all, our main target is to simulate numerical problems with tens of millions of variables, nearly 20 times the average size problem of Caserta *et al*. Therefore, we prefer to adapt our code to distributed memory machines that allow to handle much larger amount of memory. We choose a high-level technique based on distributed memory architecture as it is more suited for our purposes.

Because HPF is maintained by third-party and private companies (see the HPF official website http://hpff.rice.edu), we have chosen the SMS tool which is freely available. See Foster (1995) for a complete survey of parallel programming design and tools on Distributed Memory architectures, while refer to Nichols *et al.* (1996) and the official OpenMP web site for Shared Memory references. As far as SMS is concerned, see Govett *et al.* (2003) and the official SMS website (http://wwwad.fsl.noaa.gov/ac/sms.html). The detection of code segments that must be modified to optimize the serial code and to reduce the memory requirement is performed by the user via the application of a profiling analysis. In such a way, we can ensure a uniformly optimized serial code suitable for parallelisation. Below, we detail how this operation is carried out.

3.1. *SMS technique*

SMS has been developed by the Advanced Computing Branch of the Forecast Systems Laboratory at NOAA (National Oceanic and Atmospheric Administration) (Govett *et al.*, 2003). The user inserts directives in the form of comments (indetified by?sms$) into the existing serial Fortran code. SMS translates the code and directives into a parallel version that runs efficiently on shared and distributed memory high-performance computing platforms. The translation is realized by the Parallelising Pre-Processor (PPP), a component of SMS. In other words, SMS translates user directives into MPI-like code. The main advantage of using SMS is that such translation is hidden to the user. This is because SMS is built *on top* of MPI. As a consequence no complicated compiler-generated communication statements have to be included in the code. Moreover, SMS contains a number of features to speed up the debugging process and to support incremental parallelization. In order to obtain constructs ready to be automatically parallelised by the SMS, the first step is to upgrade some commands of the original Fortran77 code to Fortran90. In case the code is already written in Fortran90, the first step is to modify the code in such a way that it can directly understand SMS

directives. So, according to SMS parallelization philosophy, we have first to define the decomposition type through the `decomposition declaration` as in the following example

```
module decomp
!sms$distribute (DECOMP_XY. 1. 2)
end module decomp                    (3.1)
```

With the previous declaration we have created a new Fortran90 module to define decomposition structure, `DECOMP_XY`, needed to support data exchange, local and global address translation, do-loop transformations and data decomposition. The number that follows `DECOMP_XY` in the decomposition declaration is the number of dimensions involved in the decomposition declaration. Even though we deal with a 3D problem, the maximum number of dimensions allowed by SMS for parallelizing in the `decomposition declaration` is 2. The next step is to distribute the array representing the solution of our equations of motion, more specifically the array `u  (:?,?:?,?:?,?:?,?:)` representing soil displacement, as well as all other auxiliary arrays. According to the previous `decomposition declaration` we have:

```
!sms$distribute (DECOMP_XY. 1. 2) begin
   real. allocatable : : u (:?,?:?,?:?,?:?,?:)
!sms$distribute  end                 (3.2)
```

This directive links the data decomposition structures, defined in eq. (3.1), with arrays targeted for decomposition. With the previous SMS directive we have chosen to distribute the first two indices of array `u`.

Declarations (3.1) and (3.2) allow SMS to understand how the chosen arrays must be distributed among processors. This is because all information necessary to access, communicate, input and output, decomposed and non-decomposed arrays are specified in the previous two declarations. To go on with the parallelization, we insert SMS directives in the original Fortran90 code, after the declaration section. The first instruction is the `decomposition creation`

```
!sms$create_decomp(DECOMP_XY,
<nx, ny>, <1, 1>)                    (3.3)
```

where the decomposition name, DECOMP_XY,? the global size of the 1st and 2nd decomposed dimensions, `<nx, ny>` and width of the halo region, `<1, 1>`, are specified. More in details, `<nx, ny>` represents the maximum number of grid points of the 1st and 2nd dimension that must be decomposed, whereas `<1, 1>` represents the number of grid points involved in the halo region; we use a nearest neighbours algorithm in which we have specified the halo region made by just one grid point. Of course, such a halo region is in common between two neighbour processors. SMS requires the indices that have to be parallelized must be both, the first two in the array and they must refer to the grid's nodes. Such constrains might require modifications of the serial code to have the indices in correct order for the SMS parallelisation. The following old Fortran90 instruction in the serial

code `ALLOCATE (u(ndim,nx,nz,nt))` has the first index not linked with the grid's nodes, `ndim` is an index referring to the component, actually. Moreover, the indices of the grid's nodes, *i.e.*, `nx,ny,nz` are in the wrong position to be parallelized. So, according to the aforementioned SMS rules, we have been forced to change the index order as follows

```
ALLOCATE (u(nx,ny,nz,nt,ndim)         (3.4)
```

Once we have detected segments of the program that should be parallelized analyzing the code with a profiling software, we insert SMS directives in the serial code. From such profiling analysis it turned out that more than 84% of the time is spent by the serial code in executing the following section for a single time step, that's why we have focused our attention on it:

```
!sms$parallel(DECOMP_XY, <kx>, <ky>) begin
!sms$exchange (u)
.....
      .....
do kz=2,nz-1
     do ky=2,ny-1
        do kx=2, nx-1
        call stencil_full(kx,ky,kx)   ! full form stencil
      enddo
    ennddo
enddo
 .....
 .....

!sms$parallel end
 .....
 .....
subroutine stencil_full(kx,ky,kz)   ! the 3-D stencil:
  .....
  .....
unew=2.*u(kx,ky,kz,2,kul)-(u(kx,ky,kz,1,kul)*dtdt_rho*  (&
& u(kx+1,ky-1,2,ku2)-u(kx,ky-1,kz,2,ku2)) -               &
&(u(kx,ky,kz,2,ku1)-u(kx-1.ky,kz,2,ku1))))+               &
& ((muf*r1_dyky*(u(k,ky+1,kz,2,ku1)-u(kx,ky,kz,2ku1)))- &

  .....
  .....
u(kx,ky,kz,kt3,ku1)=unew
end soubroutine stencil_full                              (3.5)
```

The parallel section starts with the SMS instruction `!sms$parallel(DECOMP_XY, <kx>, <ky>) begin`. This instruction defines a region over which parallel computations will be done on each processor's local data, as defined by the given data decomposition `DECOMP_XY`. All do-loops inside a parallel region that reference the specified loop variables (`<kx>, <ky>`) will be translated.

It is worth noting that the order of the indices in the `u` array coupled with the order of the nested loops in (3.5), is the most efficient combination in respect to the so called *easy memory access patterns* problem (Dowd and Severance, 1998; Hennessy and Patterson, 2006). This holds for both serial and parallel codes provided they are written in Fortran language. For different programming languages the coupling between the order of indices in the array and the order of nested loops might be different.

The SMS directive `!sms$exchange (u)` has been introduced to communicate with neighbouring processors to update halo regions and to maintain consistency with the serial code in the updating. Such a communication is necessary because the array u shows a index dependence on the first neighbouring grid points, *e.g.* `u(kx+1,ky 1,kz,2,ku2)`. Information provided by (3.2) is used to generate the correct communication code for our exchanged variable. In other words, `!sms$exchange (u)` is in charge of the message passing. Time updating procedure has not been changed from serial to parallel code, details about such a procedure can be found in the Opr?al and Zahradnik (2002).

Probable serial parts of the code, that cannot be parallelized, are nested into a parallel one by `!sms$serial` directive. The parallel region is closed by adding the directive `!sms$parallel end`.

It is worth noting that we have obtained the parallel version inserting directives that represent only 6% of the whole serial code.

3.2. *SMS performances*

For this study, numerical tests are run on an IBM SP5 cluster, with 48 processors arranged in six symmetric multi processor (SMP) machines (8 processors each). Communication between processors is realised via shared memory within each 8-way SMP machine, while a high performance switch (HPS) is used to realize communication between the six 8-way SMP machines in a cluster. Each processor has 1.9 Ghz Power5, the integrated cluster has a peak performance rate of 364 Gflops and a global RAM of 192 Gbytes. We used the XLF IBM native Fortran third party compiler optimized according to the target architecture, moreover, we have optimized the SMS tool to the IBM SP5 cluster. In order to achieve suitable performances the first step is to balance the computational work among processors. By default, SMS uses a pre-determined set of rules to decide how grid points are assigned to each process and how many processes are allocated to each decomposed dimension. Roughly speaking, the grid-points are distributed evenly among the processes along a given decomposed dimension.

In order to adopt its domain decomposition we have to run our SMS executable code as follows

```
smsrUN NP 3DCPP_sms
```

where `3dcpp_SMS` is our executable whereas `np` is the number of processors.

Ideally, each processor will have the same number of computational grid-points. In practice, most models have computations that vary spatially so some processes may have more work than others. This is commonly known as *load imbalance*. Load imbalances slow down a parallel program because processes with less work are forced to wait for processes with more work to do.

The criterion used by SMS to divide the computational workload is to minimize information that must be exchanged among processors. However, attention should be paid in realizing the domain decomposition process.

This can be easily done by the user because SMS allows to specify the assignment of processors using a process configuration file in the form of a Fortran name list.

In details, we run our executable SMS code as follows

```
smsRun -cf my_config 3dcpp_SMS
```

where `my_config` is our configuration file
```
&decomp
decomp1_name = 'decomp_xy',
decomp1_nps = 2 23/
```

in which we specify, in the last line, the number of processors along x-direction and y-direction, respectively. In this case we have 46 processors available.

Figure 3 shows the time needed for a single time-step versus number of processors for both the domain decomposition suggested by SMS (Default in fig. 3), and the one preferred by us (User in fig. 3). Oscillations in time are clearly recognized as the number of processors increase. Such an effect is strictly linked to the load balancing problem. Indeed, in our case SMS has to divide 480 nodes along the *x* axis and 442 nodes along the *y*-axis. In the worst case with 46 processors (see fig. 3), SMS realized such division by default assigning 23 processors along *x*-axis and 2 processors along *y*-axis. This causes a big load imbalance well represented in the time needed for a single computational step.

To fix the load balancing problem, we have inverted the default SMS decomposition assigning 2 processors along *x*-axis and 23 processors along *y*-axis. Our choice, of 46 processors, improved the time needed for a single iteration by almost 19% (see fig. 3). Such a procedurehas been adopted to improve the domain decomposition for other numbers of processors.

A useful index to check any gain in performance with respect to the serial code is the Speed-up, $S(n)$. It is defined as the ratio between the real time employed by one processor to run the code, $T(1)$, and the real time needed by n processors, $T(n)$:

$$S(n) = \frac{T(1)}{T(n)}.$$

Figure 4 left panel compares the Speed-up of both SMS default domain decomposition and our specified decomposition with ideal performance. It emerges that for our modeling the Speed-up scaling is satisfactory up to 24

processors. Beyond this threshold the onset of saturation for $S(n)$ starts. Saturation is an important marker, to illustrate its meaning we have to consider that the user-hiding message passing (among processors) is a time consuming process. Saturation starts when the message-passing time is comparable with the computation time needed by each processor to run its own part of the workload. The communication time increases with the number of processors while the computational time of each processor decreases. Therefore, there is no advantage in increasing the number of processors within a Speed-up saturated regime.

In looking at fig. 4 left panel, we see that the saturation is approached through oscillations in the Speed-up values and this is not surprising taking into account the load balancing analysis discussed above.

Figure 4 right panel shows the performance of the parallel code in terms of the Efficiency, which is defined as the ratio between the Speed-up and the number of processors:

$$E(n) = \frac{S(n)}{n}.$$

By definition, Efficiency is a measure of the relevance of user-hiding message passing for a single process. From fig. 4 right panel, the order of magnitude of the improvement achieved can be seen comparing the values of the Efficiency for the same number of processors in the case of the User and Default domain decomposition. As an example, looking at fig. 4 right panel, at 36 processors we see that the Efficiency corresponding to the User decomposition is almost 10% higher that the Default one.

Moreover, in looking at the Efficiency plot we see an improvement in performances each time a new 8 processors SP5 machine is added to the cluster. This effect is better seen and recognizable in the Efficiency curve corresponding to our domain decomposition choice. In fact, the Efficiency shows a decrease followed by a flat curve almost after every 8 processors. The same behavior has been observed in Caserta *et al*. (2002) for HPF; in our case this trend is more difficult to recognize because load balancing effects are superimposed. It follows from this that advantages in using SMS are ob-
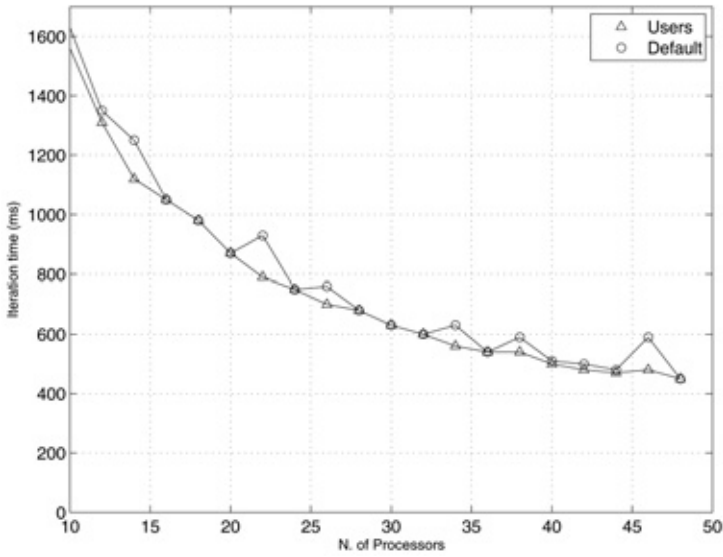
Fig. 3. Iteration time per time step (in milliseconds) vs. number of processors for the domain decomposition suggested by SMS (Default) and that one suggested by us (User). The plot starts from 10 processors in order to better magnify the differences between the two decompositions. Under 10 processors no difference takes place.
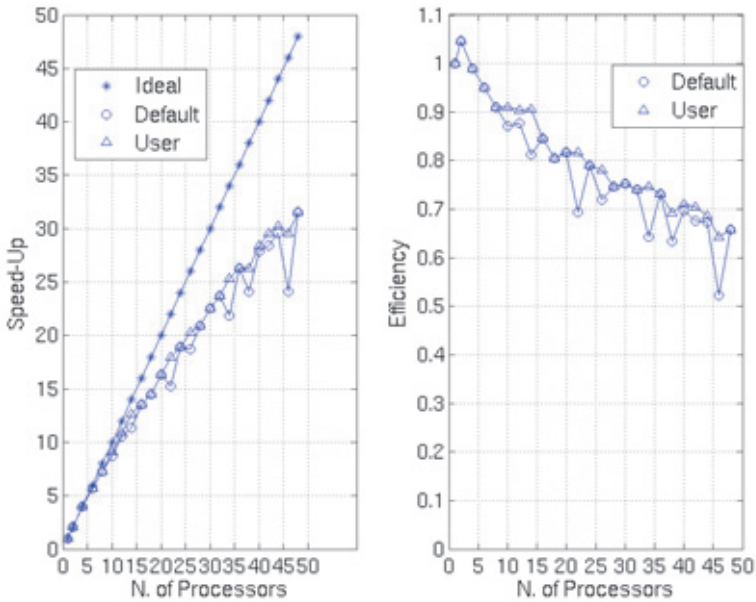

Fig. 4. Plots of Speed-up (left panel) and Efficiency (right panel) vs. number of processors for both the domain decompositions as planned and realized by SMS (Default) and as planned and realized by us (User). Compari-son shows up to 48 processors, *i.e.*, using six 8-processor SP5 machines in a cluster. Straight line with asterisks represents the ideal Speed

tained when a cluster of multiprocessor machines are used in a distributed memory environment.

4. Conclusions

We investigated a simple and efficient way to parallelise a serial code, namely 3D seismological code able to simulate the interaction between seismic radiation and near-surface geological structures. The chosen case study code (Opr?al and Zahradnik, 2002) and the case test geological site (Fäh *et al.,* 2006) are representative of a wide set of seismological problems dealing with the aforementioned dynamic interaction.

Our parallel approach is based on the SMS high-level tool. It allows the user to avoid all the low-level machinery needed to plan and realise the management of information exchanged among processors, apart from taking care of the domain decomposition problem as discussed in the previous paragraph. This does not mean algorithmic modifications in the serial code were not performed by the user to increase both the Speed-up and the Efficiency. On the contrary, these latter must be included in the profiling analysis applied to the serial code.

In the parallelisation of our case study, numerical tests indicate care must be taken in the domain decomposition process to reduce oscillations in both Speed-up and Efficiency, improving parallel performances. Generally speaking, in a shared memory environment communication is much faster because it takes place in the same cluster node. Nevertheless, we have seen less degradation of performances in adding multiprocessor machines. This phenomenon is clearer in the Efficiency plot (fig. 3 right panel) where the Efficiency remains almost constant when we add a new 8 processor machine, then in the Speed-up plot (fig. 3 left panel); this is mainly due to the load balance problem that is more evident in the Speed-up plot.

Such an effect was also observed in Caserta *et al*. (2002) with smaller size numerical problems, when a new multiprocessor machine is added under HPF compiler.

Moreover, porting from serial to parallel versions can be realized relatively simply for both environments. In fact, the porting is realized through the following simple steps:

– definition of the decomposition structure (see eq. 3.1),

– distribution of variables among processors (see eq. 3.2),

– domain decomposition creation (see eq. 3.3),

– creation of parallel region and exchange of variables among processors, *i.e*., message passing (see eq. 3.5).

Such SMS directives represent around 6% of serial code instructions.

On the other hand, SMS limitations are mainly:

– it can be used for Fortran codes only,

– it is intended for applications using structured Cartesian grids,

– maximum number of array indices that can be distributed is two. We point out that they must be the first two indices in the array. This constrain might require modifications of the serial code to have the indices in the required order. This is what we have been forced to do as in eq. 3.4.

No further limitations are arranged concerning, in particular, the numerical implementation, *i.e*., boundary elements, finite elements, spectral elements, finite differences, and so on. Under the above limitations, the simplicity and efficiency of the SMS tool are evident as it may allow broader and/or detailed physical models to be studied due to the use of parallel machines.

It is worth noting that the majority of 3D seismic codes that represent our target are written in Fortran and are based on the finite differences method on a Cartesian grid. On the other hand, no limitations so, we can conclude that for our purposes the previous limitations are not so severe.

Acknowledgements

chines at CASPUR computer centre. We also wish to thank Antonio Rovelli for help and criticism. Part of the research activities were carried out by A. Caserta, for his PhD thesis, in cooperation with the Charles University in Prague (Czech Republic) and in the frame of the projects GACR 205/07/0502 and MSM 0021620860.

REFERENCES

AKI, K. (1988): Local site effect on ground motion, in *Earthquake engineering and soil dynamics*, II: *Recent advances in ground-motion evaluation*, edited by J. LAWRENCE VON THUN, ASCE, 103-155.

AKI, K. (1993): Local site effects on weak and strong ground motions, *Tectono-physics*, **218**, 93-111.

BAO, H., J. BIELAK, O. GHATTAS, D.R. O'HALLARON, L.F. KALLIVOKAS, J.R. SHEWCHUK and J. XU (1996): *Earthquake Ground Motion Modeling on Parallel Computers*, Supercomputing '96, (Pittsburgh, Pennsylvania, November 1996).

BARD, P.-Y. (1995): Effects of surface geology on ground motion: recent results and remaining issues, in *Proceedings of the 10th European Conference on Earthquake Engineering*, (Vienna, Austria), 305-324.

BARD, P.-Y. (1998): Microtremor measurements: a tool for site effect estimation?, in *Proceeding of the Second International Symposium on the Effects of Surface Geology on Seismic Motion*, (Yokohama, Japan), pp. 1251-1279.

BIELAK, J., O. GHATTAS and H. BAO (1998): Ground motion modeling using 3D finite element methods, in *Proceedings of the 2nd International Symposium on the Effects of Surface Geology on the Seismic Motion*, (Yokohama, Japan), 121-133.

BONNEFOY-CLAUDET, S., F. COTTON and P.-Y. BARD (2006): The nature of noise wavefield and its applications for site effects studies. A literature review, *Earth Science Review,* **79**, 205-227.

CARA, F., A. ROVELLI, G. DI GIULIO, F. MARRA, T. BRAUN, G. CULTRERA, R. AZZARA and E. BOSCHI (2005): The role of site effects on the intensity anomaly of S. Giuliano di Puglia inferred from aftershocks of the Molise, Central Southern Italy, sequence, November 2002, *Bulletin of the Seismological Society of America*, **95** (4), 1457-1468.

CASERTA, A. and P. LANUCARA (2000): Computer animation as a tool to visualize effects of seismic wave propagation inside heterogeneous media, *Annali di Geofisica* **43** (1), 119-134.

CASERTA, A., F. BELLUCCI, G. CULTRERA, S. DONATI, F. MARRA, G. MELE, B. PALOMBO and A. ROVELLI (2000): Study of site effects in the area of Nocera Umbra (Central Italy) during the 1997 Umbria-Marche seismic sequence, *Journal of Seismology*, **4**, 555-565.

CASERTA, A., V. RUGGIERO and P. LANUCARA (2002): Numerical Modelling of dynamical interaction between seismic radiation and near-surface geological struc-

tures: a parallel approach, *Computer & Geoscience*, **28**, 1069-1077.

CULTRERA, G., A. ROVELLI, G. MELE, R. AZZARA, A. CASERTA and F. MARRA (2003): Azimuth dependent amplification of the weak and strong ground motions within a fault zone (Nocera Umbra, central Italy), *Journal of Geophysical Research*, **108**, 2156-2170.

DOWD, K. and C. SEVERANCE (1998): *High performance computing*, (O'Reilly, Cambridge- Kölon-Paris-Sebastopol-Tokyo), pp. 446.

DI GIULIO G., A. ROVELLI, F. CARA, R.M. AZZARA, F. MARRA, R. BASILI and A. CASERTA (2002): Long duration asynchronous ground motions in the Colforito plain, central Italy, observed on a two dimensional dense array, *Journal of Geophysical Research*, **108**, 2486-2498.

FÄH, D., C. IODICE and P. SUHADOLC (1993): A new method for realistic estimation of seismic ground motion in megacities: the case of Rome, *Earthquake Spectra,* **4,** 643-668.

FÄH, D., S. STEIMEN, I. OPRŠAL, J. RIPPERGER, J. WÖSSNER, R. SCHATZMANN, P. KÄSTLI, I. SPOTTKE and P. HUGGENBERGER (2006): The earthquake of 250 A.D. in Augusta Raurica, A real event with a 3D site effect?, *Journal of Seismology*, **10** (4), 459-477.

FOSTER, I. (1995): Designing and Building Parallel Programs: Concept and Tools for Parallel Software Engineering. *Addison-Wesley, Reading*, MA, pp. 381.

GOVETT, M., L. HART, T. HENDERSON, J. MIDDLECOFF and D. SCHAFFER (2003): The scalable modeling system: directive-based code parallelization for distributed and shared memory computers, *Parallel Computing*, **29** (8), 995-1020.

GRAVES, R.W. (1998): Three-dimensional computer simulations of realistic earthquake ground motions in regions of deep sedimentary basin. in *Proceedings 2nd International Symposium on the effects of surface geology on seismic motion, Yokohama, Japan*, pp. 103-120.

HENNESSY, J. and D. PATTERSON (2006): *Computer Architecture: A Quantitative Approach* [With CD-ROM], (Morgan Kaufmann Publishers, San Francisco, CA), pp. 672.

MITCHEL, A.R. and D.F. GRIFFITHS (1980): *The Finite Difference Method in Partial Differential Equations*, (Wiley, New York), pp. 272.

MOCZO, P., J. KRISTEK and E. BYSTRICKY (2001): Efficiency and optimization of the 3-D finite-difference modeling of seismic ground motion, *Journal of Computational Acoustics,* **9** (2), 593-609.

MOCZO, P., J. KRISTEK, M. GALIS, P. PAZAK and M. BALAZOVJECH (2007): The Finite-Difference and Finite-Element Modeling of Seismic Wave Propagation and Earthquake Motion, *Acta Physica Slovaca*, **57** (2), 177-406.

NICHOLS, B., D. BUTTLAR and J. FARRELL (1996): *Pthreads Programming*, (1st ed. O'Reilly, Sebastopol, CA), pp. 283.

OLSEN, K.B. and R.J. ARCHULETA (1996): Three-dimensional simulations of earthquakes on the Los Angeles fault system, *Bulletin of the Seismological Society of America*, **86**, 575-596.

OLSEN, K.B., A. AKINCI, A. ROVELLI, F. MARRA and L. MALAGNINI (2006): 3D ground-motion estimation in Rome, Italy, *Bulletin of the Seisological Society of*

America, **96**, 133- 146.

OPRŠAL, I. and J. ZAHRADNIK (1999) Elastic finite-difference method for irregular grids. *Geophysics,* **64** (1), 240-250.

OPRŠAL, I. and J. ZAHRADNIK (2002): Three-dimensional finite difference method and hybrid modeling of earthquake ground motion, *Journal Of Gephysisical Research*, **107**, B8, 2161.

OPRŠAL, I., J. ZAHRADNÍK, A, SERPETSIDAKI and G.-A. TSELENITS (2004): 3D hybrid simulation of the source and site effects during the 1999 Athens earthquake, in *Proc. Of 13th World Conference on Earthquake Engineering,* (Vancouver, B.C., Canada, August 1-6, 2004), Paper No. 3337, pp. 15.

OPRŠAL, I., D. FÄH, M. MAI and D. GIARDINI (2005): Deterministic earthquake scenario for the Basel area: Simulating strong motions and site effects for Basel, Switzerland, *J. Geophys. Res.,* **110** (B4), 19, B04305, doi:10.1029/2004JB003188.

OPRŠAL, I. and D. FÄH (2007): 1D vs. 3D strong ground motion hybrid modelling of site, and pronounced topography effects at Augusta Raurica, Switzerland - earthquakes or battles?, in *Proceedings of 4th International Conference on Earthquake Geotechnical Engineering June 25-28, 2007, Greece*, Paper No. 1416, pp. 12.

OPRŠAL, I., C. MATYSKA and K. IRIKURA (2009): The source-box wave propagation hybrid methods: general formulation and implementation, *Geophysical Journal International*, **176** (2), 555-564.

OPRŠAL, G.F., F. ROMANELLI and F. VACCARI (2001): Seismic wave propagation in laterally heterogeneous anelastic media: theory and applications to seismic zonation, *Advances in Geophysics*, **43**, 1-95.

PITARKA, A. (1999): 3D elastic finite difference modeling of seismic wave propagation using staggered grid non-uniform spacing, *Bulletin of the Seismological Society of America,* **89**, 54-68.

ROVELLI, A., A. CASERTA, L. MALAGNINI and F. MARRA (1994): Assessment of potential strong ground motions in the city of Rome, *Annali di Geofisica,* **37** (6), 1745-1769.

SÁNCEZ-SESMA, F.J. and F. LUZON (1995): Seismic response of three-dimensional valleys for incident P, S, and Rayleigh waves, *Bulletin. of the Seismological Society of America*, **85**, 269-284.

SORENSEN, M.B., I. OPRŠAL, S. BONNEFOY-CLAUDET, K. ATAKAN, P.M. MAI, N. PULIDO and C. YALCINER (2006): Local site effects in Ataköy, Istanbul, Turkey, due to a future large earthquake in the Marmara Sea, *Geophysical Journal International*, **167**, 1413-1424, doi: 10.1111/j.1365-246X.2006.03204.x.

ZAHRADNIK, J., P. MOCZO and F. HRON (1993): Testing four elastic finite-difference schemes for behaviour at discontinuities, *Bulletin of the Seismological Society of America,* **83**, 107-129.

ZAHRADNIK, J. and P. MOCZO (1996): Hybrid seismic modeling based on discretewave number and finite difference methods, *Pure and Applied Geophysics*, **148**, 21-38.